THÈSE

Pour l'obtention du grade de

DOCTEUR DE L'UNIVERSITÉ DE PAU ET DES PAYS DE L'ADOUR

DOMAINE DE RECHERCHE: Mathématique Appliquées

Présentée par

M. Viatcheslav VOSTRIKOV

Simulation numérique d'écoulements diphasiques immiscibles compressibles avec transport réactif en milieux poreux

Numerical simulation of two-phase multicomponent flow with reactive transport in porous media

Directeur de thèse : Brahim Amaziane

Co-directeur de thèse : Michel Kern

Soutenue le 15 décembre 2014

JURY

Mme. J. ERHEL	Directrice de Recherche, INRIA	Rapporteur
M. M. JURAK	Professeur, Université de Zagreb	Rapporteur
M. P. PONCET	Professeur, Université de Pau	Examinateur
M. E. AHUSBORDE	Chargé de Recherche, CNRS	Co-encadrant
M. B. AMAZIANE	Maître de Conférences, HDR, Université de Pau	Directeur de thèse
M. M. KERN	Chargé de Recherche, INRIA	Co-directeur de thèse

Thèse préparée au sein du Laboratoire de Mathématiques et de leurs Application de Pau (LMAP), dans l'École Doctorale des Sciences Exactes et leurs applications de l'UPPA.

Remerciements

Le travail présenté dans ce manuscrit rentre dans le cadre d'une collobaration entre l'Université de Pau et des Pays de l'Adour, Laboratoire de Mathématiques et de leurs Applications et la Maison de la Simulation. Ce travail a bénéficié du soutien financier du Conseil Régional d'Aquitaine et du CEA - INSTN Saclay.

Je tiens à remercier tout d'abord Brahim Amaziane, mon directeur de thèse, et Michel Kern, mon co-directeur de thèse, qui m'ont accompagné pendant ces trois ans. Leurs disponibilité, leurs patiences, leurs encouragements m'ont aidé tout au long de cette thèse et m'ont permis de réussir mon travail malgré toutes les difficultés auxquelles je me suis heurté.

Je remercie également Etienne Ahusborde, co-encadrant de la thèse, qui m'a accompagné pendant mon travail au Laboratoire de Mathématiques et de leurs Applications de Pau. Il m'a aidé à maîtriser un nouveau logiciel puis a apporté une contribution importante à la résolution des problémes liés à la fois à la programmation et à l'édition de la thèse.

Je remercie Jocelyne Erhel et Mladen Jurak d'avoir accepté la tâche de rapporter sur ce manuscrit. Ils ont également contribué par leurs remarques et suggestions à améliorer la qualité du rapport final. Merci également à Philippe Poncet d'avoir accepté de faire partie de mon jury de thèse.

Je voudrais également remercier tous mes collègues et amis à la Maison de la Simulation et au Laboratoire de Mathématiques et de leurs Applications de Pau pour leur accueil.

Finalement, je remercie toute ma famille pour son soutien tout le long de cette thèse notamment dans les moments les plus difficiles.

Résumé & Abstract

Résumé

Le sujet de la thèse est la simulation numérique d'un écoulement diphasique eau-gaz couplé à des réactions chimiques. Ce sujet a des applications dans de nombreux problèmes liés à l'environnement. L'application qui nous intéresse est la séquestration du dioxyde de carbone (CO_2) dans un aquifère salin.

Lors de sa capture et de son stockage, le CO_2 est tout d'abord capturé à sa source, transporté sous forme liquéfiée puis injecté à haute pression sous forme gazeuse dans un aquifère salin profond. La simulation numérique est un outil essentiel pour s'assurer que le CO_2 restera piégé pendant des centaines voire des milliers d'années. Plusieurs mécanismes de piégeage peuvent être combinés afin d'atteindre cet objectif. On s'intéresse dans cette thèse au piégeage par solubilité (le CO_2 gazeux est dissout dans l'eau lorsqu'il remonte vers la surface) et à plus long terme, au piégeage minéral (le CO_2 réagit avec la matrice rocheuse pour former des minéraux tels que la calcite par exemple). Ainsi, comprendre comment le CO_2 réagit chimiquement avec son environnement devient un enjeu important pour son devenir à long terme.

La thèse comporte 4 chapitres. Le Chapitre 1 est une introduction à la problématique générale de l'écoulement diphasique multi-composants en milieu poreux, avec ou sans réactions chimiques. Il présente une revue de la littérature, et un résumé des chapitres suivants.

Le Chapitre 2 présente une discussion détaillée des phénomènes physiques et chimiques qui rentrent en jeu, et de leur modélisation mathématique. Le modèle que nous utilisons est celui d'un écoulement diphasique à deux composants en milieu poreux, couplé au transport réactif. Ce modèle conduit à un grand nombre d'équations aux dérivées partielles, couplées à des équations algébriques décrivant l'évolution de la concentration de chaque espèce à chaque point du maillage. Une solution consistant à résoudre le système tout entier (approche totalement implicite) est possible, mais présente de nombreuses difficultés d'un point de vue numérique. Nous avons ainsi opté pour une approche découplée dans laquelle l'écoulement diphasique et le transport réactif sont calculés séquentiellement. L'un des principaux avantages de cette approche est qu'elle permet de réutiliser des codes testés et validés séparément pour chaque sous-problème. Un autre avantage est qu'elle évite de devoir résoudre un grand système souvent très mal conditionné à chaque pas de temps, comme pour le problème totalement couplé

Comme ce sont des ingrédients essentiels à notre approche, nous avons décrit en détail au Chapitre 3 les codes utilisés pour l'écoulement diphasique à deux composants ainsi que pour le transport réactif. Le cadre général que nous avons utilisé est DuMu^X

(un simulateur libre et open-source pour les écoulements en milieu poreux). Le solveur pour l'écoulement diphasique à deux composants était déjà présent dans l'environnement et nous avons validé son utilisation par de nombreux tests numériques. Nous avons par ailleurs développé de nouveaux modules, tout d'abord pour le transport seul puis pour le transport réactif, le code pour le transport réactif étant lui même basé sur une approche séquentielle itérative entre le transport et la chimie. Pour la résolution de l'équilibre chimique, nous avons utilisé le code ChemEqLib développé en interne.

Le Chapitre 4 décrit de manière détaillée la méthode utilisée pour découpler les sous-problèmes. Un inconvénient d'une telle approche est une possible perte de précision par rapport à une approche globale. C'est pour cela que nous avons bien détaillé la procédure de découplage afin que les approximations responsables d'une perte de précision soient bien identifiables. Nous décrivons ensuite le nouveau module de haut niveau réalisé pour le couplage des deux sous-problèmes (écoulement et transport réactif). L'ensemble de la méthode est validée à travers des exemples de tests pris dans la littérature et qui décrivent des scénarios typiques de stockage du CO_2.

Abstract

The subject of this thesis is the numerical simulation of water–gas flow in the subsurface together with chemical reactions. The subject has applications to various situations in environmental modeling, though we are mainly concerned with CO_2 storage in deep saline aquifers.

In Carbon Capture and Storage studies, CO_2 is first captured from its sources of origin, transport in liquefied form and injected as gas under high pressure in deep saline aquifers. Numerical simulation is an essential tool to make sure that gaseous CO_2 will remain trapped for several hundreds or thousands of years. Several trapping mechanisms can be brought to bear to achieve this goal. Of particular interest in this thesis are solubility trapping (whereby gaseous CO_2 dissolves in the brine as it moves upward) and, on a longer term, mineral trapping (which causes CO_2 to react with the surrounding rock to form minerals such as calcite). Thus, understanding how CO_2 reacts chemically becomes an important issue for its long term fate.

The thesis is composed of four chapters. The first chapter is an introduction to multicomponent two-phase flow in porous media, with or without chemical reactions. It presents a review of the existing litterature, and gives an outline of the whole thesis.

Chapter 2 presents a quantitative discussion of the physical and chemical phenomena involved, and of their mathematical modeling. The model we use is that of two-phase two-component flow in porous media, coupled to reactive transport. This model leads to a large set of partial differential equations, coupled to algebraic equations, describing the evolution of the concentration of each species at each grid point. A direct solution of this problem (a *fully coupled* solution) is possible, but presents many difficulties form the numerical point of view. Moreover, it makes it difficult to reuse codes already written, and validated, to simulate the simpler phenomena of (uncoupled) two-phase flow and reactive transport. We thus opted for a decoupled approach, where the two-phase flow and reactive transport subsystems are solved sequentially. The main advantage of this approach is that it lets us reuse well tested software codes to solve these two subsystems. Another advantage is that we avoid having to solve a very large, and possibly ill-conditioned system of equations at each time-step.

The codes we have used for both the two-phase two-component flow and the reactive transport problems are described in details in Chapter 3, as they will be essential ingredients in the solution process. The overall framework we have used is the DuMu^X library (a free and open-source simulator for flow and transport processes in porous media). The two-phase flow solver was already present in the framework (though we have validated its use). To solve the reactive transport problem, we have implemented a new module in the DuMu^X framework that solves a single phase multicomponent problem, and we have coupled it with a locally developped code for chemical equilibrium call ChemEqLib, through a sequential iterative approach.

In Chapter 4, we discuss the decoupled solution method, based on the individual codes described previusoly. A possible drawback of the approach is that some accuracy may be lost in the decoupling process. For this reason, we have gone into much detail when presenting the decoupling procedure, so that the additional approximation so introduced will be visible. We then present the high level module that implements the sequential coupling procedure. We describe the method used, and show its validation on test examples from the literature that describe typical CO_2 storage scenarios.

Résumé long

Le stockage géologique du dioxyde de carbone (CO_2) est considéré comme l'une des stratégies les plus prometteuses pour atténuer les conséquences des gaz à effet de serre qui sont les principaux responsables du réchauffement climatique. Compte tenu des échelles de temps qui interviennent (plusieurs milliers d'années), l'évaluation de la viabilité du stockage géologique nécessite l'utilisation de la simulation numérique puisque les expérimentations sont impossibles et les prédictions indispensables. Plusieurs mécanismes physiques et géochimiques de piégeage doivent être combinés afin d'assurer un niveau élevé de confinement. Le piégeage géochimique devient notamment très important sur les très longues échelles de temps. En effet, la dissolution du carbone dans l'eau se produit seulement au bout de dizaines d'années alors que la formation de minéraux carbonés peut nécessiter plusieurs milliers d'années. Il devient donc primordial de prendre en compte les interactions entre les espèces chimiques présentes en solution et la matrice rocheuse. La séquestration du CO_2 dans un aquifère salin conduit ainsi à l'étude d'un écoulement diphasique (eau-gaz) couplé avec la géochimie (étude des réactions). Les équations régissant ce modèle sont obtenues en écrivant les équations de conservation de la masse, la loi de Darcy généralisée et la loi de la pression capillaire. Le couplage avec la chimie intervient par l'intermédiaire des taux de réactions, qui peuvent être soit des fonctions (non-linéaires) données des concentrations, dans le cas de réactions cinétiques, soit inconnus pour des réactions à l'équilibre. Dans ce dernier cas, chaque réaction donne lieu à une loi d'action de masse, soit une relation algébrique liant les concentrations des espèces concernées. D'un point de vue mathématique, la simulation numérique du stockage géologique du CO_2 nécessite donc de résoudre un large système d'équations aux dérivées partielles (décrivant l'écoulement diphasique compositionnel) ainsi que des équations différentielles algébriques ou ordinaires modélisant les réactions chimiques. L'objectif de cette thèse est de proposer un méthode numérique afin de résoudre ce système.

De nombreux travaux concernant les écoulements multiphasique multicomposant d'une part et le transport géochimique d'autre part existent dans la littérature. Récemment, plusieurs références sur le couplage entre les deux problèmes sont apparues. Généralement, pour les problèmes couplés, il existe principalement deux types d'approches. La première approche est une approche complètement couplée qui consiste à résoudre un système non linéaire rassemblant toutes les équations à chaque itération en temps. La seconde approche, plus répandue dans la littérature, est une approche séquentielle. Dans ce cas, l'écoulement et le transport réactif (voire l'écoulement, le transport et la chimie) sont résolus séquentiellement à chaque itération en temps, éventuellement dans une boucle itérative. A notre connaissance, aucune étude comparative n'existe encore afin de quantifier la perte de précision de cette approche par rapport à l'approche complètement couplée, mais son gain dans la mise en œuvre et l'économie en temps de calcul sont assez évidents. Ainsi, c'est cette approche que nous avons choisie de suivre dans cette thèse.

Le premier chapitre de cette thèse en présente la problématique. Nous avons effectué une revue de l'état de l'art et une liste non exhaustive de références sur les différents modèles utilisés pour le stockage du CO_2 est proposée. Le premier modèle considéré

est un modèle d'écoulement diphasique compositionnel sans réaction chimique. Dans la revue de l'état de l'art, nous nous sommes focalisés sur une des principales difficultés numérique de ce modèle, à savoir le choix des variables physiques à utiliser pour la gestion de l'apparition ou la disparition d'une phase. Nous avons ensuite décrit un modèle d'écoulement diphasique compositionnel avec transport réactif. Par définition, ce modèle tient compte des réactions géochimiques. Là encore, une revue de l'état de l'art est proposée d'une part pour les principales approches utilisées dans la littérature (approche totalement couplée et approche séquentielle) et d'autre part sur les méthodes utilisées pour résoudre le problème de transport réactif (approche séquentielle itérative ou non, approche globale implicite...).

Dans le second chapitre, nous avons décrit en détail le modèle physique utilisé pour un écoulement multiphasique multicomposant avec transport réactif. Le système d'équations obtenu comporte des équations aux dérivées partielles provenant essentiellement des équations de conservation de la masse couplées à des équations algébrique provenant de la chimie. Notre choix d'approche séquentielle nous a conduit à diviser ce système en deux sous-systèmes: le premier étant dédié à un écoulement diphasique avec deux constituants (eau-CO_2) et le second au transport réactif. Pour cette raison, nous avons aussi décrit en détail les deux modèles physiques utilisés dans ces sous-systèmes.

Dans le troisième chapitre, nous nous sommes focalisés sur la simulation numérique de chacun de ces deux sous-problèmes. Nous avons décidé d'utiliser un logiciel nommé DuMu^X. DuMu^X (DUNE for Multi-Phase, Component, Scale, Physics,..) est une plateforme de simulation numérique pour des problèmes de transport et d'écoulement en milieu poreux. DuMu^X inclut plusieurs modèles standards de complexité variée, allant du simple écoulement monophasique isotherme à un écoulement multiphasique multicomposant non-isotherme. L'utilisation d'un environnement existant et bien concu tel que DuMu^X pour implémenter nos algorithmes a présenté plusieurs avantages. L'environnement fournit en effet la plupart des outils numériques nécessaires pour l'implémentation de nouvelles méthodes numériques (gestion du maillage, discrétisation spatiale et temporelle, solveurs...). Pour le premier sous-problème (écoulement deux-phases deux-constituants), nous avons utilisé un modèle déjà existant dans DuMu^X. Ce modèle utilise une approche totalement implicite. La discrétisation spatiale est réalisée par une approche volumes-finis centrés aux sommets tandis que pour la discrétisation temporelle on utilise un schéma d'Euler implicite. Nous avons réalisé plusieurs cas test existants dans la littérature qui nous ont confirmé les capacités du simulateur choisi. Pour le second sous-problème (transport réactif), nous avons choisi une approche séquentielle itérative (SIA) qui consiste à résoudre successivement les équations de transport et l'équilibre chimique. Dans ce cas, nous avions donc besoin d'une part d'un solveur pour résoudre les équations de transport et d'autre part d'un solveur pour résoudre l'équilibre chimique. Pour le problème de transport, nous avons tout d'abord implémenté dans DuMu^X un modèle d'écoulement monophasique multicomposant en modifiant un modèle existant. Ce nouveau modèle a été validé sur un cas test analytique. Pour la résolution de l'équilibre chimique, nous avons utilisé le code ChemEqLib développé en interne. A nouveau, différents cas tests ont été réalisés et ont validé le code. Finalement, nous avons couplé ces deux modules afin de réaliser l'approche séquentielle

itérative dans l'environnement de DuMu^X puis validé notre nouveau module de transport réactif par différents cas tests.

La principale contribution de la thèse figure dans le quatrième chapitre où nous présentons notre approche séquentielle pour la résolution de l'écoulement diphasique multicomposant avec transport réactif. L'approche séquentielle consiste à résoudre successivement l'écoulement diphasique et le transport réactif. Dans la littérature, plusieurs codes utilisent cette approche mais la procédure de couplage entre les deux sous-problèmes n'est pas toujours explicite. Nous souhaitions donc proposer un algorithme où le couplage entre les deux sous-problèmes est justifié de facon rigoureuse. L'idée principale de notre approche est la séparation des composants chimiques en composants dominants et en composants mineurs. Cette séparation est basée sur l'influence qu'ont ces composants sur les paramètres physiques. Ainsi les composants dominants possèdent des concentrations élevées par rapport aux composants mineurs et ont par conséquent une grand influence sur certains paramètres physiques tels que les densités de chaque phase, les viscosités, etc. Nous avons ainsi reformulé le modèle physique initial en introduisant cette notion de séparation entre les composants dominants et mineurs. Cette nouvelle formulation facilite le découplage car on peut identifier plus facilement deux sous-problèmes. Dans un premier temps, on résout un écoulement simplifié avec deux phases et deux constituants en considérant l'eau et le CO_2 comme des composants dominants. On obtient alors l'évolution des pressions, des saturations et des concentration de l'eau et du CO_2. Les contributions des composants mineurs sont alors soit négligées, soit explicitées, c'est à dire prises à l'itération précédente. Dans un second temps, on résout un problème de transport réactif pour les composants mineurs grâce à la vitesse calculée par le sous-problème régissant l'écoulement. En retour, le transport réactif calcule comment la matrice est dissoute, permettant la mise à jour de la porosité. Cet algorithme a été implémenté dans DuMu^X en couplant les deux modules présentés et validés dans le second chapitre. Finalement, notre approche a été validée par plusieurs cas test, ce qui a montré son bien fondé.

Plusieurs perspectives sont désormais envisageables. Tout d'abord, il faudrait réaliser des tests de convergence et des études de robustesse de la méthode de couplage que nous avons proposée pour s'assurer de sa précision. Il faudrait aussi mieux comprendre l'influence des composants mineurs sur l'écoulement et le cas échéant, développer puis tester une stratégie itérative pour le couplage écoulement-transport réactif. Nous avons considéré que toutes les réactions chimiques sont à l'équilibre. Il faudrait donc aussi pouvoir aussi prendre en compte des réactions cinétiques, et des réactions mixtes équilibre-cinétique. Enfin, il faudrait procéder à l'implémentation 3D parallèle de notre stratégie. L'environnement de DuMu^X est déjà parallélisé mais la difficulté est de concevoir une stratégie d'équilibrage de charge qui soit valable à la fois pour la chime et l'écoulement.

Contents

List of Figures

List of Tables

Chapter 1

General Introduction

Contents

1.1 Introduction

This chapter gives a general introduction to the topic of the thesis and a short overview of its contributions.

In the second section we describe the goal of a geological CO_2 storage. In the third section we give a short review of a first type of existing physical models which can be used for description of CO_2 storage process. These models consider a two-phase multicomponent flow in porous media. In the fourth section we present the second type of models: two-phase multicomponent flow in porous media with reactive transport that additionally takes into consideration the chemical processes observed during CO_2 storage in a saline aquifer. Also in this section we describe two possible approaches for the numerical simulations of such type of physical models: fully-coupled approach or sequential approach and compare their main advantages and technical difficulties. In the last section of the general introduction we give an outline of the thesis contents.

1.2 Description of the geological storage of CO_2

This section is based on the book "Geological storage of CO_2. Modelling approaches for large-scale simulation", Nordbotten, J. M. and Celia, M.A. [49].

Global warming The global climate is a highly complex system that depends on many parameters and has been subject to various changes within geological times. During the last decades, a trend of rising average global temperature has been observed. Increasingly scientists are connecting rising temperatures with increasing amounts of greenhouse gases in the atmosphere. Greenhouse gases absorb radiation within the thermal infrared range emitted from the surface of the earth and can therefore cause a heating-up of the atmosphere.

The primary greenhouse gases in the Earth's atmosphere are water vapor, ozone, carbon dioxide, methane, nitrous oxide. These gases reside naturally in the atmosphere and greatly affect the temperature of the Earth: without them, Earth's surface would average about 33 °C colder. Due to human activities, the amounts of three of them (carbon dioxide, methane, nitrous oxide) have been increasing since the beginning of the industrial revolution. With respect to the anthropogenic greenhouse gases, CO_2 is the most abundant, because it is emitted into the atmosphere in large quantities.

The atmospheric concentrations of CO_2 have increased since the beginning of the industrial era in the second half of the 18th century from 280 ppm (parts per million), which had persisted for the previous 10,000 years with a variability of maximal 20 ppm, to a value of 379 ppm in 2005. Several scenarios describing the emission of greenhouse gases and models for the estimation of their influence on the global climate have been examined by the members of the Intergovernmental Panel on Climate Change (IPCC). Depending on the assumptions and the climate model, global temperature increases between 1 and 6 °C were predicted by the year 2100. It is very likely that such temperature change can cause that a lot of regions could face dramatic problems as a result of changed local climate.

Solution - underground storage To prevent catastrophic climate change in the near future, humankind should significantly reduce the level of greenhouses gas emission, especially carbon dioxide emission. Some possible ways of decreasing CO_2 emissions are the following:

- Improving the energy efficiency of existing technologies: the use of less energy, for the same output diminishes emitted CO_2.
- Using alternative energy sources: wind, solar and hydro-power do not produce CO_2 emissions. Biomass/wood as a fuel emits only the amount of carbon dioxide that was extracted from the atmosphere in the first place; it is emission neutral.
- Capturing CO_2 and storing it for long periods of time (hundreds of years) in geological formations.

The subject of this thesis is the investigation of this last possibility - the long-term storage of CO_2 in deep aquifers, known as Carbon Capture and Storage (CCS).

Physical phenomena during storage process In order to act as a climate change mitigation measure CCS needs to be implemented globally on a large scale. Currently, there are only a few large-scale saline aquifer storage projects, such as the Sleipner project in the North Sea (Torp and Gale [65]), the Snohvit project (Maldal and Tappel [41]) in the Barents Sea or Lacq-Rousse project [55] in Aquitaine. For the efficient

implementation of this technology, large-scale projects accompanied by detailed monitoring, risk and feasibility studies are crucial.

One important pillar for the realization of CO_2 storage projects is numerical modelling. Based on geological data, numerical models can be applied for a first screening of potential storage sites. Further, they are needed for risk assessment, capacity estimates and feasibility evaluations. The requirements on the modelling tools are high. Depending on the specific question, they need to be capable of describing complex processes observed during CO_2 sequestration in geological media such as:

Physical processes

- Static trapping (using structural and stratigraphic traps or man-made caverns, etc.): the flow of CO_2 is impeded by a physical low-permeability barrier.
- Residual CO_2 trapping: the CO_2 is trapped in the pore space at irreducible gas saturation; the flow of CO_2 is not possible because of the inter-facial tension between CO_2 and formation water.
- Hydrodynamic trapping: a combination of different mechanisms, including all the possible physiochemical mechanisms.

Chemical processes

- Solubility trapping: as the carbon dioxide flows in the subsurface, it dissolves in the brine which initially fills the pores of the storage formation; dissolved CO_2 mass does not flow upwards because of density differences.
- Mineral trapping: depending on the properties of brine and rock, the CO_2 reacts with the formation and forms minerals.

Static and hydrodynamic trappings are the most important trapping mechanism while CO_2 is being injected into the formation and as long as the plume is moving in the subsurface. With time the plume stagnates and residual and solubility trapping become the predominant CO_2 traps. After at least several hundreds of years, mineral trapping may become the most important trapping mechanism.

Appropriate model The aim of this work is to build a geochemical model that can describe the physical and chemical processes observed during CO_2 sequestration. The physical model elaborated in this thesis is based on the model of two-phase multicomponent flow in porous media with incorporation of the different types of chemical reactions between the chemical components.

1.3 Two-phase multicomponent flow in porous media: models and review of existing work

This section aims at giving a brief description of the physical model of two-phase multicomponent flow in porous media and gives a short overview of existing works.

Generally the physical model used for the simulation of CO_2 sequestration describes a system that contains two phases (liquid and gas) and two base components (water

and carbon dioxide). Such models may or not take into account the effects caused by the presence of other chemical component and chemical reaction among them. In this section, we consider models without chemistry. They are able to simulate the physical processes observed during CO_2 sequestration in geological media such as static and hydrodynamic trapping. There are several books available on fluid flow in porous media that explain the basics of two-phase flow (for instance, Bear [12], Pinder [53], Chen *et al* [21]). Here we will give a short list of physical relations involved in the considered model (a detailed form of relations will be given further in Chapter 2).

The governing equations for the simultaneous flow of liquid and gaseous phases are the mass conservation laws, Darcy's law, state equations and closure relations. The considered system involves two components (water and CO_2) present in both phases and mass transfer between different phase states of these components. Because of mass interchange between the phases, mass is not conserved within each phase, but the total mass of each component is conserved. Therefore, for each component in the physical model, we formulate a mass conservation law for its total mass. These equations express the variation of component mass caused by different physical processes observed in the flow: advection, diffusion, dispersion and mass removal (accumulation) through sinks (sources).

The second type of governing equations for two-phase two-component flow is Darcy's law. The original form of the law describes fluid flow in a porous medium on the macroscale and states that flow velocity (Darcy's velocity) is proportional to the ratio between permeability tensor and fluid viscosity and the gradient of fluid pressure. Darcy's law is analog to the momentum conservation law from the Navier-Stokes equations. Originally Darcy's law was determined experimentally, but it has since been derived from the Navier-Stokes equations via an homogenization procedure. For two-phase flow, Darcy's law is commonly extended to Darcy-Muskat's law by introducing of the relative permeability of each phase and referring to phase pressures. The existence of different pressures in each phase implies that their values should be coupled through the capillary pressure law.

The first two types of governing equations are conservation relations. In general case the physical description of the system involves third type of such conservation relations: energy conservation law. In this thesis, for all studied systems we consider only isothermal cases. For this reason, we do not include the energy conservation law in the physical model.

The following type of governing equation is state equations. This type of relations expresses the compressibility of the phases as functions of phase pressures, temperature and concentrations of components. The actual form of these relations is strongly dependent on the range of observed pressures and temperature values. For example, the compressibility of gas phase for atmospheric pressure and room temperature is close to the compressibility of ideal gas (density is proportional to the pressure), but with the increase of pressure the compressibility gradually decreases.

The last type of governing equations is closure relations. Such type of relations expresses the evident algebraic relations between system variables and completes the system of equations. The concrete choice of primary variables defines the list of closure relations. A standard choice for the primary variables for two-phase two-component flow is the pressure of one phase and the saturation of the other phase.

A great challenge in this context is the disappearance of the gas phase, which has

been studied in many recent papers, as the saturations cannot be used as primary variable here. A valid choice in the one-phase region would be one phase pressure and the mass fraction of CO_2 in the liquid phase. Several approaches to treat this problem exist.

For instance, Class *et al.* [23] switch primary variables according to the local phase state which is defined by switching criteria presented in the form of a set of inequalities.

Jaffré *et al.* [34] add the mass fraction of CO_2 as third primary variable to the liquid phase pressure and liquid phase saturation and use additional nonlinear complementarity constraints that describe the transition from one-phase to two-phase region, to close the system.

An analog approach was proposed by Lauser *et al.* in article [39] for general case of multiphase multicomponent flow. Authors of this article include phase transitions in the nonlinear system of equations: the transition conditions are formulated as a set of local inequality constraints, which are then directly integrated into the nonlinear solver using a nonlinear complementarity function.

Abadpour *et al.* [7] and Panfilov *et al.* [50] extend the saturation to artificial negative values, so that the system of mass conservation laws does not degenerate in the one phase region and the saturation can still be used as a primary variable.

Bourgeat *et al.* [14, 15] use persistent variant of the primary variables: dissolved gas mass concentration and liquid pressure that are defined both for liquid saturated and unsaturated regions.

Neumann *et al.* [48] propose a set of primary variables that consists of gas pressure and capillary pressure. To make this set uniform for both saturated and unsaturated by gas phase regions, in the absence of the gas phase the authors define the gas pressure as the corresponding pressure to the value of CO_2 mass fraction dissolved in the liquid phase.

Amaziane *et al.* [10] also use a persistent set of primary variable set that does not depend on phase transitions. As first primary variable the authors propose to use a global pressure variable, which partially decouples the system of equations. As a second persistent variable the authors introduce the total gas component mass density defined in one-phase and two-phase zones.

Marchand *et al.* in their works [42, 43, 44] present another persistent set of primary variables that contains the total molar fraction of the gas component and mean pressure which equals the pressure of the remaining phase when one of them disappears.

1.4 Two-phase multicomponent flow in porous media with reactive transport: application to geological storage of CO_2

As gaseous CO_2 dissolves in water, various minerals present in the rock matrix (such as calcite or quartz) also get dissolved, and this in turn creates acidification of the

medium. It is thus important to take into account a complex liquid phase, and also some reactions between the liquid species and various minerals. Indeed there appear the additional source/sink terms attributed to these chemical reactions [35] in mass conservation laws. The model presented in the previous section is limited to 2 components in the liquid phase. Here we discuss how the model can be extended to take into account these chemical reactions by addition of other chemical components present in the system. Note that chemistry can in turn have an influence on the flow, for instance through a modification of the porosity (and then also permeability) caused by a change in the mineral content of the host rock. The new extended model is called two-phase multicomponent flow in porous media with reactive transport.

1.4.1 Models with reactive transport

The governing equations for two-phase multicomponent flow in general are similar to two-phase two-component flow and can be arranged in the following groups: the mass conservation laws, Darcy-Muskat's law , states equations and closure relations.

The considered system in addition to water and CO_2 involves other chemical components formed in liquid phases during geological storage of CO_2 in an aquifer (such as H^+, OH^-, HCO_3^-, ...) and mass transfer between different chemical components caused by the presence of chemical reactions. In the general case, we formulate mass conservation laws for the mass of each component present in the chemical system. But because of mass interchange between the component caused by chemical reactions, we add a new source terms in these mass conservations laws that represent increasing or decreasing of chemical component mass under the influence of chemical reactions involving considered component. One has to introduce a distinction based on the time scale of the chemical reactions as compared to a typical time scale of the flow. Most aqueous phase reactions are much faster than the flow, whereas this may not be the case for reactions with minerals. Slow reactions (and in principle, all chemical reactions) should be modeled as kinetic reactions, with rates being known functions of all concentrations. For fast reactions, the possible discrepancy in time scales will introduce difficulties for the time integration scheme, and it is customary to model fast reactions as equilibrium reactions. However, this simplifications implies that the reaction rates are no longer explicit functions. They become unknowns of the problem, and have to be complemented by a mass action law for each reaction [56]. In these case the mass conservation laws should be rewritten in terms of total mass of components by making linear combinations in order to eliminate source terms formed by chemical rates of equilibrium reaction. This procedure is described in the papers (Saaltink *et al.* [28, 57], Kräutle [36]). Also we should notice that chemical rates of slow kinetic reactions are not eliminated after linear combinations.

The other types of governing equations are similar to the equations in the two-phase two-components flow but can have some minor changes caused by the presence of other chemical components except of water and carbon dioxide. For example, the state equation for liquid equation can express additional dependence of the liquid phase density on the concentrations of various chemical components (such as salt (NaCl) or dissolved carbon dioxide).

The final system of equations contains both non-linear partial differential equations (mass conservation laws for total mass) and algebraic relations (mass action laws and

closure relations). The standard choice of primary variables is the concentrations of chemical components, phase pressures and phase saturations. The obtained system is strongly coupled and its numerical simulation presents significant computational difficulties, such as a relatively large set of governing equations (in comparison to model of two-phase two-component flow), or additional coupling of equations through mass action laws. To resolve these difficulties, two different approaches for numerical simulation of two-phase multicomponent flow in porous media with reactive transport have been developed: a fully coupled approach, and a sequential one. The descriptions of physical models of two-phase multicomponent with reactive transport, that underlie the different numerical simulators, can be found in the following works: [26], [59] and [74].

1.4.2 Approaches for coupling flow/transport with chemistry

1.4.2.1 Fully coupled approaches

The first approach for solving two-phase multicomponent flow in porous media with reactive transport is the solution of an entire strongly coupled system of equations. The main disadvantage of such approach is the large number of system variables connected with increasing of governing equations in comparison with two-phase two-component flow. The Jacobian matrix resulting from such a fully coupled system is very large and the procedure for solving of resulting linear system involves considerable difficulties connected with additional coupling of governing equations through mass action laws.

Because of those numerical difficulties, there are only few numerical simulators of two-phase multicomponent flow that use the fully coupled approach. The numerical simulator developed by Fan *et al.* [26] solves the entire system of mass conservation laws and mass action laws by construction of the global Jacobian matrix. Another numerical simulator is the one developed by Saaltink *et al.* [59]. The main feature of this simulator is that instead of solving a system of mass action laws coupled with expression of total masses, the authors use a pre-calculated tabulated function that returns the concentrations of all component at chemical equilibrium according to the value of gas pressure. Such a choice reduces the list of primary variables only to phase pressures and saturations and, consequently, decreases the size of resulting Jacobian matrix. On the other hand, such a choice requires performing a significant amount of pre-computations of function that returns the values of chemical equilibrium for each component. The values of this function are specific for each chemical system and each change in the list of chemical components or reactions requires the complete recalculation.

1.4.2.2 Sequential (iterative) approaches

The second approach is a sequential (iterative) approach. The underlying concept of sequential approach as applied to the two-phase multicomponent flow in porous media with reactive transport is a splitting of the entire system into a subsystem of two-phase two-component flow for water and carbon dioxide, and a subsystem of reactive transport, that contains mass conservation laws for the other chemical components as well as mass action laws of chemical reactions. After solution of the two-phase two-component

flow subsystem, the fluid velocities and phase saturations are used to simulate reactive transport of other components.

Sequential approach will work best when the configuration of the flow is only slightly affected by distribution of chemical components with the exception of water and carbon dioxide. This assumption is usually valid if the mass of water and carbon dioxide constitutes almost the entire mass of mobile liquid and gas phases. The usage of a sequential approach decreases the complexity of the original fully coupled system of governing equations for two-phase multicomponent flow in porous media with reactive transport and replaces the solution of the original problem by sequential solutions of simpler sub-problems. The other advantage of this approach, that numerical simulator for two-phase two-component flow and reactive transport are already well developed and can be simply implemented.

The sequential approach is more widespread in numerical simulators than the fully-coupled approach. Among the existing simulators we can note the following: HYDROGEOCHEM [72], IPARS [68], TOUGHREACT [70], STOMP [69], PFLOTRAN [31, 32], MIN3P [45], NUFT [33], CORE^{2D} V4 [60] (all described in the book [74]). All these codes use a similar algorithm, decoupling the original problem into two-phase two-component flow and reactive transport, but at the same time they have some differences in the realization of interaction between the two sub-systems and in the particular realization of each sub-system.

We will detail some of the different choices made in the codes, to show how they can influence: first, the coupling between flow and reactive transport, whether or not the coupling is iterative, the physical model for the flow part, and the way the reactive transport problem is solved.

Interaction between sub-systems. The first distinguishing point is the realization of feedback interaction from the reactive transport module to the two-phase two-component flow module. After the solution of the reactive transport sub-problem, the new distribution of chemical components can cause changes in the physical parameters that can modify two-phase two-component flow path characteristics. This feedback between flow and chemistry can be considered in different ways. For examples in such codes as HYDROGEOCHEM, TOUGHREACT, PFLOTRAN, the feedback interaction from the reactive transport module to the two-phase two-component flow module takes into account modifications of internal flow parameters such as porosity, permeability, tortuosity or viscosity caused by changes in distribution of chemical component described by the reactive transport module. The codes NUFT and STOMP, in addition to this type of interaction, introduce an additional source term in the mass conservation laws of two-phase two-component flow module that expresses mass changes of carbon dioxide or water caused by its participation in the chemical reaction.

Iterative or non-iterative scheme. The other distinguishing point is the usage of iterative or non-iterative schemes. By non-iterative schemes we mean a single time solution of each subsystem for each time step. In iterative schemes each subsystem is solved several times with the latest update of physical parameters until the updates become sufficiently small and begin to satisfy some convergence criteria. This scheme significantly increases the time of calculation but can give more precise coupling of

sub-problems. The non-iterative scheme is used in NUFT. An iterative scheme is used in HYDROGEOCHEM, IPARS and TOUGHREACT.

Two-phase two-component flow subsystem. In addition to differences in the realization of interaction between sub-systems, the numerical simulators can use different approach for simulation of two-phase two-component flow and reactive transport subsystem. So for example, as a physical model for two-phase two-component numerical codes IPARS, TOUGHREACT, STOMP, PFLOTRAN, CORE^{2D} V4 use classical list of governing equations based on mass conservation laws as described in section 1.3. At the same time, other group of numerical simulators (HYDROGEOCHEM, MIN3P, NUFT) use simplified physical model of two-phase two-component flow based on Richard's equation. On the one hand such choice of physical model imposes significant restrictions on the applicability of the numerical simulator, since Richard's equation can be used only in the case of static gas pressure. But on the other hand, it reduces the number of governing equations and, consequently, the resulting computational part. During the process of carbon storage in deep aquifer we observe the wide range of gas pressure and its time evolution and, by this reason, the formulation in Richard's equation is not suitable for such investigations.

Reactive transport subsystem. The reactive transport sub-problem can in its turn be solved by using one of the following techniques, as described in [71], [58]

SNIA - Sequential Non-Iterative Approach. Total masses (concentrations) in mass conservation laws are divided into two separate terms: total liquid masses and total solid masses. Instead of concentration of the components, the total mass of liquid components are used as primary variables. In a first step we fix the first approximation of total solid mass from the value at the previous time step. Then the mass conservation laws are solved as transport equation for total liquid mass with fixed value of total solid mass. In a second step using the new value of total liquid mass and mass action laws we update the value of total solid mass.

SIA - Sequential Iterative Approach. This algorithm is similar to SNIA algorithm except that the described procedure is repeated several times at each time step with the last update of total solid mass until the changes in total mass after next iteration became significantly small. For instance, the details of SNIA and SIA algorithms can be found in the works [20], [71], [58] or further in Chapter 3 of this thesis.

GIA - Global Implicit Approach. This algorithm solves entire coupled system of mass conservation laws of transported components and mass action laws. In one of the most popular variants of global approach, local algebraic equations of mass action laws are treated by direct substitutional approaches (DSA): the algebraic equations are solved for certain variables, and these variables are eliminated in the remaining differential equations of mass conservation laws [71], [38]. The second variant of global approach is the differential and algebraic equations (DAE) approach in which the mass conservation equations and mass action laws are solved simultaneously as a system. For example such type of algorithm is used in works [25], [32] and [11].

The results and performance of numerical simulators for reactive transport based on SNIA, SIA and GIA approaches were compared for the 1D and 2D subproblems of test case of the MoMaS benchmark [19] in [18]. This comparison demonstrates that numerical simulators using sequential approach for reactive transport can achieve the same accuracy as the numerical simulator based on fully-implicit approach. Its also shows that fully-coupled simulators can be implemented quite efficiently.

Sequential Iterative Approach for reactive transport sub-problem is used in the following numerical simulators: TOUGHREACT, STOMP, CORE^{2D} V4. The different variations of Global Implicit Approach are used in HYDROGEOCHEM, PFLOTRAN, MIN3P, NUFT.

1.4.2.3 Comparison of numerical approaches

In this section we presented two approaches for numerical simulation of two-phase multicomponent flow with reactive transport: fully-coupled approach and sequential one. As was already mentioned each approach has its own advantages and disadvantages. On the one hand a fully coupled approach should provide a good degree of accuracy, but it is very expensive in terms of computational time. On the other hand, a sequential approach enables to simplify the original problem and reduces the cost of calculations (if we use non-iterative algorithm) but it can be less accurate. The degree of accuracy of sequential approach can be increased by using of an iterative algorithm, but in this case the numerical simulator, based on a sequential approach, can lose the computational time advantage in comparison with fully-coupled approach if the number of iterations will be large.

From this perspective, a criterion of practicality came to the forefront for the choice of a numerical approach to the problem. Numerical simulator based on fully-coupled approach must be developed only as a single module. At the same time, a numerical simulator based on a sequential approach can be separated into independent modules that are responsible for the solution of each subproblems. Validation of each module can be performed separately without the need to solve immediately complete two-phase multicomponent benchmarks. For this reason, in our work we decided to develop a numerical simulator using sequential scheme. As a model for two-phase two-component flow subsystem we chose the formulation based on the classical mass conservations laws, since as was already mentioned Richard's equation can be used only in the case of static gas pressure. For the numerical simulation of the reactive transport system we decide to use a Sequential Iterative Approach since in this case the development of a code can be facilitated by the possibility of using of modular approach in comparison with the Global Implicit Approach. At the same time, as was noted before the numerical simulator based on SIA can provide the same degree of accuracy as the simulator based on GIA.

1.5 Outline of the thesis

The main objective of this thesis is the development of a numerical simulator that will enable the investigation of physical and chemical processes observed during geological storage of CO_2 in deep aquifer.

At first, we figure out, that investigated phenomena can be sufficiently described by the physical model of two-phase multicomponent with reactive transport flow in porous media. The second chapter of this thesis presents the basic definitions used in the physics of porous media and general equations and physical laws used for the construction of a physical model of two-phase flow.

As was already mentioned, the entire system of equation of this physical model contains large number of strongly coupled partial differential equations and algebraic relations. Applying the sequential approach, we split the original system of equations into two subsystems: the subsystem of two-phase two-component flow and subsystem of reactive transport. For this reason, in the second chapter, in addition to the description of two-phase multicomponent flow, we give a detailed description of the physical models of two-phase two-component flow and reactive transport.

The choice of the sequential approach gave us the opportunity to develop a new numerical tool for simulation of two-phase multicomponent flow in porous media with reactive transport on the basis of existing open source code for simulation of two-phase two-component flow for the first sub-problem: DuMu^X [2]. In the third chapter of this thesis we provide a brief description of this software and present the results of simulation for several test cases which demonstrate the capabilities of the chosen simulator.

As a numerical algorithm for the simulation for the second sub-problem of reactive transport we have chosen a Sequential Iterative approach (SIA) which separates task of finding solution for the original problem into two subtasks: finding of chemical equilibrium and resolving of transport equations. For the numerical simulations of this problem we have created a new module **1pNc** of DuMu^X that implements the proposed SIA algorithm. This module is coupled with a locally developed code for chemical equilibrium called ChemEqLib. The detailed description of the used numerical algorithm for the reactive transport and the results of simulation, that validate the elaborated code, are also given in the third chapter of the thesis.

The main objective of the fourth chapter is the construction of a numerical simulator for two-phase multicomponent flow with reactive transport on the basis of previously elaborated simulators for two-phase two-component flow and reactive transport. In this chapter we present our variant of the sequential algorithm that is based on idea of the separation of primary components into two groups of dominant and minor components. To illustrate the methodology of proposed decoupling algorithm we apply it to the specific case of the geological storage of CO_2. Finally, we present the constructed numerical simulator for two-phase multicomponent flow and demonstrate its capabilities performing two different test cases.

Chapter 2

Physical modelling of two-phase multicomponent flow with chemical reactions

Contents

2.1 Introduction

The second chapter of this thesis is devoted to the physical modelling of two-phase multicomponent flow with chemical reactions.

In the first section of this chapter we present the basic definition used in the physics of porous media and general equations and laws used for the construction of a physical model of two-phase flow. As background material for this part, we used the books [21], [53] and the article [46] where the authors describe the status of modelling two-phase systems.

In the second section we focus on questions connected with modelling of geochemical reactions. In this section we give physical formulation of chemical reactions depending on their type, equilibrium and kinetic, and show how chemical reactions are coupled with mass balance equations. At the end of this section, we present the final system of equations used for modelling the general case of two-phase multicomponent flow.

In the third and fourth sections, we consider in detail particular cases of geochemical system: two-phase two-component H_2O-CO_2 flow and one-phase reactive transport.

2.2 Two-phase multicomponent flow

2.2.1 Basic definitions and notations

Introduce the following set of notations:

- ϕ - porosity [-],
- $\alpha = l, g$ - phase: mobile l = liquid (wetting phase) and g = gas (non-wetting phase), or immobile s = solid,
- i - index of chemical component,
- ρ_α - density of phase α [kg/m^3],
- $\rho_{\alpha,\text{mol}}$ - molar density of phase α [mol/m^3],
- ρ_α^i - partial density of component i in phase α [kg/m^3],
- X_α^i - mass ratio of component i in phase α [-],
- $c_{\alpha,i}$ -concentration of component i in phase α (number of molecules of component i in unit volume of phase α) [mol/m^3],
- $c_{p\alpha}$ -vector of concentrations of primary components i in phase α (number of molecules of component i in unit volume of phase α) [mol/m^3],
- $c_{s\alpha}$ -vector of concentrations of secondary components i in phase α (number of molecules of component i in unit volume of phase α) [mol/m^3],
- c - vector of concentrations of all components [mol/m^3],
- x_α^i - molar ratio of component i in phase α [-],
- S_α- saturation of phase α [-],

- M_i - molar mass of component i [kg/mol],
- p_α - pressure of phase α [Pa],
- $\overrightarrow{q_\alpha}$ - Darcy velocity of phase α [m/s],
- p^i_α - partial pressure of component i in phase α [Pa],
- p_c - capillary pressure [Pa],
- μ_α - viscosity of phase α [Pa/s],
- $\overrightarrow{j^i_\alpha}$ - diffusion-dispersion vector for component i in phase α,
- D^i_α - diffusion-dispersion tensor for component i in phase α,
- $\rho^i_{\alpha,\text{mol}}$ - partial molar density of component i of phase α [mol/m^3],
- $k_{r\alpha}$ - relative permeability for phase α [-],
- K - absolute permeability of the medium [m^2]
- S - salinity, mass ratio of salt in the liquid phase [-],
- T - temperature of the system [K]

The general mathematical model for two-phase flow in porous media is based on the following types of relations:

- continuum balance equations,
- Darcy-Muskat's law,
- Capillary pressure law,
- Equation of state (EOS),
- Relation for diffusion-dispersion vector,
- Closure relations.

2.2.2 Continuum balance equations

We suppose that the system consists of N_p phases and N_c components. The components are considered independently of the phases, *i.e* each component is present at most in one phase. If some chemical compounds are present in two phase states of a system, then we consider the different phase states of these compounds as different components.

In the general mathematical model we take the mass balance equation for species in the current phase as the general set of governing equations:

$$\frac{\partial}{\partial t}(\phi S_\alpha \rho_\alpha X^i_\alpha) + \nabla.(\overrightarrow{j^i_\alpha} + \rho_\alpha X^i_\alpha \overrightarrow{q_\alpha}) = R^i_{\alpha,\text{mas}} + F^i_{\alpha,\text{mas}}, \tag{2.1}$$

where $i = 1,...,N_c$ denotes the component index, $\alpha = 1,...,N_p$ is the phase index, $R^i_{\alpha,\text{mas}}$ is the general species reaction term for component i (component mass in unit

volume formed by internal chemical reactions) [kg/m^3] and $F^i_{\alpha,\text{mas}}$ is the general species external source term (component mass in unit volume) [kg/m^3].

The above mass balance equation is valid for the component of phases involved in flow. But in addition to mobile components we include the components which form an immobile solid phase: $\overrightarrow{q}_s = 0$. For such components the mass balance equation can be written in the following form:

$$\frac{\partial}{\partial t}((1-\phi)\rho_s X^i_\alpha) = R^i_{s,\text{mas}} + F^i_{s,\text{mas}}. \tag{2.2}$$

In addition to the formulation in terms of conservation of mass, we may alternatively use the quantity balance equations as the general set of governing equations.

There are two variants of quantity balance equations, which differ in the sets of primary variables:

In terms of concentrations:

- mobile phases

$$\frac{\partial}{\partial t}(\phi S_\alpha c_{\alpha,i}) + \nabla.\Big(\frac{1}{M_i}\overrightarrow{j^i_\alpha} + c_{\alpha,i}\overrightarrow{q_\alpha}\Big) = R^i_{\alpha,\text{mol}} + F^i_{\alpha,\text{mol}}, \tag{2.3}$$

- immobile solid phase

$$\frac{\partial}{\partial t}((1-\phi)c_{s,i}) = R^i_{\alpha,\text{mol}} + F^i_{\alpha,\text{mol}}. \tag{2.4}$$

In terms of molar fractions:

- mobile phases

$$\frac{\partial}{\partial t}(\phi S_\alpha \rho_{\alpha,\text{mol}} x^i_\alpha) + \nabla.\Big(\frac{1}{M_i}\overrightarrow{j^i_\alpha} + \rho_{\alpha,\text{mol}} x_{\alpha,i}\overrightarrow{q_\alpha}\Big) = R^i_{\alpha,\text{mol}} + F^i_{\alpha,\text{mol}}, \tag{2.5}$$

- immobile solid phase

$$\frac{\partial}{\partial t}((1-\phi)\rho_{s,\text{mol}} x^i_\alpha) = R^i_{\alpha,\text{mol}} + F^i_{\alpha,\text{mol}}, \tag{2.6}$$

Equations (2.1, 2.2), (2.3, 2.4), (2.5, 2.6) can easily be transformed from one to another via the following list of equivalences:

$$\frac{\rho_\alpha X^i_\alpha}{M_i} = c_{\alpha,i} = \rho_{\alpha,\text{mol}} x^i_\alpha, \tag{2.7}$$

$$R^i_{\alpha,\text{mas}} = M_i R^i_{\alpha,\text{mol}}, \tag{2.8}$$

$$F^i_{\alpha,\text{mas}} = M_i F^i_{\alpha,\text{mol}}. \tag{2.9}$$

Since the considered model describes the material system in porous media, a momentum balance equation is typically reduced to two-phase form of Darcy-Muskat's law.

Since here we consider the case of an isothermal system we do not consider the energy balance equation.

2.2.3 Darcy-Muskat's law

As already mentioned, in the models of two-phase flow the momentum balance equations are reduced to the Darcy-Muskat's law, which represents the dependence of average velocity $\overrightarrow{q}_\alpha$ of the flow on the phase pressure p_α. The extended two-phase form of Darcy's law (Darcy-Muskat's law) for liquid (wetting l) and gaseous (non-wetting g) phases can be written as follow:

$$\overrightarrow{q}_\alpha = -\frac{k_{r\alpha}(S_l)}{\mu_\alpha} K(\nabla p_\alpha - \rho_\alpha \overrightarrow{g}). \tag{2.10}$$

For the description of the functional form of the dependence of relative permeability $k_{r\alpha}$ on the saturation there exist several different model.

The two widely used models are:

Van-Genuchten's model [67]:

$$k_{rl} = \sqrt{\frac{S_l - S_{lr}}{1 - S_{lr}}} \left(1 - \left(1 - \left(\frac{S_l - S_{lr}}{1 - S_{lr}}\right)^{\frac{1}{n}}\right)^m\right)^2, \tag{2.11}$$

$$k_{rg} = \left(1 - \frac{S_l - S_{lr}}{1 - S_{lr}}\right)^{\frac{1}{3}} \left(1 - \left(\frac{S_l - S_{lr}}{1 - S_{lr}}\right)^{\frac{1}{n}}\right)^{2m}, \tag{2.12}$$

where

- S_{lr} is the residual liquid saturation,
- m, n are constants, $n > 1$, $m = 1 - \frac{1}{n}$.

Brooks and Corey's model [16]:

$$k_{rl} = \left(\frac{S_l - S_{lr}}{1 - S_{lr}}\right)^{-l+1+\frac{2}{\lambda}}, \tag{2.13}$$

$$k_{rg} = \left(1 - \frac{S_l - S_{lr}}{1 - S_{lr}}\right)^b \left(1 - \left(\frac{S_l - S_{lr}}{1 - S_{lr}}\right)^{1+\frac{2}{\lambda}}\right), \tag{2.14}$$

where $l, b, \lambda > 0$ are constants.

Both models are empirical, and therefore the parameters for these velocity-saturation relationships $(m, l, b, \lambda, S_{lr})$ can be found by fitting the functional forms to experimental data.

2.2.4 Capillary pressure law

The capillary pressure p_c is the difference in pressure between two different phases.

$$p_c = p_g - p_l. \tag{2.15}$$

From physical experiments and observations, it is usually assumed that the value of the capillary pressure in a porous medium for the mixture of gas and liquid phases depends on the saturation of the liquid phase. To describe the functional form of this dependence , we can use one of the two following models:

Van-Genuchten's model [67]:

$$p_c = \frac{1}{\alpha}\Big(\Big(\frac{S_l - S_{lr}}{1 - S_{lr}}\Big)^{-\frac{1}{m}} - 1\Big)^{\frac{1}{n}}, \tag{2.16}$$

Brooks and Corey's model [16]:

$$p_c = \frac{1}{\varepsilon}\Big(\frac{S_l - S_{lr}}{1 - S_{lr}}\Big)^{-\frac{1}{\lambda}}, \tag{2.17}$$

where $\alpha, m, n, \varepsilon, \lambda$ are constants.

The parameters of the models $\alpha, m, n, \varepsilon, \lambda, S_{lr}$ can be found by fitting the functional forms to experimental data.

2.2.5 State equation

In the description of two-phase flow, the state equation relates the density of the phase ρ_α and the primary variables such as the phase pressure p_α and the mass ratio of the component X_α^i (or concentrations c_i). As in the case of the capillary pressure, this relation is usually empirical and its functional form is obtained from physical experiments and observations.

Liquid phase:

The equation of state for the liquid phase in general form can be written as:

$$\rho_l \equiv \rho_l(p_l, X_l^1, ...X_l^{N_c}). \tag{2.18}$$

In the literature, we can find more specific functional form of this equation:

- Sometimes we can suppose that the liquid phase is incompressible and then we can use the simplest form of EOS: $\rho_l = const$.
- In [62] the author proposes the following EOS for the density of the liquid phase: $\rho_l X_l^{H_2O} = const$, where $X_l^{\mathrm{H_2O}}$ is the mass ratio of H_2O in the liquid phase ($X_l^i = \frac{c_i M_i}{\rho_l}$).
- In [14] for the density of the liquid phase, the authors use a typical equation for simulation of oil reservoirs: $\rho_l = \frac{\rho_l^{std}}{B_l(p_l)}$, where $B_l(p_l)$ is the liquid formation volume factor, which is an empirical function.
- In [8] the author offers two variants of an equation of state for the liquid phase:

  1) $\rho_l \equiv \hat{\rho}_l(T,p) + \triangle\rho(T,p,X_l^{\mathrm{CO_2}}) + \triangle\rho(S)$,
  2) $\rho_{\mathrm{pure}} = \frac{\rho_1}{1 - X_l^{\mathrm{CO_2}} + \frac{X_l^{\mathrm{CO_2}}}{M_{\mathrm{CO_2}}}\rho_{\mathrm{pure}} V_\phi(T)}$,

  where ρ_{pure} is the density of pure water ($X_l^{\mathrm{CO_2}} = 0$) and $V_\phi(T)$ is the apparent molar volume of dissolved CO_2,

Gas phase:

In general, the gas phase is assumed to be a mixture of different components and instead of one equation of state we introduce the partial pressure p_i for each component of the mixture and describe its dependence from the component concentration c_i:

$p_i(c_i)$. At the same time the phase pressure is the sum of partial pressures of all gaseous components (Dalton's law):

$$p_g = \sum_{i=1}^{N_g} p_i, \tag{2.19}$$

where N_g is the number of gas components.

For the definition of the relation between partial pressure of component and its concentration we can use different models of gas:

- **Ideal gas**. For an ideal gas we get the required dependence immediately from Clapeyron law: $p_i = c_i RT$, where T is the temperature of the gas and R is the universal gas constant.
- **Peng-Robinson's model**. The dependence is obtained from Peng-Robinson equation of state [52], $p_i = \frac{c_i}{1-bc_i}RT - \frac{\alpha a c_i^2}{(1+2bc_i-b^2c_i^2)}$ where a, b are known experimental constants, α is a known experimental function of temperature.
- **Special case for** CO_2. For modelling of gas CO_2, we can use [63] where the authors propose the functional of equation of state for a wide range of temperatures and pressures. In this article they obtain the functional form of EOS from the Helmholtz energy of gas $\phi = \phi^0 + \phi^r$, where ϕ^0 corresponds to the ideal gas behavior and ϕ^r corresponds to the residual fluid behavior of CO_2.

  $$p_{CO_2}(c_{CO_2}) = c_{CO_2} RT(1 + \delta\phi^r(\delta, T)) \tag{2.20}$$

  where

  - $\delta = \frac{c_{CO_2}}{c_{CO_2,crit}}$,
  - $c_{CO_2,crit}$ is a known experimental constant,
  - $\phi^r(\delta, T)$ is a function obtained from experimental data (the exact form is given in [63]).

2.2.6 Relation for diffusion-dispersion vector

This relation describes the dependence of the diffusion-dispersion vector on the primary variables such as the phase pressure p_α and mass ratio of the component X^i_α (or concentrations c_i). At the micro-scale we know Fick's law: the diffusion-dispersion vector is proportional to the gradient of concentrations. For macroscale of the porous media, we have to use an empirical analogue of this law, sometimes replacing the component concentration c_i by mass ratio of the component X^i_α or molar ratio of the component x^i_α:

- $\overrightarrow{j^i_\alpha} = -D^i_\alpha \nabla c_i$ [28],
- $\overrightarrow{j^i_\alpha} = -\rho_\alpha \overline{D^i_\alpha} \nabla X^i_\alpha$ [8],
- $\overrightarrow{j^i_\alpha} = -\rho_{\alpha,\mathrm{mol}} \widehat{D^i_\alpha} \nabla x^i_\alpha$ [14].

where $D_\alpha^i, \overline{D_\alpha^i}, \widehat{D_\alpha^i}$ are diffusion-dispersion tensors.

In the considered literature, we have not found clear criteria saying how one can make a choice between these variants. The proposed functional forms of diffusion-dispersion vector are only approximations and are not based on specific physical laws. Therefore, often the choice is made for convenience: if the model uses concentrations as principal variables, then the diffusion-dispersion vector is assumed linearly dependent on the concentration [28].

In practice the difference between the variants is likely not very large. For example, assume that the vector is linearly dependent on the concentration gradient. From the definition of concentration we have the following identities:

$$\nabla c_i = \nabla \frac{X_\alpha^i \rho_\alpha}{M_i} = \frac{1}{M_i}\big(\rho_\alpha \nabla X_\alpha^i + X_\alpha^i \nabla \rho_\alpha\big) = \frac{\rho_\alpha X_\alpha^i}{M_i}\Big(\frac{\nabla X_\alpha^i}{X_\alpha^i} + \frac{\nabla \rho_\alpha}{\rho_\alpha}\Big). \tag{2.21}$$

In most cases, the density of the phase ρ_α varies much less than the mass fraction X_α^i so that $\frac{\|\nabla \rho_\alpha\|}{\rho_\alpha} \ll \frac{\|\nabla X_\alpha^i\|}{X_\alpha^i}$. Then we can say that the diffusion-dispersion vector is linearly dependent on the mass fraction gradient and we can suppose that the diffusion-dispersion tensors D_α^i and $\overline{D_\alpha^i}$ coincide up to a factor of proportionality $\frac{1}{M_i}$. So it is sufficient to describe only one tensor D_α^i. Usually the model developed by Young [73] is used for the description of this tensor:

$$D_\alpha^i = \phi S_\alpha \tau D_\alpha^{diff} I + d_T |\overrightarrow{q_\alpha}| I + (d_L - d_T)\frac{\overrightarrow{q_\alpha} \otimes \overrightarrow{q_\alpha^t}}{|\overrightarrow{q_\alpha}|} \tag{2.22}$$

where

- τ - tortuosity factor (measure of the irregularity of the flow paths) [-],
- D_α^{diff} - diffusion coefficient of phase α [m^2/s],
- d_L, d_T - longitudinal and transversal dispersion coefficients [m^2/s],
- $I \in \mathbb{R}^{3\times 3}$ - identity matrix.

2.2.7 Closure relations

The above relations are of physical nature. But in addition to them we have the closure relations that are directly derived from the definitions of some variables. Thus from the definitions of the saturation of phase S_α and mass ratio of component X_α^i we can obtain the following closure relations:

$$\sum_i X_\alpha^i = 1, \quad \forall \alpha, \tag{2.23}$$

$$\sum_\alpha S_\alpha = 1. \tag{2.24}$$

2.3 Model for chemistry.

2.3.1 Stoichiometry

Consider a chemical system with N_c different components and N_r chemical reactions among them:

$$\sum_{j=1}^{N_c}(\mathbb{S})_{ij}\overline{c}_j \rightleftharpoons 0 \quad i = 1,..,N_r, \tag{2.25}$$

where

- $\mathbb{S} \in \mathbb{R}^{N_r \times N_c}$ is the stoichiometric matrix,
- $\overline{c} \in \mathbb{R}^{N_c}$ is the vector of component notations.

Depending on the rate of chemical reaction we divide the set of chemical reaction into two groups: equilibrium reactions (fast rate) and kinetic (slow rate) reactions. In the considered chemical system we have N_{re} equilibrium reactions and N_{rk} kinetic reactions. In more detail the difference between two types of reactions is explained in the following subsection. According to the proposed separation of chemical reactions we can distinguish sub-matrices $\mathbb{S}_e$ (stoichiometric equilibrium matrix) and $\mathbb{S}_k$ (stoichiometric kinetic matrix) such that $\mathbb{S} = \begin{pmatrix} \mathbb{S}_e \\ \mathbb{S}_k \end{pmatrix}$ with $\mathbb{S}_e \in \mathbb{R}^{N_{re} \times N_c}$ and $\mathbb{S}_k \in \mathbb{R}^{N_{rk} \times N_c}$.

We suppose that the matrix $\mathbb{S}_e$ is a full rank matrix. This means that using linear transformations we can reduce matrix $\mathbb{S}_e$ to the following form:

$$\mathbb{S}_e = (-\mathbb{I} \mid \mathbb{S}'_e), \tag{2.26}$$

where $\mathbb{I} \in \mathbb{R}^{N_{re} \times N_{re}}$ is the identity matrix and $\mathbb{S}'_e \in \mathbb{R}^{N_c - N_{re} \times N_{re}}$.

Therefore the equations of chemical equilibrium reactions can be represented in the following way:

$$\overline{c}_{si} \rightleftharpoons \sum_{j=1}^{N_c - N_{re}} (\mathbb{S}'_e)_{ij}\overline{c}_{pj}, \quad i = 1, \ldots, N_{re}, \tag{2.27}$$

where on the left side $\overline{c}_s \in \mathbb{R}^{N_{re}}$ is the vector of components considered as the product of reaction among the components of vector $\overline{c}_p \in \mathbb{R}^{N_c - N_{re}}$ on the right side of the expression. The chemical components which are represented in vector $\overline{c}_p$ are called **primary** components, whereas those in vector $\overline{c}_s$ are called **secondary** components.

In the simulations, we consider each component in one of three different phases: mobile (liquid), fixed (solid) or gaseous. For convenience, we divide the chemical components into groups according to their phase states:

- $\overline{c}_{pl} \in \mathrm{Re}^{N_{pl}}$ is the vector of mobile primary components (liquid phase) ,
- $\overline{c}_{ps} \in \mathrm{Re}^{N_{ps}}$ is the vector of fixed primary components (solid phase),
- $\overline{c}_{sl} \in \mathrm{Re}^{N_{scl}}$ is the vector of mobile secondary components (liquid phase),
- $\overline{c}_{ss} \in \mathrm{Re}^{N_{scs}}$ is the vector of fixed secondary components (solid phase),

- $\overline{c}_{sg} \in \mathrm{Re}^{N_{scg}}$ is the vector of gas secondary components (gas phase).

The absence of gas primary components is due to the fact that we assume that gas components participate only in exchange reactions with their own liquid forms. Therefore we can always suppose that the liquid form in such reactions will be a primary component and the gas form will be secondary.

Taking into account the new notation, we can rewrite the chemical equilibrium reactions in a more detailed form:

$$\begin{pmatrix} -\mathbb{I} & 0 & 0 & \mathbb{S}_{ll} & \mathbb{S}_{ls} \\ 0 & -\mathbb{I} & 0 & \mathbb{S}_{sl} & \mathbb{S}_{ss} \\ 0 & 0 & -\mathbb{I} & \mathbb{S}_{gl} & 0 \end{pmatrix} \begin{pmatrix} \overline{c}_{sl} \\ \overline{c}_{ss} \\ \overline{c}_{sg} \\ \overline{c}_{pl} \\ \overline{c}_{ps} \end{pmatrix} \rightleftharpoons 0 \tag{2.28}$$

or

$$\begin{pmatrix} \overline{c}_{sl} \\ \overline{c}_{ss} \\ \overline{c}_{sg} \end{pmatrix} \rightleftharpoons \begin{pmatrix} \mathbb{S}_{ll} & \mathbb{S}_{ls} \\ \mathbb{S}_{sl} & \mathbb{S}_{ss} \\ \mathbb{S}_{gl} & 0 \end{pmatrix} \begin{pmatrix} \overline{c}_{pl} \\ \overline{c}_{ps} \end{pmatrix}. \tag{2.29}$$

2.3.1.1 Example

To illustrate the notations proposed above, we consider as example the chemical system of the SHPCO2 Benchmark [30].

In the SHPCO2 Benchmark we have $N_c = 10$ different chemical components. The list of components is shown in the following table:

Name of component	Phase
OH^-	Liquid
HCO_3^-	Liquid
H_2O	Liquid
H^+	Liquid
Ca^{+2}	Liquid
$CO_{2(l)}$	Liquid
$SiO_{2(l)}$	Liquid
$SiO_{2(s)}$	Solid
$CaCO_3$	Solid
$CO_{2(g)}$	Gas

The chemical components of the system participate in $N_{re} = 4$ equilibrium chemical reactions and in $N_{rk} = 1$ kinetic reactions.

Equilibrium reactions:

Hydrolysis of water:

- $OH^- - H_2O + H^+ \rightleftharpoons 0$,

$CO_{2(l)}$ dissociation:

- $HCO_3^- - H_2O + H^+ - CO_{2(l)} \rightleftharpoons 0$,

Dissolution-precipitation of calcite:

- $-H_2O + 2\,H^+ - CO_{2(l)} - Ca^{+2} + CaCO_3 \rightleftharpoons 0$,

$CO_{2(g)}$ dissociation in water:

- $CO_{2(g)} - CO_{2(l)} \rightleftharpoons 0$.

Kinetic reactions:

Dissolution-precipitation of quartz:

- $SiO_{2(s)} - SiO_{2(l)} \rightleftharpoons 0$.

For the vector of notations $\bar{c} = (OH^-, HCO_3^-, CaCO_3, CO_{2(g)}, H_2O, H^+, Ca^{+2}, CO_{2(l)}, SiO_{2(l)}, SiO_{2(s)})^T$, the stoichiometric matrices of equilibrium reactions $\mathbb{S}_e$ and kinetic reactions $\mathbb{S}_k$ take the following form:

$$\mathbb{S}_e = \begin{pmatrix} -1 & 0 & 0 & 0 & 1 & -1 & 0 & 0 & 0 & 0 \\ 0 & -1 & 0 & 0 & 1 & -1 & 0 & 1 & 0 & 0 \\ 0 & 0 & -1 & 0 & 1 & -2 & 1 & 1 & 0 & 0 \\ 0 & 0 & 0 & -1 & 0 & 0 & 0 & 1 & 0 & 0 \end{pmatrix}, \tag{2.30}$$

$$\mathbb{S}_k = \begin{pmatrix} 0 & 0 & 0 & 0 & 0 & 0 & 0 & 0 & -1 & 1 \end{pmatrix}. \tag{2.31}$$

As the vectors of primary components and secondary components we can choose the following vectors:

- $\bar{c}_p = (H_2O, H^+, Ca^{+2}, CO_{2(l)}, SiO_{2(l)}, SiO_{2(s)})^T \in \mathbb{R}^{N_c - N_{re}}$,
- $\bar{c}_s = (OH^-, HCO_3^-, CaCO_3, CO_{2(g)})^T \in \mathbb{R}^{N_{re}}$.

Then

- $\bar{c}_{pl} = (H_2O, H^+, Ca^{+2}, CO_{2(l)}, SiO_{2(l)})^T$ - sub-vector of mobile primary components,
- $\bar{c}_{ps} = (SiO_{2(s)})^T$ - sub-vector of fixed primary components,
- $\bar{c}_{sl} = (OH^-, HCO_3^-)^T$ - sub-vector of mobile secondary components,
- $\bar{c}_{ss} = (CaCO_3)^T$ - sub-vector of fixed secondary components,
- $\bar{c}_{sg} = (CO_{2(g)})^T$ - sub-vector of gas secondary components.

Thus in the presented primary and secondary components, the matrices $\mathbb{S}'_e, \mathbb{S}_{ll}, \mathbb{S}_{ls}, \mathbb{S}_{sl}, \mathbb{S}_{ss}, \mathbb{S}_{gl}$ take the following form:

$$\mathbb{S}'_e = \left(\begin{array}{ccccc|c} 1 & -1 & 0 & 0 & 0 & 0 \\ 1 & -1 & 0 & 1 & 0 & 0 \\ \hline 1 & -2 & 1 & 1 & 0 & 0 \\ \hline 0 & 0 & 0 & 1 & 0 & 0 \end{array}\right), \tag{2.32}$$

$$\mathbb{S}_{ll} = \begin{pmatrix} 1 & -1 & 0 & 0 & 0 \\ 1 & -1 & 0 & 1 & 0 \end{pmatrix}, \tag{2.33}$$

$$\mathbb{S}_{ls} = \begin{pmatrix} 0 \\ 0 \end{pmatrix}, \tag{2.34}$$

$$\mathbb{S}_{sl} = \begin{pmatrix} 1 & -2 & 1 & 1 & 0 \end{pmatrix}, \tag{2.35}$$

$$\mathbb{S}_{ss} = \begin{pmatrix} 0 \end{pmatrix}, \tag{2.36}$$

$$\mathbb{S}_{gl} = \begin{pmatrix} 0 & 0 & 0 & 1 & 0 \end{pmatrix}. \tag{2.37}$$

2.3.2 Balance equations

In order to formulate the equations of mass conservation we suppose that the considered chemical system participates in two-phase multicomponent flow and therefore we use the same mass balance equations as in the previous section. Also we make the following convention: if a component is denoted by $\overline{c}_j$, then its concentration is c_j.

For convenience we will use the balance equations in terms of concentrations:

- mobile phase ($\alpha = l, g$) (2.3)

$$\frac{\partial}{\partial t}(\phi S_\alpha c_{\alpha,i}) + \nabla.(\overrightarrow{j^i_\alpha} + c_{\alpha,i}\overrightarrow{q_\alpha}) = R^i_{\alpha,\text{mol}} + F^i_{\alpha,\text{mol}} \tag{2.38}$$

- solid phase ($\alpha = s$) (2.4)

$$\frac{\partial}{\partial t}((1-\phi)c_{s,i}) = R^i_{s,\text{mol}} + F^i_{s,\text{mol}}. \tag{2.39}$$

We suppose that the system doesn't have external sources ($F^i_{\alpha,\text{mol}} = 0$). In the considered chemical system the general species reaction term $R^i_{\alpha,\text{mol}}$ can be expressed through the rates r_j of chemical reactions:

$$R^i_{\alpha,mol} = \sum_{j=1}^{N_{re}} (\mathbb{S}_e)_{ji} r_{ej} + \sum_{j=1}^{N_{rk}} (\mathbb{S}_k)_{ji} r_{kj} \tag{2.40}$$

where r_e is the vector of rates of equilibrium reactions and r_k is the vector of rates of kinetic reactions. The chemical reaction rate describe the number of mole produced by reaction in the unit volume during the fixed period of time [mol/m^{3}s].

We now return to the question of differences between the kinetic and equilibrium reactions. As previously mentioned, the main distinction is the value of the reaction rate. This difference also causes that we use a different mathematical model for each type of reaction. In the case of kinetic reaction the rate is slow relatively to the considered time scale and therefore we can determine the reaction rate of each kinetic reaction as function of concentrations of components involved in this reaction: $r_{ki} \equiv r_{ki}(c)$. In the case of equilibrium reaction the rate is fast relatively to the considered time scale and therefore we can suppose that the components involved in equilibrium reaction are always at the equilibrium state, which is described by a special relation: the mass action

law. It also means that the reaction rate of each equilibrium reaction is an unknown function and we should eliminate the vector r_e in the balance equations (2.38), (2.39).

For convenience we rewrite the system of balance equation in vector form. For this purpose, we introduce the following notations:

- θ_α - volumetric factor, part of unit volume that is occupied by phase α ($\theta_l = S_l\phi$, $\theta_g = S_g\phi$, $\theta_s = 1-\phi$),
- $\theta \in \mathbb{R}^{N_c \times N_c}$ - volumetric matrix, diagonal matrix such that $\theta_{ii} = \theta_\alpha$ if component i is present in phase α,
- $\mathbb{M}_\alpha \in \mathbb{R}^{N_c \times N_c}$ - matrix of presence in phase, diagonal matrix such that $m_{ii} = 1$ if component is present in phase α and $m_{ii} = 0$ - otherwise.

If we order the vector of chemical components as $\overline{c} = (\overline{c}_{sl}, \overline{c}_{ss}, \overline{c}_{sg}, \overline{c}_{pl}, \overline{c}_{ps})^T$, the matrices θ, $\mathbb{M}_l$, $\mathbb{M}_g$ take the following forms:

$$\theta = \begin{pmatrix} S_l\phi\mathbb{I} & & & & \\ & (1-\phi)\mathbb{I} & & & \\ & & S_g\phi\mathbb{I} & & \\ & & & S_l\phi\mathbb{I} & \\ & & & & (1-\phi)\mathbb{I} \end{pmatrix} \tag{2.41}$$

$$\mathbb{M}_l = \begin{pmatrix} \mathbb{I} & & & & \\ & 0 & & & \\ & & 0 & & \\ & & & \mathbb{I} & \\ & & & & 0 \end{pmatrix} \tag{2.42}$$

$$\mathbb{M}_s = \begin{pmatrix} 0 & & & & \\ & \mathbb{I} & & & \\ & & 0 & & \\ & & & 0 & \\ & & & & \mathbb{I} \end{pmatrix} \tag{2.43}$$

$$\mathbb{M}_g = \begin{pmatrix} 0 & & & & \\ & 0 & & & \\ & & \mathbb{I} & & \\ & & & 0 & \\ & & & & 0 \end{pmatrix} \tag{2.44}$$

We also introduce the advection-diffusion operator for each phase ($\overrightarrow{j}_\alpha^i = \tau S_l D_\alpha \nabla c_i$ for $\alpha = l, g$ and $\overrightarrow{j}_\alpha^i = 0$ for $\alpha = s$):

- Liquid phase:

$$L_l(c) = \nabla.(c\overrightarrow{q_l}) + \nabla.(-\tau S_l D_l \nabla c), \tag{2.45}$$

- Solid phase:

$$L_s(c) = 0, \tag{2.46}$$

- Gas phase:

$$L_g(c) = \nabla.(c\overrightarrow{q_g}) + \nabla.(-\tau S_l D_g \nabla c) \tag{2.47}$$

Using the above notation we can write the set of quantity balance equations (2.38), (2.39) for each component in vector form:

$$\frac{\partial(\theta c)}{\partial t} + \mathbb{M}_l L_l(c) + \mathbb{M}_g L_g(c) = \mathbb{S}_e^T r_e + \mathbb{S}_k^T r_k. \tag{2.48}$$

As indicated previously we need to eliminate the vector of equilibrium rates r_e in balance equations (2.48)

Since $\mathbb{S}_e \in \mathbb{R}^{N_{re} \times N_c}$ is a full rank matrix and $N_{re} < N_c$, we can always find an elimination matrix $\mathbb{U} \in \mathbb{R}^{N_c - N_{re} \times N_c}$ of full rank such that $\mathbb{U}\mathbb{S}_e^T = 0$. If $\mathbb{S}_e = (-\mathbb{I}|\mathbb{S}'_e)$ then a possible choice for $\mathbb{U}$ is $\mathbb{U} = (\mathbb{S}'^T_e|\mathbb{I})$: $\mathbb{U}\mathbb{S}_e^T = (\mathbb{S}'^T_e|\mathbb{I})\begin{pmatrix} -\mathbb{I}^T \\ \mathbb{S}'^T_e \end{pmatrix} = \mathbb{S}'^T_e - \mathbb{S}'^T_e = 0$.

As an example we present the matrix $\mathbb{U}$ for the case of the chemical system (2.28).

$$\mathbb{U} = \begin{pmatrix} \mathbb{S}_{ll}^T & \mathbb{S}_{sl}^T & \mathbb{S}_{gl}^T & \mathbb{I} & 0 \\ \mathbb{S}_{ls}^T & \mathbb{S}_{ss}^T & 0 & 0 & \mathbb{I} \end{pmatrix}. \tag{2.49}$$

Multiplying (2.48) by the matrix $\mathbb{U}$ we obtain:

$$\frac{\partial(\mathbb{U}\theta c)}{\partial t} + L_l(\mathbb{U}\mathbb{M}_l c) + L_g(\mathbb{U}\mathbb{M}_g c) = \mathbb{U}\mathbb{S}_k^T r_k(c). \tag{2.50}$$

For a more explicit way of writing of the equations, we introduce the vectors of total phase concentrations $T_\alpha = \mathbb{U}\mathbb{M}_\alpha c \in \mathbb{R}^{N_c - N_{re}}$. Then the equations (2.50) can be rewritten in the following form:

$$\frac{\partial(\phi S_l T_l)}{\partial t} + \frac{\partial(\phi S_g T_g)}{\partial t} + \frac{\partial((1-\phi)T_s)}{\partial t} + L_l(T_l) + L_g(T_g) = \mathbb{U}\mathbb{S}_k^T r_k(c). \tag{2.51}$$

Thus, the resulting set of balance equation (2.51) contains N_{re} equations less than original set (2.38), (2.39).

2.3.2.1 Example

To demonstrate the algorithm for deducing the balance equations (2.51), we return to the chemical system of the SHPCO2 Benchmark, presented in section 2.3.1.1

For the vector of concentrations $c = (c_{OH^-}, c_{HCO_3^-}, c_{CaCO_3}, c_{CO_{2(g)}}, c_{H_2O}, c_{H^+}, c_{Ca^{+2}}, c_{CO_{2(l)}}, c_{SiO_{2(l)}}, c_{SiO_{2(s)}})^T$, the volumetric matrix θ, matrices of presence in the phase $\mathbb{M}_l$, $\mathbb{M}_s$,$\mathbb{M}_g$ and elimination matrix $\mathbb{U}$ take the following view:

$$\theta = \mathrm{diag}\Big(\boxed{\phi S_l,\ \ \phi S_l,}\ \boxed{1-\phi,}\ \boxed{\phi S_g,}\ \boxed{\phi S_l,\ \ \phi S_l,\ \ \phi S_l,\ \ \phi S_l,\ \ \phi S_l,}\ \boxed{1-\phi}\Big) \tag{2.52}$$

$$\mathbb{M}_l = \mathrm{diag}\Big(\boxed{1,\ \ 1,}\ \boxed{0,}\ \boxed{0,}\ \boxed{1,\ \ 1,\ \ 1,\ \ 1,\ \ 1,}\ \boxed{0}\Big) \tag{2.53}$$

$$\mathbb{M}_s = \mathrm{diag}\Big(\boxed{0,\ \ 0,}\ \boxed{1,}\ \boxed{0,}\ \boxed{0,\ \ 0,\ \ 0,\ \ 0,\ \ 0,}\ \boxed{1}\Big) \tag{2.54}$$

$$\mathbb{M}_g = \mathrm{diag}\left(\begin{array}{|c|c|c|c|c|c|c|c|c|c|}\hline 0, & 0, & 0, & 1, & 0, & 0, & 0, & 0, & 0, & 0 \\ \hline\end{array}\right) \tag{2.55}$$

$$\mathbb{U} = (\mathbb{S}_e'^T|\mathbb{I}) = \left(\begin{array}{cccc|cccccc} 1 & 1 & 1 & 0 & 1 & 0 & 0 & 0 & 0 & 0 \\ -1 & -1 & -2 & 0 & 0 & 1 & 0 & 0 & 0 & 0 \\ 0 & 0 & 1 & 0 & 0 & 0 & 1 & 0 & 0 & 0 \\ 0 & 1 & 1 & 1 & 0 & 0 & 0 & 1 & 0 & 0 \\ 0 & 0 & 0 & 0 & 0 & 0 & 0 & 0 & 1 & 0 \\ 0 & 0 & 0 & 0 & 0 & 0 & 0 & 0 & 0 & 1 \end{array}\right) \tag{2.56}$$

Thus we can find the vectors of the total phase concentrations T_l, T_g T_s for this example of chemical system:

$$T_l = \mathbb{U}\mathbb{M}_l c = \begin{pmatrix} c_{H_2O} + c_{OH^-} + c_{HCO_3^-} \\ c_{H^+} - c_{OH^-} - c_{HCO_3^-} \\ c_{Ca^{+2}} \\ c_{CO_{2(l)}} + c_{HCO_3^-} \\ c_{SiO_{2(l)}} \\ 0 \end{pmatrix} \tag{2.57}$$

$$T_s = \mathbb{U}\mathbb{M}_s c = \begin{pmatrix} c_{CaCO_3} \\ -2c_{CaCO_3} \\ c_{CaCO_3} \\ c_{CaCO_3} \\ 0 \\ c_{SiO_{2(s)}} \end{pmatrix} \tag{2.58}$$

$$T_g = \mathbb{U}\mathbb{M}_g c = \begin{pmatrix} 0 \\ 0 \\ 0 \\ c_{CO_{2(g)}} \\ 0 \\ 0 \end{pmatrix} \tag{2.59}$$

Using the obtained matrices θ, $\mathbb{M}_l$, $\mathbb{M}_s$,$\mathbb{M}_g$, $\mathbb{U}$ and the vectors T_l, T_g T_s we can write the balance equations (2.51). The resulting set of balance equation (2.51) contains $N_c - N_{re} = 6$ equations.

2.3.3 Mass action laws

In the previous section, we saw that in a chemical system such as (2.38) there are $N_c - N_{re}$ balance equations. For a complete description of the system we need N_r additional relations that describe the equilibrium among the components of equilibrium chemical reactions: mass action laws.

In addition to its concentration, each chemical component is also characterized by its chemical *activity*. For convenience, we make the following convention: we denote

the activity of component $\overline{c}_j$ by $\hat{c}_j$. For the chemical reactions (2.27) the mass action law connects the chemical activity of components in the following way:

$$\hat{c}_{si} = K_i \prod_{j=1}^{N_c - N_{re}} \hat{c}_{pj}^{(\mathbb{S}'_e)_{ij}} \quad i = 1, .., N_{re}, \tag{2.60}$$

where K_i is the equilibrium constant of the chemical reaction i. Define $\log c$ for a vector c with $c_i > 0$ by

$$(\log c)_i = \log c_i. \tag{2.61}$$

Then if we apply a logarithm to (2.60), we can rewrite it in vector form:

$$\log \hat{c}_s = \log K + \mathbb{S}'_e \log \hat{c}_p. \tag{2.62}$$

The value of chemical activity represent the real chemical potential of component in the system. This potential depends on various number of factors: temperature, pressure, concentration. To reflect such dependency from external conditions there exist different mathematical models of activity. The simple linear function form of activity of component i in general case can be represented in the following way

$$\hat{c}_i = \gamma_i z_i \tag{2.63}$$

where the meaning of z_i and γ_i depends on the phase.

For aqueous solute components:

1) γ_i is the activity coefficient, the ratio of the chemical activity of any components to its molality, concentration or molar concentration,

2) $z_i = m_i = \frac{c_l^i}{c_l^{H_2O} M_{H_2O}}$ - molality of component i in liquid phase.

For gaseous components:

1) γ_i is the fugacity coefficient, the ratio of the chemical activity of any gas component to its partial pressure,

2) $z_i = p_g^i$ is the partial pressure of the component i in the gas phase.

For mineral components:

1) γ_i is the activity coefficient,

2) $z_i = x_s^i$ is the molar ratio of the component i in the solid phase.

In the following text, for simplicity, we choose the ideal model of component activity for liquid components:

$$\hat{c}_i = c_i, \tag{2.64}$$

i.e. instead of the component activity we will use its concentration.

For solid components the usual convention is to take constant activity:

$$\hat{c}_i = 1. \tag{2.65}$$

As an example, we write the mass action laws for the case of the chemical system (2.28):

$$\begin{cases} \log c_{sl} &= \log K_{sl} + \mathbb{S}_{ll} \log c_{pl} + \mathbb{S}_{ls} \log c_{ps}, \\ \log c_{ss} &= \log K_{ss} + \mathbb{S}_{sl} \log c_{pl} + \mathbb{S}_{ss} \log c_{ps}, \\ \log c_{sg} &= \log K_{sg} + \mathbb{S}_{gl} \log c_{pl}. \end{cases} \tag{2.66}$$

where $K_{c_{sl}}, K_{c_{ss}}, K_{c_{sg}}$ are the parts of vector of equilibrium constants K which correspond to the reaction of production of liquid, solid and gaseous secondary components.

2.3.4 Final system of equations of coupled two-phase multicomponent flow and chemistry

Finally, the set of mass action laws replaces the eliminated equations in the set of balance equation (2.51). Thus for the construction of the physical model for two-phase multicomponent flow with chemical reactions, we should combine the set of balance equation, mass action laws and all additional relation required for two-phase multicomponent flow (gas phase(g), liquid phase(l)):

- Balance equations for total concentrations (2.51) - $N_c - N_{re}$ equations,
- Mass action laws (2.66) - N_{re} equations,
- Capillary pressure law (2.15) - 1 equation,
- Density state equations for liquid and gas phases - 2 equations,
- Closure relation for phase composition (2.24) - 1 equation.

In summary, the system of equations consists of $N_c - N_{re}$ partial differential equations and $N_{re} + 4$ algebraic equations.

The main unknown of the problem of two-phase multicomponent flow with chemical reactions are:

- pressures of liquid and gas phases p_l, p_g - 2 unknowns,
- saturations of liquid and gas phase S_l, S_g - 2 unknowns,
- vector of concentrations $c = \begin{pmatrix} c_{sl} \\ c_{ss} \\ c_{sg} \\ c_{pl} \\ c_{ps} \end{pmatrix}$ - N_c unknowns.

In total, the system has $N_c + 4$ unknowns for a total of $N_c + 4$ equations.

Therefore the final system can be written as follows:

$$\begin{cases} \dfrac{\partial(\phi S_l T_l)}{\partial t} + \dfrac{\partial(\phi S_g T_g)}{\partial t} + \dfrac{\partial((1-\phi)T_s)}{\partial t} + L_l(T_l) + L_g(T_g) &= \mathbb{U}\mathbb{S}_k^t r_k(c), \\ \log c_{sl} &= \log K_{c_{sl}} + \mathbb{S}_{ll} \log c_{pl} + \mathbb{S}_{ls} \log c_{ps}, \\ \log c_{ss} &= \log K_{c_{ss}} + \mathbb{S}_{sl} \log c_{pl} + \mathbb{S}_{ss} \log c_{ps}, \\ \log c_{sg} &= \log K_{c_{sg}} + \mathbb{S}_{gl} \log c_{pl}, \\ \rho_l &= \rho_l(p_l, c_{pl}, c_{sl}), \\ \rho_g &= \rho_g(p_g, c_{sg}), \\ p_c(S_l) &= p_g - p_l, \\ S_l + S_g &= 1. \end{cases} \tag{2.67}$$

2.4 An example of two-phase two-component flow (H_2O-CO_2)

2.4.1 General information

In this section we consider in detail a particular case of two-phase multicomponent flow. The considered system is partially miscible and isothermal. In this system we have two phases: liquid (l) and gas (g) and 3 chemical compounds: water (H_2O), carbon dioxide(CO_2) and salt. Water and carbon dioxide are present in both phases, salt is only present in the liquid phase. Thus in the system we have 5 components. Also in the system we have two equilibrium chemical reactions: $H_2O_{(l)} \rightleftharpoons H_2O_{(g)}$ phase exchange reaction for water component and $CO_{2(l)} \rightleftharpoons CO_{2(g)}$ phase exchange reaction for carbon dioxide component.

2.4.2 Continuum balance equations

As was already explained in subsection 2.2.2, the system of balance equation consists of mass balance equations for each component of the system. But in this system we suppose that the mass concentration of the salt, called salinity, is known. Therefore the balance equation for salt is absent and instead of a balance equation for the water component we consider the balance equation for mix of water and salt, called brine (the mass fraction of brine is equal to the sum of water mass fraction and salinity $X_l^b = X_l^{H_2O} + S$). For convenience of notation the water component in the gas phase is denoted like the brine component in gas phase ($X_g^b = X_g^{H_2O}$) and the chemical reaction of water exchange $H_2O_{(l)} \rightleftharpoons H_2O_{(g)}$ is replaced by the chemical reaction of brine exchange $\text{brine}_{(l)} \rightleftharpoons \text{brine}_{(g)}$. Thus the system of balance equations consists of 4 equations for brine component in the liquid phase,brine component in the gas phase, carbon dioxide in the liquid phase, carbon dioxide in the gas phase. Since there are two equilibrium chemical reactions in the system we perform the elimination procedure described in 2.3.2.

The elimination matrix $\mathbb{U}$ for the considered chemical system has the simple form $\mathbb{U} = \begin{pmatrix} 1 & 0 & 1 & 0 \\ 0 & 1 & 0 & 1 \end{pmatrix}$ for the concentration vector $c = \begin{pmatrix} c_{\text{brine}_l} \\ c_{CO_{2(l)}} \\ c_{\text{brine}_g} \\ c_{CO_{2(g)}} \end{pmatrix}$. Hence we obtain two balance equations that express the sum of mass balance equations in different phases for each component: brine and CO_2.

Mass balance equation for brine component:

$$\frac{\partial}{\partial t}(\phi(S_l\rho_l X_l^b + S_g\rho_n X_g^b)) + \nabla.(\overrightarrow{j_l^b} + \overrightarrow{j_g^b}) + \nabla.(\rho_l X_l^b \overrightarrow{q_l} + \rho_g X_g^b \overrightarrow{q_g}) = F^b. \tag{2.68}$$

Mass balance equation for CO_2 component:

$$\frac{\partial}{\partial t}(\phi(S_l\rho_l X_l^{CO_2} + S_g\rho_g X_g^{CO_2})) + \nabla.(\overrightarrow{j_l^{CO_2}} + \overrightarrow{j_g^{CO_2}}) + \nabla.(\rho_l X_l^{CO_2} \overrightarrow{q_l} + \rho_g X_g^{CO_2} \overrightarrow{q_g}) = F^{CO_2}. \tag{2.69}$$

2.4.3 Darcy-Muskat's law, relative permeability and capillary pressure law

In this model we use the same relations for Darcy-Muskat's law, relative permeability and capillary pressure law as in the general case of two-phase multicomponent flow (subsection 2.2.3, subsection 2.2.4).

Since here we consider the case of an isothermal system, we don't consider the energy balance equation.

2.4.4 Equation of state

Liquid phase: The form of the state equation of the liquid phase in the considered model is based on the results of articles [29] and [9] and expressed in the following form:

$$\rho_l(p_l, x_l^{\mathrm{CO}_2}, S, T) = \rho_{brine}(p_l, S, T) + \rho_{\mathrm{H_2O-CO_2}}(p_l, x_l^{\mathrm{CO}_2}, T) - \rho_{\mathrm{H_2O}}(p_l, T), \quad (2.70)$$

where

- $\rho_{brine}(p_l, S, T)$ - density of pure brine (only water and salt are presented in the liquid phase),
- $\rho_{\mathrm{H_2O-CO_2}}(p_l, x_l^{\mathrm{CO}_2}, T)$ - density of mixture of water and carbon dioxide (only water and carbon dioxide are presented in the liquid phase),
- $\rho_{\mathrm{H_2O}}(p_l, T)$ -density of pure water (only water is presented in the liquid phase).

Detailed descriptions of brine density and pure water density is given in article [9], the density of mixture of water and carbon dioxide - [29],

Gas phase:

The relation of density of the gas phase $\rho_g(p_g, T)$ in the considered model is taken from the article [63].

2.4.5 Mass action laws. Solubility model

In the considered model we have two mass action laws for the exchange reaction of brine and carbon dioxide components:

$$\begin{cases} \widehat{c}_g^{\,b} &= K_{\mathrm{H_2O}} \widehat{c}_l^{\,b} \quad \text{(Raoult's law)}, \\ \widehat{c}_g^{\,\mathrm{CO}_2} &= K_{\mathrm{CO}_2} \widehat{c}_l^{\,\mathrm{CO}_2} \quad \text{(Henry's law)}, \end{cases} \quad (2.71)$$

where $K_i(p_g, T)$ - coefficient of equilibrium for the component i.

For activity of the gas components we use the following relations:

$$\begin{aligned} \widehat{c}_g^{\,b} &= \Phi_{\mathrm{H_2O}} p_g x_g^b, \\ \widehat{c}_g^{\,\mathrm{CO}_2} &= \Phi_{\mathrm{CO}_2} p_g x_g^{\mathrm{CO}_2}, \end{aligned} \quad (2.72)$$

where $\Phi_i(p_g, T)$ is the fugacity coefficient of the component i for the CO_2-H_2O mixture.

For activity of the liquid components we use the following relations:

$$\begin{aligned} \widehat{c}_l^{\,b} &= \gamma_{\mathrm{H_2O}} x_l^b, \\ \widehat{c}_l^{\,\mathrm{CO}_2} &= \gamma_{\mathrm{CO}_2} x_l^{\mathrm{CO}_2} \end{aligned} \quad (2.73)$$

The relation (2.73) is valid only when the salinity of the liquid phase is zero ($S = 0$).

Under the condition of zero salinity we can combine the equations (2.71) with the closure relation for molar fractions and obtain the following system:

$$\begin{cases} \widehat{x}_g^b &= A\widehat{x}_l^b, \\ \widehat{x}_l^{\mathrm{CO}_2} &= B\widehat{x}_g^{\mathrm{CO}_2}, \\ \widehat{x}_g^b + \widehat{x}_g^{\mathrm{CO}_2} &= 1, \\ \widehat{x}_l^b + \widehat{x}_l^{\mathrm{CO}_2} &= 1, \end{cases} \tag{2.74}$$

where

- $A = \frac{K_{\mathrm{H_2O}}\gamma_{\mathrm{H_2O}}}{\Phi_{\mathrm{H_2O}}p_g}$ and $B = \frac{K_{\mathrm{CO_2}}\gamma_{\mathrm{CO_2}}}{\Phi_{\mathrm{CO_2}}p_g}$.

As long as we know the value of the pressure of the gas phase, the system of the algebraic equations (2.74) is closed. This means that using this system of equations we can find the component composition of each phase for any given value of pressure. The obtained system of equations is called a **solubility model**. The solution of solubility model can be represented as a vector function $\psi : \mathbb{R} \to \mathbb{R}^4$ such that

$$\psi(p_g) = \begin{pmatrix} \widehat{x}_g^b \\ \widehat{x}_g^{\mathrm{CO}_2} \\ \widehat{x}_l^b \\ \widehat{x}_l^{\mathrm{CO}_2} \end{pmatrix}. \tag{2.75}$$

Therefore we can eliminate the molar fraction of components (or their concentrations) from the list of primary variables of the final system replacing the mass action laws and the closure relation for the molar fractions by new state equation (2.75). This approach is used for example in the simulator DuMu^X.

As was already mentioned above,the obtained solubility model is valid only for the case of zero salinity. In the case when salinity is different from zero in order to find the component composition of phases we use an algorithm proposed in the article [64].

1) In a **first stage** we calculate the molar fractions for the system without salt. Denote by $\widehat{x}_l^b, \widehat{x}_g^b, \widehat{x}_l^{\mathrm{CO}_2}, \widehat{x}_g^{\mathrm{CO}_2}$ molar fractions of components for system with $S = 0$. The values of molar fractions are the solutions of the system (2.74).

2) In a **second stage** we adapt the solution for pure case to obtain the component composition for the case when $S > 0$. This stage can be divided in 4 steps:

Step 2.a: At first we calculate the molality of $\mathrm{CO_2}$ for pure case ($S = 0$):

$$\widehat{m}_{\mathrm{CO_2}} = \frac{55.508\ \widehat{x}_{\mathrm{CO_2}}}{1 - \widehat{x}_{\mathrm{CO_2}}}, \tag{2.76}$$

Step 2.b: Find the molality of $\mathrm{CO_2}$ for media with salinity S from the following equation:

$$\gamma^*(m_{\mathrm{NaCl}}, p_g, T) = \frac{\widehat{m}_{\mathrm{CO_2}}}{m_{\mathrm{CO_2}}}, \tag{2.77}$$

where $m_{\mathrm{NaCl}} = \frac{S}{0.058(X_w^b - S)}$. The actual form of coefficient γ^* can be found in [64].

Step 2.c: Transform molality of $\mathrm{CO_2}$ to molar fraction in the liquid phase:

$$x_l^{\mathrm{CO}_2} = \frac{m_{\mathrm{CO_2}}}{m_{\mathrm{CO_2}} + m_{\mathrm{NaCl}} + 55.508}, \tag{2.78}$$

Step 2.d: Calculate the molar fraction of brine component in the gas phase:

$$x_g^b = A\left(1 - x_l^{\mathrm{CO}_2} - \frac{\rho_l S}{58}\right). \tag{2.79}$$

2.4.6 Viscosity

Liquid phase:
As a model for the viscosity of the liquid phase, we take the equation given in the article [9] that represents the dependence on salinity and temperature:

$$\mu_l(S,T) = (0.1 + 0.333(S + 1.65 + 91.9))\exp(-A), \tag{2.80}$$

where $A(T)$ - known function of temperature T.

Gas phase:
As a model for the viscosity of the gas phase, we take the equation which is given in the article [27] and represents the dependence on pressure and temperature:

$$\mu_n(p_g,T) = \mu_0(T) + \Delta\mu(\rho_g(p_g,T),T). \tag{2.81}$$

2.4.7 Relation for diffusion-dispersion vector

For diffusion-dispersion vector we use the following expression:

$$\overrightarrow{j_\alpha^k} = \tau\phi S_\alpha \rho_{molar,\alpha} D_\alpha^k \nabla x_\alpha^k \tag{2.82}$$

where

- D_α^k - diffusion-dispersion tensor,
- τ - tortuosity (in our tests $\tau = 1$),
- $\rho_{molar,\alpha} = \rho_\alpha(\frac{x_\alpha^b}{0.018} + \frac{x_\alpha^{\mathrm{CO}_2}}{0.044})$ - molar density of phase α.

In our model we suppose that the dispersion is equal to 0 and therefore diffusion-dispersion tensor is isotropic.

In almost all tests we suppose that the diffusion-dispersion coefficients D_α^k for all components are constant and we take:

$$D_\alpha^k = 2\times 10^{-9}\mathrm{m}^2/\mathrm{s} \quad \forall\alpha, \ \forall k \tag{2.83}$$

2.5 One-phase reactive transport

In this section we consider in detail a simplified model of two-phase multicomponent flow - a one-phase reactive transport. The system considered in this section contains only one mobile phase - liquid phase ($S_l = 1$). Therefore the equation of the capillary pressure and the closure relation for the phase saturations disappear from the physical model of one-phase reactive transport and the phase saturations are excluded from the list of variables. We also assume that the pressure (p_l) and consequently the velocity field ($\overrightarrow{q_l}$) of the liquid phase is already known from a flow simulation. Therefore there

is no need for Darcy-Muskat's law and state equations. As in section 2.3, in the considered system we have N_c different chemical component and N_r chemical reactions: N_{re} equilibrium reactions and N_{rk} kinetic reactions.

Finally, the physical model consist of $N_c - N_{re}$ balance equations and N_{re} mass actions laws. The vector of component concentrations c is the vector of system unknowns.

2.5.1 Balance equations

Each component is in one of two different phases: mobile (liquid), fixed (solid). We divide the chemical components into the following groups:

- $\overline{c}_{pli}$ - mobile primary component,
- $\overline{c}_{psi}$ - fixed primary component,
- $\overline{c}_{sli}$ - mobile secondary component,
- $\overline{c}_{ssi}$ - fixed secondary component.

For the vector of chemical components $\overline{c} = (\overline{c}_{sl}, \overline{c}_{ss}, \overline{c}_{sg}, \overline{c}_{pl}, \overline{c}_{ps})^T$ matrices $\mathbb{S}_e$, $\mathbb{S}'_e$, $\mathbb{M}_l$, $\mathbb{M}_s$ and $\mathbb{U}$ take the following forms:

$$\mathbb{S}_e = \begin{pmatrix} -\mathbb{I} & 0 & \mathbb{S}_{ll} & \mathbb{S}_{ls} \\ 0 & -\mathbb{I} & \mathbb{S}_{sl} & \mathbb{S}_{ss} \end{pmatrix} \tag{2.84}$$

$$\mathbb{S}'_e = \begin{pmatrix} \mathbb{S}_{ll} & \mathbb{S}_{ls} \\ \mathbb{S}_{sl} & \mathbb{S}_{ss} \end{pmatrix} \tag{2.85}$$

$$\mathbb{M}_l = \begin{pmatrix} \mathbb{I} & & & \\ & 0 & & \\ & & \mathbb{I} & \\ & & & 0 \end{pmatrix} \tag{2.86}$$

$$\mathbb{M}_s = \begin{pmatrix} 0 & & & \\ & \mathbb{I} & & \\ & & 0 & \\ & & & \mathbb{I} \end{pmatrix} \tag{2.87}$$

$$\mathbb{U} = \begin{pmatrix} \mathbb{S}_{ll}^T & \mathbb{S}_{sl}^T & \mathbb{I} & 0 \\ 0 & \mathbb{S}_{ss}^T & 0 & \mathbb{I} \end{pmatrix}, \tag{2.88}$$

Thus,we can write the resulting set of balance equation which contains $N_c - N_{re}$ equations:

$$\frac{\partial(\phi T_l)}{\partial t} + \frac{(1-\phi)\partial(T_s)}{\partial t} + L_l(T_l) = \mathbb{U}\mathbb{S}_k^T r_k(c). \tag{2.89}$$

where $T_\alpha = \mathbb{U}\mathbb{M}_\alpha c$ for $\alpha = l, s$.

2.5.2 Mass action laws

The resulting set of mass action laws for one-phase reactive flow has the following form:

$$\begin{cases} \log c_{sl} &= \log K_{c_{sl}} + \mathbb{S}_{ll} \log c_{pl} + \mathbb{S}_{ls} \log c_{ps}, \\ \log c_{ss} &= \log K_{c_{ss}} + \mathbb{S}_{sl} \log c_{pl} + \mathbb{S}_{ss} \log c_{ps}, \end{cases} \tag{2.90}$$

where $K_{c_{sl}}, K_{c_{ss}}$ - the parts of vector of equilibrium constants K .

The resulting system of equations for one-phase reactive transport is combined from equations (2.89) and (2.90).

Chapter 3

Description and validation of the numerical tools

Contents

3.1 Introduction

The main objective of the third chapter is the numerical simulations of the physical models for two-phase two-component flow and one-phase reactive transport considered in the previous chapter. Construction of effective numerical simulators for these two models is a necessary first step towards the development of more complex simulator for two-phase multicomponent reactive flow.

For the simulation of two-phase two-component flow (H_2O-CO_2) we decided to use the numerical simulator DuMu^X. In the second section of this chapter, we provide a brief description of this software and in the third section give the results of simulation for several test cases which demonstrate its capabilities.

As numerical algorithm for the simulation of one-phase reactive transport, we have chosen a sequential approach which separates task of finding solution for the original problem into two subtasks: finding of chemical equilibrium and resolving of transport equations. In the fourth section we define the problem of chemical equilibrium, present its numerical simulator ChemEqLib. Performing several test cases, we verify abilities of this code.

Further, in the fifth section we consider the second sub-problem: one-phase multicomponent transport. For the numerical simulations of this problem, we create a new module which we call **1pNc** in DuMu^X. To validate the elaborated code, we perform the test case with a known analytical solution.

On the basis of numerical simulators for chemical equilibrium problem and one-phase multicomponent transport, using sequential iterative approach as numerical algorithm, we developed a new numerical simulator for one-phase reactive transport. In the final sixth section we present this new simulator and perform different validation tests.

3.2 Description of DuMu^X

DuMu^X [2] is a free and open-source simulator for flow and transport processes in porous media. It is based on DUNE [4], the Distributed and Unified Numeric Environment, a modular toolbox for solving partial differential equations with grid-based methods.

DuMu^X includes several standard models of varying complexity, ranging from stationary isothermal single-phase single-component flow to transient non-isothermal multiphase compositional flow. All models employ efficient nonlinear solvers in close combination with a sophisticated time step management. The capabilities of DUNE are heavily exploited to offer various spatial discretization schemes as well as the possibility of parallel computations.

DuMu^X is coded in C++ and employs high-level generic programming techniques. The basic principle of DuMu^X code designing is modularity. DuMu^X provides shelves of modularized objects, enabling the user to choose the appropriate parts according to the handled problem. The user is able to select each part of the implementation at each shelve through specially developed **property system**. The main shelves of this modular setup are:

- numerical schemes,

- control strategies for the simulation,
- model concepts,
- material systems: multitude of substances (components), material laws.

3.2.1 Numerical schemes.

In selection of appropriate numerical schemes, DuMu^X let us choose between two existing standard approaches for the solution of porous media problems: a coupled fully-implicit approach and a decoupled semi-implicit approach. The fully-implicit approach discretizes the original coupled balance equations by an implicit method in time. For the implicit approach DuMu^X uses one of two spatial discretization methods: cell centered finite volume method and box method which unites the advantages of the finite-volume and finite-element methods. The decoupled approach manipulates the balance equations toward one equation for the pressure and one or more mass or energy balance equations where the pressure equation is solved implicitly while the transport is solved explicitly. In comparison to a fully implicit approach, the decoupled structure allows the use of different discretization methods for different equations. The standard method used in the decoupled schemes is a cell centered finite volume method. For both the coupled fully-implicit and decoupled schemes, the linearized problem obtained after the procedure of spatial and time discretization is resolved by one of the linear solver (such as GMRES or others) implemented in DUNE.

3.2.2 Control strategies.

In DuMu^X, both the coupled fully-implicit and decoupled schemes use the same code for the time-step control: the period of simulation, at first, is divided into episodes, defined as time periods where boundary conditions, source terms are differentiable with respect to time. Then simulation time is advanced by the minimum of the time-step suggested by numerical schemes or the time span until the end of episodes. For the coupled fully-implicit schemes, the time step is controlled based on the number of iterations required by the Newton method to achieve convergence for the last time integration. For the decoupled schemes, the time-step size is calculated by CFL-like criteria.

3.2.3 Model concepts.

At the level of selection of appropriate models, for handled problem, DuMu^X provides a broad range. An overview of the currently available models is given in Table 3.1. Each model can be chosen largely independent from the problem description (exact form of material laws, components properties etc.).

coupled-fully implicit	decoupled semi-implicit
1p, 1p2c, 2p, 2pni, 2p2c, 2p2cni, 2pdfm, 2pni, 3p, 3p3c, 3p3cni, co2, co2ni, mpnc, Richards	1p, 2p, 2p2c

Table 3.1: Currently available models within DuMu^X

In the names of models in Table 3.1, the following nomenclature is used: **p** stands for phase, **c** for component and **ni** for non-isothermal. The description of each model can be found in [3].

3.2.4 Material systems.

The DuMu^X material system constitutes a framework that allows a convenient definition and usage of parameters and material laws. This framework has a modular structure and is separated into the following parts.

Components. The term component stands for constituents of the phases which can be associated with a unique chemical species or with a group of species exploiting similar physical behavior. Each component is implemented as a class consisting of member functions describing the physical properties of the component. This ranges from simple constants like molar mass to complex relationships like the density depending on pressure and temperature.

FluidSystems. A **FluidSystem** describes the properties of the participating fluid phases. This includes phase densities and viscosities as well as fugacities and diffusion coefficients of components inside phases. The properties of the fluid phases usually depend on their current composition which is described in a seperate object of type **FluidState** containing the saturation and mole fraction values. A **FluidSystem** is implemented in the same way as a component.

FluidMatrixInteractions. This module collects the material laws which describe interactions of fluid phases with the porous medium, i.e capillary pressure law and relative permeability. A collection of standard laws is provided, e.g. Van-Genuchten [67] and Brooks and Corey models [16]. Each material law uses a set of appropriately definable parameters of type **MaterialLawParams**, which may depend on the location inside the domain.

SpatialParameters. This part collects all parameters that may vary depending on the location within the porous medium. It admits a local assignment of purely intrinsic properties like porosity, permeability or heat capacity.

Up to now, DuMu^X is an academic research code and thus primarily targeted towards researchers and particularly PhD students to code, test and apply new mathematical and numerical modeling approaches. Thanks to the abstraction principles employed in the basic DUNE framework, this can be achieved without any knowledge of the underlying detailed implementations. Still, a profound knowledge of advanced C++ programming techniques is required from the current users and developers.

3.3 Two-phase two-component flow (H_2O-CO_2)

3.3.1 Implementation in Dumu^X

The physical model of two-phase two-component flow (H_2O-CO_2) was described in section 2.4. The numerical simulator for this system is already implemented in DuMu^X in the module called **CO2**. This module is based on another DuMu^X module which is

developed for more general case of two-phase two-component flow. Below we give a brief description of the main features of the modules **2p2c** and **CO2**.

The two-phase, two-component model: TwoPTwoCModel 2p2c This model implements two-phase two-component flow of two compressible and partially miscible phases $\alpha \in (l(\text{liquid phase}), g(\text{gas phase})$ composed of the two components $i \in (w(\text{water}), a(\text{air}))$ and uses fully-implicit approach. All equations are discretized using a vertex-centered finite volume (box) scheme as spatial discretization and the implicit Euler method as time discretization.

By using relations for the capillary pressure $p_c = p_g - p_l$ relative permeability $k_{r\alpha}$ and taking advantage of the fact that $S_l + S_g = 1$ and $x_l^w + x_l^a = 1$, the number of unknowns can be reduced to two. The used primary variables are either p_l and S_g or p_g and S_l. By default, the model uses p_l and S_g. In this model there is primary variable switch which can change the second primary variable depending on the phase state:

- both phases are present: saturation S_g is second primary variable as long as $0 < S_g < 1$,
- only liquid phase is present: the mole fraction of air in the liquid phase x_l^a is second primary variable as long as the maximum mole fraction is not exceeded ($x_l^a < x_{l,\max}^a$),
- only gas phase is present: the mole fraction of water in the gas phase x_g^w is second primary variable as long as the maximum mole fraction is not exceeded ($x_g^w < x_{g,\max}^w$).

The CO_2 model: CO2 The **CO2** model is derived from the 2p2c model. In the **CO2** model the phase switch criterion is different from the 2p2c model. The phase switch occurs when the equilibrium concentration of a component in a phase is exceeded, instead of the sum of the components in the virtual phase (the phase which is not present) being greater that unity as done in the **2p2c** model. The **CO2** model do not use constraint solver for calculating the mole fractions as is the case in the 2p2c model. Instead mole fractions are calculated immediately in the **FluidSystem** with a given temperature, pressure and salinity. Additionally, instead of direct calculations the values of gas phase density is computed by linear interpolation of tabulated function [63] obtained by external calculations.

3.3.2 Numerical simulations

We present four test cases showing how to use the **CO2** model of Dumu^X to simulate two-phase two-component flow (H_2O-CO_2). Because we have used the code without new developments, we do not include detailed quantitative comparisons with the original source.

3.3.2.1 Test case of Neumann, Bastian and Ippisch

Description of Test 1. The description of the first test is taken from the article [48].

In this test, CO_2 is injected into the lower part Γ_{in} of the left border of the rectangular domain 600 × 100 m with a flux of $q_{CO_2}^{in}$. The domain is located at 800 m under the

surface. Top, bottom and left (except injection zone Γ_{in}) sides of the domain have no-flux boundary conditions. For the Dirichlet boundary on the right side, we choose hydrostatic pressure for the liquid phase (3.1) and zero value for the mass fraction of CO_2 in the liquid phase.

$$p_l = p_{atm} + (h_{depth} - y)\rho_l g, \tag{3.1}$$

where h_{depth} is the depth of the bottom boundary of the domain and y is vertical coordinate counted from the level of this boundary.

At the initial time, we have only the liquid phase ($S_l = 1$), hydrostatic pressure for the entire domain (3.1) and zero mass fraction of CO_2 in the liquid phase ($X_l^{CO_2} = 0$). The size of injection zone Γ_{in} is equal to 2 m. The physical parameters for this test can be found in Table 3.2. Mesh parameters are given in Table 3.3.

Parameter	Value	Parameter	Value
ϕ	0.2	$q^{in}_{CO_2}$	4. 10^{-2} [kg/m^{2}s]
S_{lr}	0.0	S_{gr}	0.0
λ	2.0	p_e	10^3 [Pa]
K	10^{-12} [m^2]	p_{atm}	10^5 [Pa]
T	313.15 [K]	Salinity	0.0

Table 3.2: Physical parameters for the test case of Neumann et al.

Size	600 × 100 [m]
Number of elements	120 × 20

Table 3.3: Parameters of the mesh for the test case of Neumann et al.

Results of simulation. The results of this test are shown in Figure 3.1. The saturation of the gas phase is represented at 3 different periods of simulation: 7, 20, 65 days. Also in this figure the contour lines depict the molar fraction of CO_2 in the liquid phase. For comparison, at the Figure 3.2 original results obtained by Neumann et al. in [48] are presented.

In this test, the CO_2 migrates upward by buoyancy effect until it reaches the top of the domain with no-flux conditions and then is driven to the right by advective forces.

When we compare our results with those of Neumann et al. [48], we observe that the evolution of the saturation and mass fraction for CO_2 are similar, but that some differences can be seen. The shapes of the contour lines are slightly different, and the same is true for the maximum values. These differences may be related to the fact that some of the physical laws and its realization in two codes may be differ for example realization of solubility model or viscosity model . Also the mechanism of primary variable switch used in [48] does not match to those used in DuMu^X. Last and possibly the most important factor is that the exact length of injection zone Γ_{in} is not indicated [48].

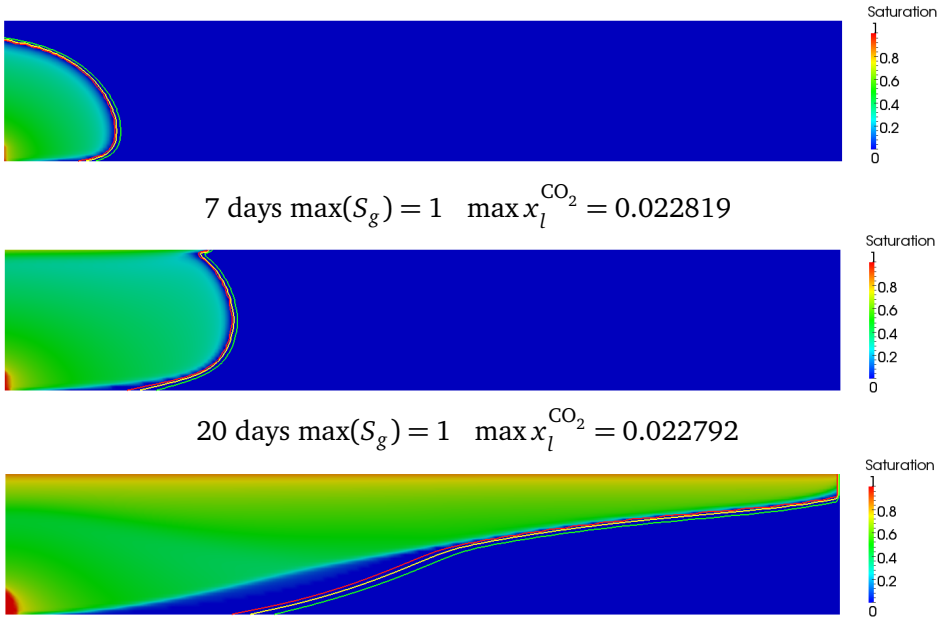

7 days $\max(S_g) = 1 \quad \max x_l^{CO_2} = 0.022819$

20 days $\max(S_g) = 1 \quad \max x_l^{CO_2} = 0.022792$

65 days $\max(S_g) = 1 \quad \max x_l^{CO_2} = 0.022$

Figure 3.1: Results of simulation. CO_2 saturation and molar fraction of dissolved CO_2 in the liquid phase (contour lines for $x_l^{CO_2} = 0.05, 0.011, 0.016$).

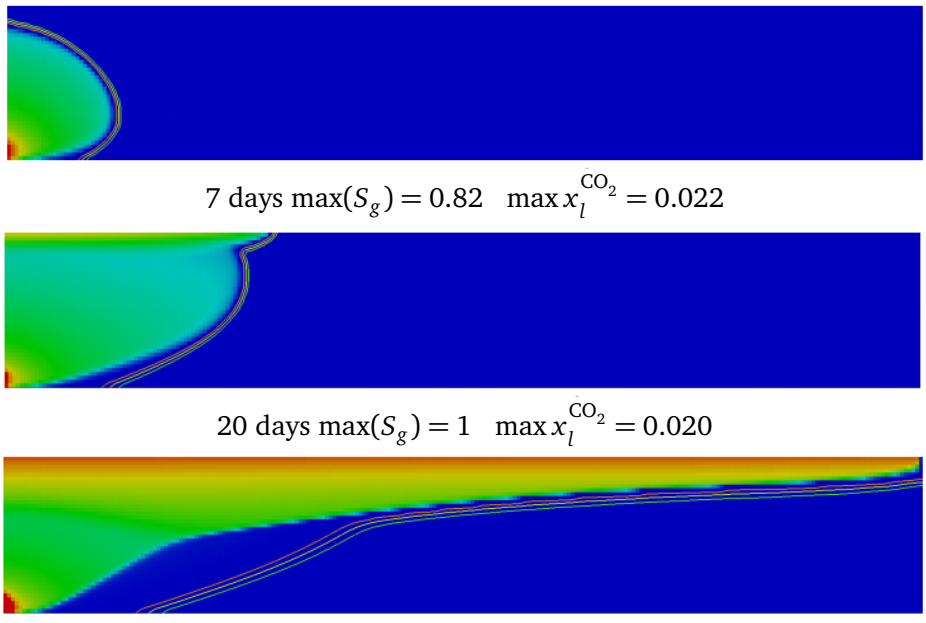

7 days $\max(S_g) = 0.82 \quad \max x_l^{CO_2} = 0.022$

20 days $\max(S_g) = 1 \quad \max x_l^{CO_2} = 0.020$

65 days $\max(S_g) = 1 \quad \max x_l^{CO_2} = 0.020$

Figure 3.2: Neumann et al. results. CO_2 saturation and molar fraction of dissolved CO_2 in the liquid phase (contour lines for $x_l^{CO_2} = 0.05, 0.011, 0.016$).

3.3.2.2 Test case of Bielinski (bottom Injection)

Description of Test 2. The description of the second test is taken from [8]. In this test, we consider a rectangular domain 3000 × 1000 m. The domain is located at 1500 m under the surface. The model domain contains two different sub-domains Ω_1 at the top and the bottom and Ω_2 in between. Ω_2 is a thick layer with low value of permeability that prevents the carbon dioxide from rising towards the surface. Top and almost all bottom of the domain have no-flux boundary conditions. The left and the right parts are Dirichlet boundaries with hydrostatic pressure (3.1) and zero condition for CO_2 mass fraction in the liquid phase $X_l^{CO_2} = 0$. At the central part of the bottom boundary there is time limited injection of CO_2 ($q^{in}_{CO_2}$).

Initially we have only the liquid phase ($S_l = 1$), hydrostatic pressure for the entire domain (3.1) and zero mass fraction of CO_2 in the liquid phase ($X_l^{CO_2} = 0$). The physical parameters are given in Table 3.4. The geometry of the domain is shown in Figure 3.3. The domain is discretized by a mesh of 150 × 50 elements.

Parameter	Value	Parameter	Value
ϕ	0.2	$q^{in}_{CO_2}$	0.02 [kg/m^{2}s] if $t < 40$ days and 0 otherwise
S_{lr}	0.2	S_{gr}	0.05
λ	2.0	p_e	10^3 [Pa]
K_{Ω_1}	10^{-12} [m^2]	K_{Ω_2}	10^{-14} [m^2]
T	303.15 [K]	Salinity	0.25

Table 3.4: Physical parameters for bottom injection test.

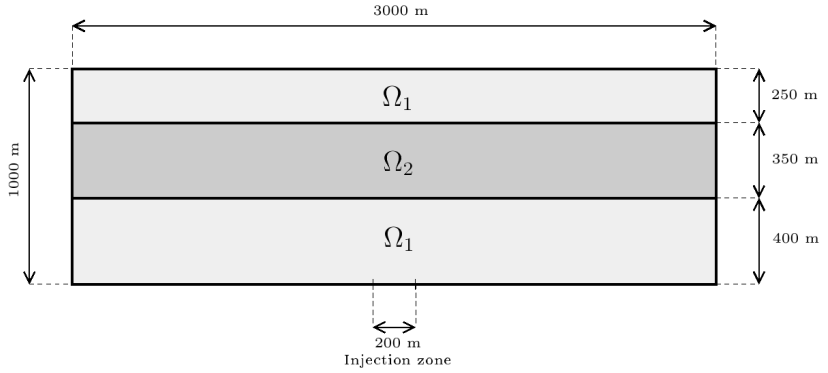

Figure 3.3: Geometry of the domain for bottom injection test.

Results of simulation. The saturation of the gas phase is represented in Figure 3.4 at different times of the simulation: 1, 10, 100 years of simulation. In this figure we see how CO_2 enters the domain from below and migrates upward by the influence of flow induced by injection and the influence of gravity (buoyancy effect) until it hits the layer of low permeability. It penetrates the layer, but quickly stops moving, because the residual saturation is reached and no more CO_2 flows into the domain.

The distribution of CO_2 in the liquid phase is represented in Figure 3.5. In this figure we see that the movement of the carbon dioxide in the liquid phase almost coincides with the movement of the gas phase. But at $t = 100$ years we find that under the influence of gravity the liquid phase saturated by CO_2 starts to fall due to its higher density than unsaturated liquid phase.

The obtained results are not exactly the same as those given in [8] but basic tendencies observed in the flow coincide. The observed difference can be explained by difference in undetermined physical properties of the test case. For example form of Henry's and Raoult's laws, viscosity model, state equations of densities are not given in [8]. But despite this we can conclude that the basic tendencies observed in the flow coincide.

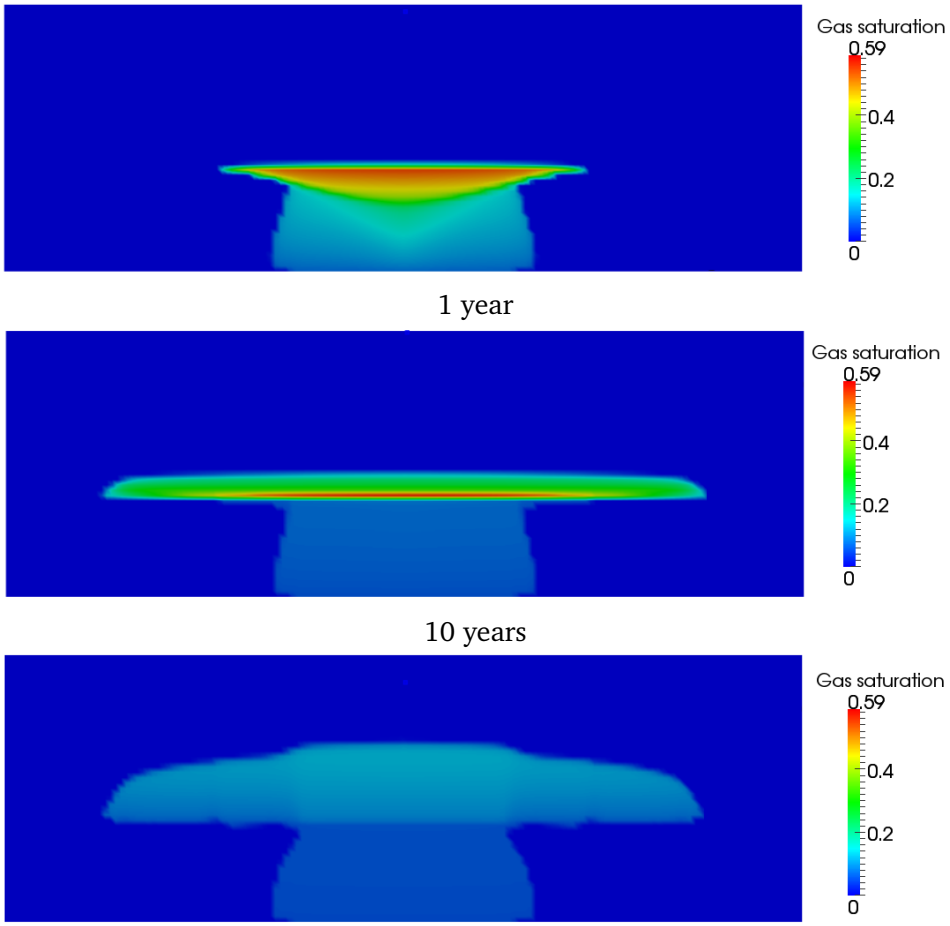

Figure 3.4: Saturation of the gas phase for bottom injection test.

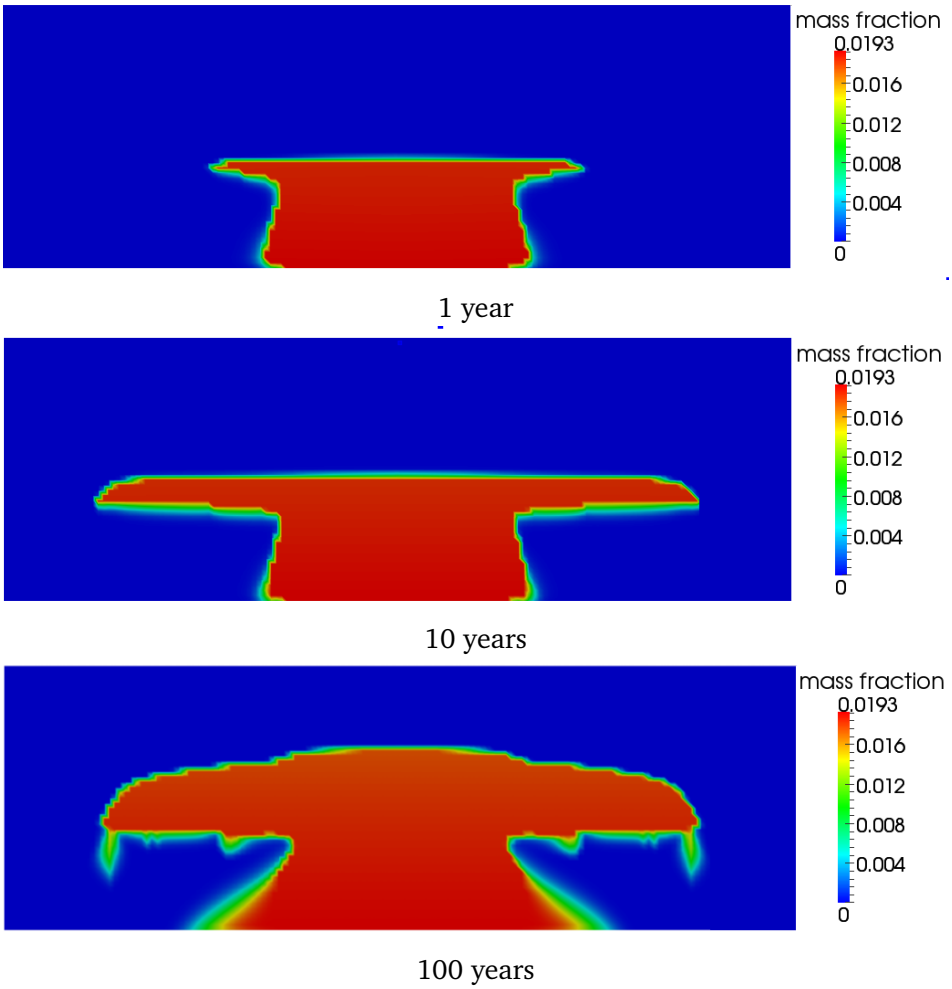

Figure 3.5: Mass fraction of CO_2 in the liquid phase for bottom injection test.

3.3.2.3 Test case of Bielinski (fingering)

Description of Test 3. The description of the third test is again taken from [8]. In this test we consider a rectangular domain of size 50 m×20 m. The domain is located at 1500 m under the surface. Bottom, right and left sides of the domain have no-flux boundary conditions. For the Dirichlet boundary on the top side, we have hydrostatic pressure for the liquid phase and 5 % value for the gas phase saturation. Initially we have two layers in the domain with different physical parameters. In the top layer both phases are present, the saturation of the gas phase equals 5 %. In the bottom layer there is only the liquid phase, the mass fraction of CO_2 in the liquid phase is zero ($X_l^{CO_2} = 0$). Also we set hydrostatic pressure for the entire domain at the initial time. The physical parameters are given in Table 3.5. The domain is discretized by a mesh of 100 × 40 elements. The length of mesh element equals 0.3125 m.

Parameter	Value	Parameter	Value
ϕ	0.2	thickness of top layer	5 [m]
S_{lr}	0.2	S_{gr}	0.05
λ	2.0	p_e	10^3 [Pa]
K	10^{-12} [m^2]	p_{atm}	10^5 [Pa]
T	303.15 [K]	S	0.0

Table 3.5: Physical parameters for fingering test .

Results of simulation. The distribution of carbon dioxide in the liquid phase obtained in our simulations is represented in Figure 3.6 after two years of simulated time.

The density of the water saturated by CO_2 is higher then the density of the pure water. This difference under influence of gravity force creates the instability in the domain. Numerical errors of solver (round-off, accuracy etc.) break unstable equilibrium state of the system and caused the movement called fingering.

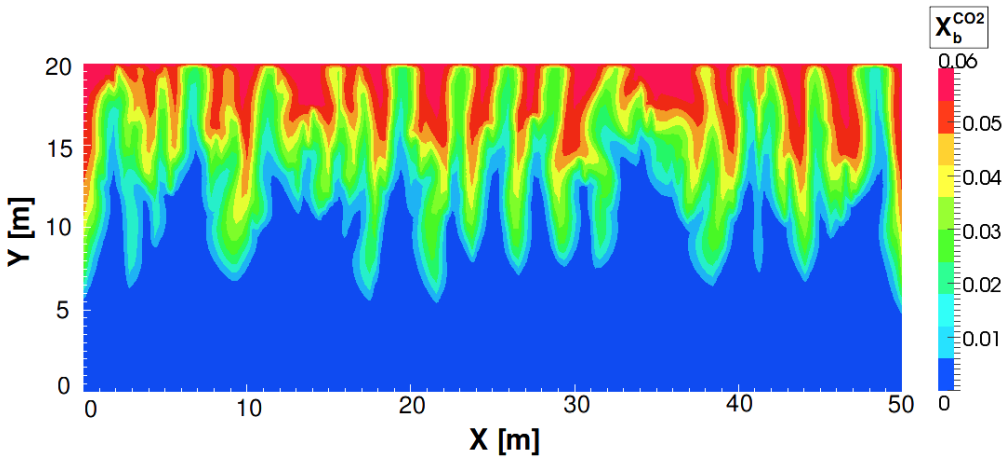

Our results

Figure 3.6: Fingering caused by density differences: the value of mass fraction of dissolved CO_2 in the liquid phase after 2 years of simulation.

3.3.2.4 Test case of Class et al. (leaky well)

Description of Test 4. The fourth test is an adaptation of a three-dimensional test described in [22] to two-dimension. In this test we consider a rectangular domain 201 m×160 m. The domain is located at 800 m under the surface. The model domain contains three different sub-domains with different values of physical parameters: Ω_1 at the top and the bottom, Ω_2 in between and Ω_3. Ω_2 is the impermeable layer that prevents the carbon dioxide from rising towards to surface. Ω_3 is a thin vertical pipe with high permeability located in the center of the domain and crossing the entire area (see Figure 3.7). The top and the bottom of the domain have no-flux boundary conditions. For the Dirichlet boundary on the right and left side we have hydrostatic pressure for the liquid phase and $X_l^{CO_2} = 0$. CO_2 is injected in a zone at the left side of the bottom layer at the rate $q^{in}_{CO_2}$.

Initially, we have only the liquid phase ($S_l = 1$), hydrostatic pressure for the entire domain (3.1) and zero mass fraction of CO_2 in the liquid phase ($X_l^{CO_2} = 0$). The physical parameters of the test can be found in Table 3.6. The geometry of the layers is described in Table 3.7. The domain is discretized by a mesh of 201 × 160 elements.

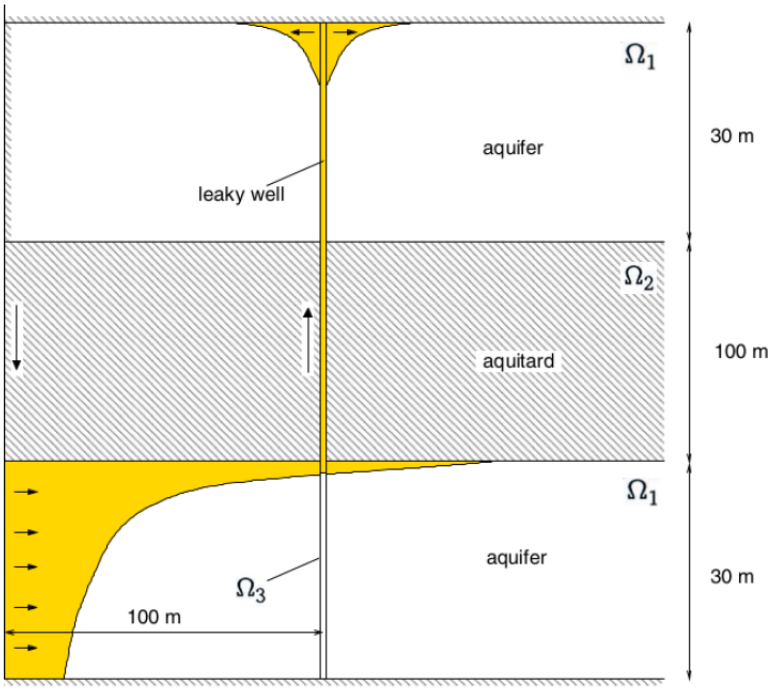

Figure 3.7: Geometry of the domain for leaky well test (taken from [22]).

Results of simulation. The results of this test are shown in Figure 3.8. The saturation of the gas phase is represented at 3 different periods of simulation: 100, 150, 200 days. The CO_2 migrates upward by buoyancy effect until it reaches the impermeable layer Ω_2 and then moves to the right by advective forces. Then CO_2 comes to the tube Ω_3 and moves to the top of domain. Finally, carbon dioxide reaches the top of the domain with noflux condition and under the influence of advection moves to the left or right side of

Parameter	Value	Parameter	Value
ϕ	0.15	$q^{in}_{CO_2}$	4.708 10^{-4} [kg/m^{2}s]
S_{lr}	0.2	S_{gr}	0.05
λ	2.0	p_e	10^4 [Pa]
K_{Ω_1}	10^{-14} [m^2]	K_{Ω_2}	10^{-21} [m^2]
K_{Ω_3}	10^{-12} [m^2]		
T	303.15 [K]	S	0.25

Table 3.6: Physical parameters for leaky well test.

Size	201 × 160 [m]
Thickness of bottom layer	30 [m]
Thickness of middle layer	100 [m]
Thickness of top layer	30 [m]
Diameter of tube Ω_3	1 [m]

Table 3.7: Parameters of the mesh for leaky well test.

the domain.

The obtained results are difficult to compare with results presented in [22] since our simulations are only two-dimensional adaptation of three dimensional test case and thus we can not observe the effects caused by existence of the additional dimension. But despite this, we can observe that the main tendencies in spreading of injected carbon dioxide gas are similar and have the identical time scale.

3.3.3 Summary

In this section we have realized four different test cases for the two-phase two-component H_2O-CO_2 flow. Performing these tests we verify the capabilities of DuMu^X simulator. The principle studies were set up the CO_2 flow in the subsurface on different time and space scales. Summarizing the obtained results we can conclude that:

- The **2p2c** module in Dumu^X gives us all the necessary tools to define the geometric parameters of numerical tests, to describe the types of boundary and initial conditions, to use the different variants of physical laws of model (Henry's and Raoult's laws, state equations).

- The results obtained on these test cases show behavior consistent with what is theoretically expected.

- Comparison of our results with the results obtained by other authors shows that DuMu^X simulator is capable to demonstrate the similar evolution of two-phase two-component flow as other numerical simulators.

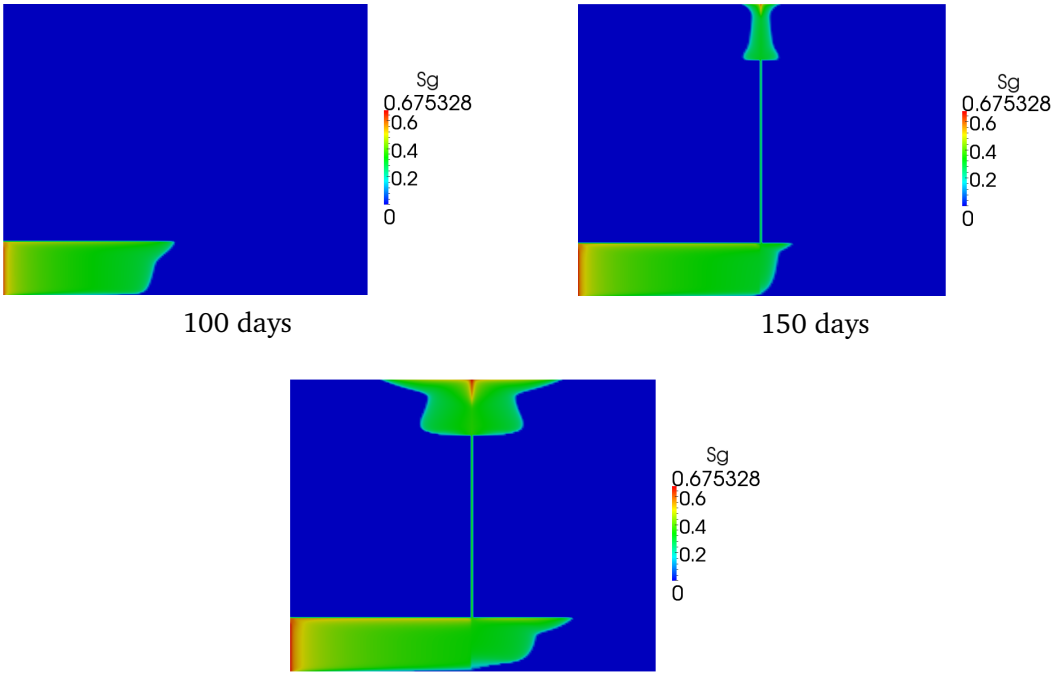

Figure 3.8: Saturation of the gas phase for leaky well test.

3.4 Chemistry

3.4.1 Resolution of chemical equilibrium systems

3.4.1.1 System of equations

In the previous chapter we derived the system of equations of coupled two-phase multicomponent flow (2.67). The solution of this system gives the evolution of the concentration of the components as a function of time. In this section, we consider the case of a closed chemical system, i. e. we want to find the solutions of chemical equilibrium for given values of the total concentrations. For this case, the balance equation for total concentration is used to fix a linear combination of the component concentrations. The final system of equations is obtained by combining these mass balance equations with the mass action laws:

$$\begin{cases} \log \hat{c}_{sl} &= \log K_{sl} + \mathbb{S}_{ll} \log \hat{c}_{pl} + \mathbb{S}_{ls} \log \hat{c}_{ps}, \\ \log \hat{c}_{ss} &= \log K_{ss} + \mathbb{S}_{sl} \log \hat{c}_{pl} + \mathbb{S}_{ss} \log \hat{c}_{ps}, \\ \log \hat{c}_{sg} &= \log K_{sg} + \mathbb{S}_{gl} \log \hat{c}_{pl}. \\ \mathbb{U}\theta c &= \begin{pmatrix} \phi S_l \mathbb{S}_{ll}^T c_{sl} + (1-\phi)\mathbb{S}_{sl}^T c_{ss} + \phi S_g \mathbb{S}_{gl}^T c_{sg} + \phi S_l c_{pl} \\ \phi S_l \mathbb{S}_{ls}^T c_{sl} + (1-\phi)\mathbb{S}_{ss}^T c_{ss} + (1-\phi) c_{ps} \end{pmatrix} = \overline{T} = \phi S_l T_l + T_s + \phi S_g T_g. \end{cases} \tag{3.2}$$

where $\mathbb{U}$ is the elimination matrix defined previously in section 2.3.2.

The obtained system of equations (3.2) are closed and have the set of unknowns consisting of component concentrations $c = \left(c_{sl},\ c_{ss},\ c_{sg},\ c_{pl},\ c_{ps}\right)^T$, while the values of vector of total concentration $\overline{T}$ and vector of equilibrium constants $K = \left(\ K_{sl},\ K_{ss},\ K_{sg}\right)^T$ are given. Thus we have a system of equations with N_c unknowns and with N_c equa-

tions.

The system of equations (3.2) is nonlinear and the existence and uniqueness of solution isn't proven in the general case. But for special cases of two-phase system (liquid and solid) there are results [36] that demonstrate the existence of solutions for such system of equations.

3.4.1.2 Solution method

Types of chemical reactions The proposed formulation of chemical equilibrium problem can involve both homogeneous (aqueous complexation) and heterogeneous reactions (mineral dissolution/precipitation and ion exchange).

Homogeneous reactions involve only the liquid phase. Relations between components activities are expressed by mass action laws

$$(\log \hat{c}_{sl})_i = (\log K_{sl})_i + (\mathbb{S}_{ll} \log \hat{c}_{pl})_i. \tag{3.3}$$

For the sake of simplicity, we assume that all components of homogeneous reactions have ideal activity, and do not take into account the correction term ($\hat{c}_i = c_i$).

Heterogeneous reactions in contrast define the inter-phase chemical interactions and contain both solid and liquid or gas components.

Heterogeneous ion exchange reactions can involve different solid components. In a similar way to homogeneous reactions the component activities are coupled by mass action laws

$$(\log \hat{c}_{ss})_i = (\log K_{ss})_i + (\mathbb{S}_{sl} \log \hat{c}_{pl})_i + (\mathbb{S}_{ss} \log \hat{c}_{ps})_i. \tag{3.4}$$

The activity model of solid components involved in ion exchange reaction has a complex physical basis, but for simplicity further in this work we use for such solid component the same ideal activity model as for the liquid components.

Heterogeneous precipitation-dissolution reactions describe the interaction of one solid component (mineral) with the set of liquid components. The presence of these reactions in a chemical system adds the following difficulty: it is in general not known a priori which of the minerals are present in the system and which are completely dissolved. The presence of a mineral means that the liquid phase is saturated with respect to the corresponding precipitation-dissolution reaction and the activities of the involved components in the reaction are coupled by

$$(\hat{c}_{ss})_i = (\log K_s s)_i + (\mathbb{S}_{sl} \hat{c}_{pl})_i. \tag{3.5}$$

If the liquid phase is undersaturated, then the corresponding mineral is fully dissolved and its concentration is equal zero: $(\hat{c}_{ss})_i = 0$. The condition for liquid phase saturation will be given later.

From the above brief description of chemical reaction types we can conclude that basic aspects of modeling (mass action law, activity) for homogeneous and ion exchange reaction are similar. In contrast for the description of precipitation-dissolution reactions, we should introduce additional conditions which define whether the liquid phase is saturated or not. For this reason, first, we consider the process of finding solutions of chemical equilibrium for a chemical system that contains only homogeneous and ion exchange reactions. The algorithm used for precipitation-dissolution reactions will be detailed later.

System of homogeneous and ion exchange reactions. As stated above, we assume that liquid and solid components involved in homogeneous and ion exchange reactions have the same ideal activity model. This implies that the mass action laws of chemical reactions provide an explicit expression for the concentrations of secondary components $\left(c_{sl},\ c_{ss}\right)^T$ in terms of primary component concentrations $\left(c_{pl},\ c_{ps}\right)^T$:

$$\begin{pmatrix} c_{sl} \\ c_{ss} \end{pmatrix} = \begin{pmatrix} e^{(\log K_{sl} + \mathbb{S}_{ll} \log c_{pl})} \\ e^{(\log K_{ss} + \mathbb{S}_{sl} \log c_{pl} + \mathbb{S}_{ss} \log c_{ps})} \end{pmatrix}, \tag{3.6}$$

where we use the convention that $(e^c)_i = e_i^c$.

The total concentrations of primary component of considered chemical system is given by following formula:

$$\begin{pmatrix} \overline{T}_{pl} \\ \overline{T}_{ps} \end{pmatrix} = \begin{pmatrix} \phi c_{pl} + \phi \mathbb{S}_{ll}^T c_{sl} \\ \phi c_{ps} + \phi \mathbb{S}_{sl}^T c_{sl} + (1-\phi)\mathbb{S}_{ss}^T c_{ss} \end{pmatrix}. \tag{3.7}$$

Lumping all the terms into the right hand side of (3.7), we can construct the following linear function F:

$$F(c_{sl}, c_{ss}, c_{pl}, c_{ps}) = \begin{pmatrix} \overline{T}_{pl} \\ \overline{T}_{ps} \end{pmatrix} - \begin{pmatrix} \phi c_{pl} + \phi \mathbb{S}_{ll}^T c_{sl} \\ \phi c_{ps} + \phi \mathbb{S}_{sl}^T c_{sl} + (1-\phi)\mathbb{S}_{ss}^T c_{ss} \end{pmatrix} = 0 \tag{3.8}$$

Using the explicit dependence of secondary component concentrations from primary component concentrations (3.6), we can eliminate the secondary components from (3.6) to obtain a new nonlinear function, which depends only on primary component concentrations:

$$\overline{F}(c_{pl}, c_{ps}) = F(e^{(\log K_{sl} + \mathbb{S}_{ll} \log c_{pl}}, e^{(\log K_{ss} + \mathbb{S}_{sl} \log c_{pl} + \mathbb{S}_{ss} \log c_{ps})}, c_{pl}, c_{ps}) \tag{3.9}$$

Thus, the solution of chemical equilibrium of the system with homogeneous and ion exchange reactions for given values of the total concentrations can be found by solving the nonlinear system of equation:

$$\overline{F}(c_{pl}, c_{ps}) = 0. \tag{3.10}$$

Instead of primary component concentrations, we use the logarithms of concentrations as variables of system (3.10). The new variables provide better scaling of values in the solution vector and guarantee positivity of component concentrations. For solving system (3.10), we use a variant of Newton's method and its modifications [54].

Systems with mineral components. In this paragraph we describe the algorithm for finding the chemical equilibrium for a system of reduced complexity without homogeneous and ion exchange reactions. For this we consider a chemical system that contains N_s minerals and N_l liquid components. We also assume that all reactions are mineral precipitation equilibrium reactions, one for each component. As primary components we choose all liquid components (c_{pl}), as secondary - minerals ($c_{ss,\text{mineral}}$). The system of chemical reaction in this case can be written in the following way:

$$\overline{c}_{ss,\text{mineral}} \rightleftharpoons \mathbb{S}_{sl,\text{mineral}} \overline{c}_{pl} \tag{3.11}$$

Then the total concentrations of primary liquid component can be found from the following formula:

$$\overline{T}_{pl} = \phi c_{pl} + (1-\phi)\mathbb{S}^T_{sl,\text{mineral}} c_{ss,\text{mineral}} \tag{3.12}$$

If it is known that no complete dissolution of minerals takes place, then the equilibrium conditions can be expressed by the mass action laws with ideal activities for liquid components and constant activity (set to unity) for the minerals:

$$0 = (\log K_{ss,\text{mineral}})_j + (\mathbb{S}_{sl,\text{mineral}} \log c_{pl})_j, \quad j = 1,..,N_s. \tag{3.13}$$

or $E(c_{pl})$ where

$$E(c_{pl}) := -\log K_{ss,\text{mineral}} - \mathbb{S}_{sl,\text{mineral}} \log c_{pl}, \tag{3.14}$$

under condition of positive primary liquid component concentrations.

Condition (3.13), expressing saturation of the fluid with respect to the corresponding reaction, has only to be fulfilled if the corresponding mineral is present,i.e., when $(c_{ss,\text{mineral}})_j > 0$.

Also we cannot exclude the possibility that the fluid is undersaturated and the mineral j fully dissolved, i.e.

$$E_j(c_{pl}) = (-\log K_{ss,\text{mineral}})_j - (\mathbb{S}_{sl,\text{mineral}} \log c_{pl})_j \geq 0 \quad \text{and} \quad (c_{ss,\text{mineral}})_j = 0. \tag{3.15}$$

A general unified formulation for the saturated and the unsaturated situation can be expressed as a nonlinear system of complementarity conditions [37]:

$$(E(c_{pl}) = 0 \text{ and } c_{ss,\text{mineral}} \geq 0) \quad \text{or} \quad (E(c_{pl}) \geq 0 \text{ and } c_{ss,\text{mineral}} = 0). \tag{3.16}$$

where all inequalities are to be understood componentwise. A well known solution strategy for problem (3.16) and (3.12) (proposed by [13] and used in ChemEqLib is to make an assumption as to which subset of minerals is present, and to solve only the corresponding equations from (3.16) together with (3.12) by finding a root of nonlinear vector function $G(c_{pl}, c_{ss,\text{mineral}})$ such that

$$G = \begin{pmatrix} G_1 \\ G_2 \end{pmatrix} : \mathbb{R}^{N_l+N_s} \longrightarrow \mathbb{R}^{N_l+N_s} \tag{3.17}$$

where

$$G_1 = T_{pl} - \phi c_{pl} - (1-\phi)\mathbb{S}^T_{sl,\text{mineral}} c_{ss,\text{mineral}} \tag{3.18}$$

and

$$(G_2)_j = E_j(c_{pl}) \text{ if mineral } j \text{ is present} \quad \text{or} \quad (G_2)_j = (c_{ss,\text{mineral}})_j \text{ if mineral } j \text{ is dissolved.} \tag{3.19}$$

In contrast to (3.10) in the system of equation

$$G(c_{pl}, c_{ss,\text{mineral}}) = 0 \tag{3.20}$$

the concentration of secondary components $c_{ss,\text{mineral}}$ are not eliminated from the list of system variables. Also the component concentrations in system (3.20) can not be replaced by its logarithms for the reason that zero or negative values are possible for mineral components [61]. The obtained solution of (3.20) should be checked if it is physical or not. If not (concentration of some minerals are negative or liquid phase is oversaturated), then the assumption must be modified following certain heuristic rules and the computation must be repeated until a physical solution is found. The scheme of this algorithm is shown in Figure 3.9.

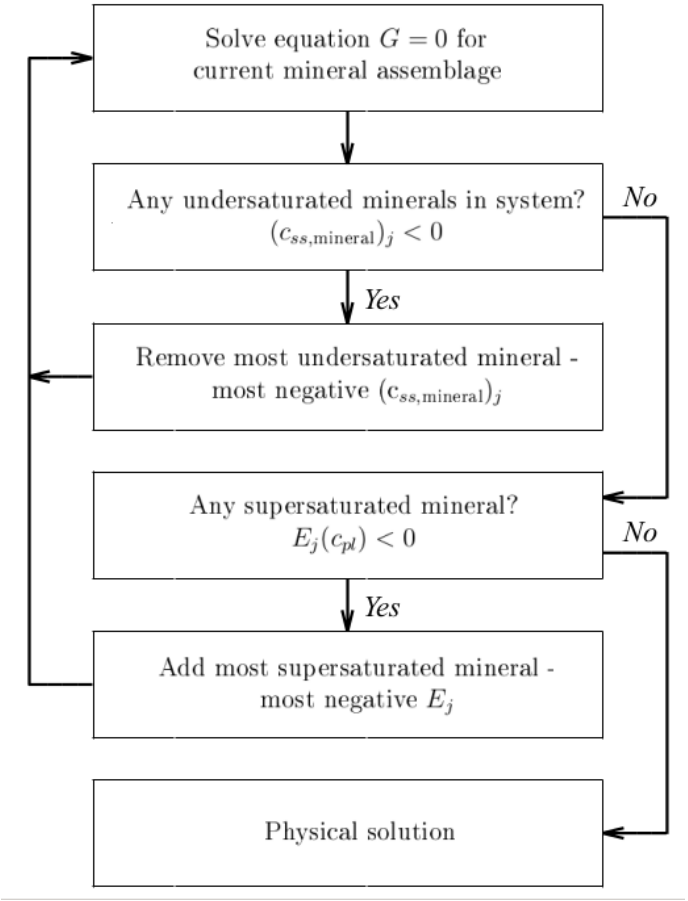

Figure 3.9: Procedure of finding the physical solution in a chemical system with mineral components (taken from [13]).

The main disadvantages of this strategy is that one nonlinear system must be solved several times for each mineral configuration. Although there is no proof that this procedure converges, in practice it was found to be efficient. A more rigorous method, based on semi-smooth Newton method, has been proposed by S. Kräutle [37] (but it was not been yet implemented in our code).

3.4.1.3 Software

As software for our simulations we use code the ChemEqLib realised in C++ language by Michel Kern [1]. For description of the chemical system with this code we use two input files:

- **nameofproblem.pot** - in this file we describe the stoichiometric part of the problem: number of each type of components, the set of primary and secondary components, chemical reactions and their equilibrium constants.
- **nameofproblem.exp** - in this file we indicate the value of vector of total concentrations T.

From this input data, the program construct the function $\overline{F}$ (3.10) or G in (3.20). Then using tools from the library GNU Scientific Library (GSL) [6] for multidimensional root-

finding for nonlinear system of equations, the program finds the root of the equation by Newton's method. Also there is external loop for the case with precipitated components which gives the opportunity to define if precipitated component should be active or not.

3.4.2 Verification examples

For verification of the ChemEqLib code we complete three different tests. For each test we give the information about the chemical system in the form of **Morel's tableau** [47]. Also we add the values of the vector T in this table and indicate the concentrations of all components as result of calculations.

3.4.2.1 Ion exchange "ex11"

Description of Test 1. For the first test we take a system with 6 components and 2 chemical reactions from [17]. The Morel's tableau of this chemical system is given in Table 3.8. In this table we also indicate the value of the total concentrations.

	K^+	Ca^{2+}	Al^{3+}	KX	$\log K$
K^+	1	0	0	0	0
Ca^{2+}	0	1	0	0	0
Al^{3+}	0	0	1	0	0
KX	0	0	0	1	0
CaX_2	-2	1	0	2	0.81
AlX_3	-3	0	1	3	0.125
Total conc.	$-1\cdot10^{-2}$	$3\cdot10^{-3}$	$2\cdot10^{-3}$	$1.2\cdot10^{-2}$	

Table 3.8: Parameters for ions exchange test.

Results of simulation. In this test case we suppose that all components have the same ideal model of activity. Therefore the vector of variable of the function $\overline{F}$ (3.10) consists only of concentrations of primary components: K^+, Ca^{2+}, Al^{3+}, KX. In Table 3.9 we give the value of their concentrations and compare our results with J. Carrayrou's results [17]. From this comparison we can see that the results are identical. Also we compare the efficiency of different methods of root finding. In Table 3.10 we indicate the number of iterations which is necessary for convergence of the different methods where "**newton**" corresponds to Newton's Method (the standard root-finding algorithm

Name of component	Concentration(our solution)	Carrayrou's solution
K^+	$7.637\cdot10^{-4}$	$7.637\cdot10^{-4}$
Ca^{2+}	$1.674\cdot10^{-4}$	$1.674\cdot10^{-4}$
Al^{3+}	$3.005\cdot10^{-4}$	$3.005\cdot10^{-4}$
KX	$1.237\cdot10^{-3}$	$1.237\cdot10^{-3}$

Table 3.9: Solution of ions exchange test.

Method	Number of iterations
newton	7
hybridj	16
hybridsj	16

Table 3.10: Convergence of ions exchange test.

without globalization), "**hybridsj**" is a modified version of Powell's Hybrid method, "**hybridj**" is an unscaled version of "hybridsj" method.

More detailed description of these multidimensional root-finding methods are given in the documentation of the GSL library [5]. All root-finding methods used in our simulations are iterative. Thereby for each of these algorithms we should define initial approximation of solution (initial point). In preliminary tests, we found out that the most effective variant of initial component concentrations is the concentration equal to the total concentration. Thus in this and following tests in this section we use the vector of total concentrations as initial approximation.

3.4.2.2 Galic acid

Description of Test 2. For the second test we take a more complex system with 17 components and 14 chemical reactions [17]. The Morel's tableau of this chemical system is given in Table 3.11. In this table we also indicate the value of total concentrations.

	H^+	Al^{3+}	H_3L	Log K
H^+	1	0	0	0
Al^{3+}	0	1	0	0
H_3L	0	0	1	0
OH^-	-1	0	0	-14
H_2L^-	-1	0	1	-4.15
HL^{2-}	-2	0	1	-12.59
L^{3-}	-3	0	1	-23.67
$AlHL^+$	-2	1	1	-4.93
AlL	-3	1	1	-9.43
AlL_2^{3-}	-6	1	2	-21.98
AlL_3^{6-}	-9	1	3	-37.69
$Al_2(OH)_2(HL)_3^{2-}$	-8	2	3	-22.65
$Al_2(OH)_2(HL)_2L^{3-}$	-9	2	3	-27.81
$Al_2(OH)_2(HL)L_2^{4-}$	-10	2	3	-32.87
$Al_2(OH)_2L_3^{5-}$	-11	2	3	-39.56
$Al_4L_3^{3-}$	-9	4	3	-20.25
$Al_3(OH)_4(H_2L)^{4+}$	-5	3	1	-12.25
Total conc.	pH=5.8	10^{-3}	10^{-3}	

Table 3.11: Parameters for test galic acid test.

Results of simulation. In this test case we suppose that all components have the same ideal model of activity. The concentration of primary component H^+ is fixed at the level pH=5.8 or $[H^+]=1.58\cdot 10^{-6}$ mol. Therefore the variables of function $\overline{F}$ (3.10) are only the concentrations of the remaining two primary components: Al^{3+}, H_3L. In Table 3.12 we give the values of their concentrations. Again, results are in agreement with J. Carrayrou's results [17].

Name of component	Concentration(our solution)	Carrayrou's solution
Al^{3+}	$2.03\cdot 10^{-5}$	$2.03\cdot 10^{-5}$
H_3L	$2.59\cdot 10^{-7}$	$2.59\cdot 10^{-7}$

Table 3.12: Solution of galic acid test.

Also we compare the efficiency of different methods of root finding. In Table 3.13 we indicate the number of iterations necessary for convergence of method.

Method	Number of iterations
newton	39
hybridj	71
hybridsj	69

Table 3.13: Convergence of galic acid test.

3.4.2.3 Iron diagram

Description of Test 3. In the third test we consider the chemical system of iron compounds with 14 components and 10 chemical reactions [17]. The Morel's tableau of this chemical system is given in Table 3.14. In this table we also indicate the value of total concentrations. In this test we have two types of components with different model of activity. Components of first group (H^+, e^- (free electrons), OH^-, H_2CO_3, HCO_3^-, CO_3^{2-}, Fe^{2+}, Fe^{3+}, $FeOH^{2+}$, $Fe(OH)_4^-$) are liquid and have ideal activity. Components of second group (Fe(s), $FeCO_3$(s), $Fe(OH)_2$(s), $Fe(OH)_3$(s)) have fixed activity and may precipitate. The concentrations of primary component H^+ and e^- are imposed ($pH=-\log c_{H^+}$ and $pe=-\log c_{e^-}$). As primary component we choose: H^+, e^-, HCO_3^-, Fe^{2+}.

Results of simulation. Values of pH and pe vary from pH=0 to pH=15 with step ΔpH= 0.1 and from pe=-15 to pe=20 with step Δpe= 0.1. For each particular value of pH and pe we compare concentrations of iron compounds of system (Fe^{2+}, Fe^{3+}, $FeOH^{2+}$, $Fe(OH)_4^-$, Fe(s), $FeCO_3$(s), $Fe(OH)_2$(s), $Fe(OH)_3$) and mark the compound with maximal concentration. In Figure 3.10 distribution of dominant component of system depending on the concentration of imposed components H^+ and e^- is shown.

Correct distribution of dominant component of the considered chemical system is shown in Figure 3.11 and taken from [17].

From a comparison of the two diagrams we can find that the distribution of dominant component basically resembles, but in our result (Figure 3.10) we can detect instable areas (dotted areas) near to the border of dominant component regions. The

	H^+	e^-	HCO_3^-	Fe^{2+}	Log K
H^+	1	0	0	0	0
OH^-	0	0	0	0	-14
H_2CO_3	1	0	1	0	6.3
HCO_3^-	0	0	1	0	0
CO_3^{2-}	-1	0	1	0	-10.3
Fe^{2+}	0	0	0	1	0
Fe^{3+}	0	-1	0	1	-13
$FeOH^{2+}$	-1	-1	0	1	-15.2
$Fe(OH)_4^-$	-4	-1	0	1	-34.6
Fe(s)	0	2	0	1	-14.9
$FeCO_3$(s)	-1	0	1	1	0.2
$Fe(OH)_2$(s)	-2	0	0	1	-13.3
$Fe(OH)_3$(s)	-3	-1	0	1	-16.5
Total conc.	pH	pe	10^{-3}	10^{-5}	

Table 3.14: Parameters for iron diagram test.

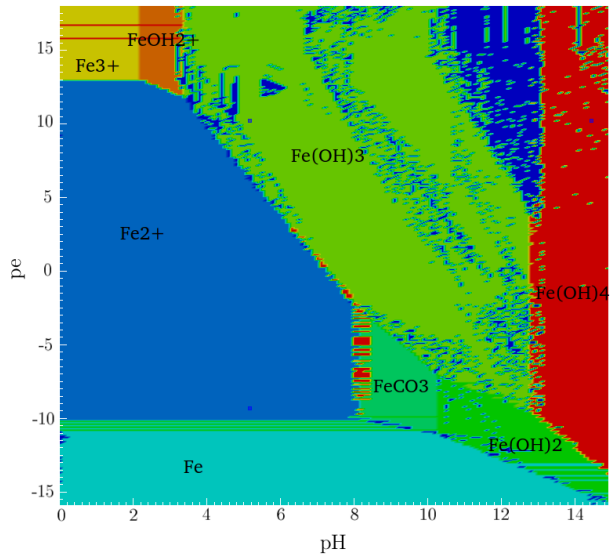

Figure 3.10: pe-pH diagram (our result).

appearance of these areas is related with poor convergence of root-finding method for nonlinear chemical equilibrium problem into them. The main reason for not convergence is a wrong choice of initial approximation. Close to the border between different dominant component regions the domain of appropriate initial approximations decreases and in some cases root-finding method used in ChemEqLib doesn't converge to the right solution. In our simulations we simply use the vector of total concentrations as initial approximation. More intelligent and adaptive approach for initial point selection could significantly reduce the size of zones without convergence.

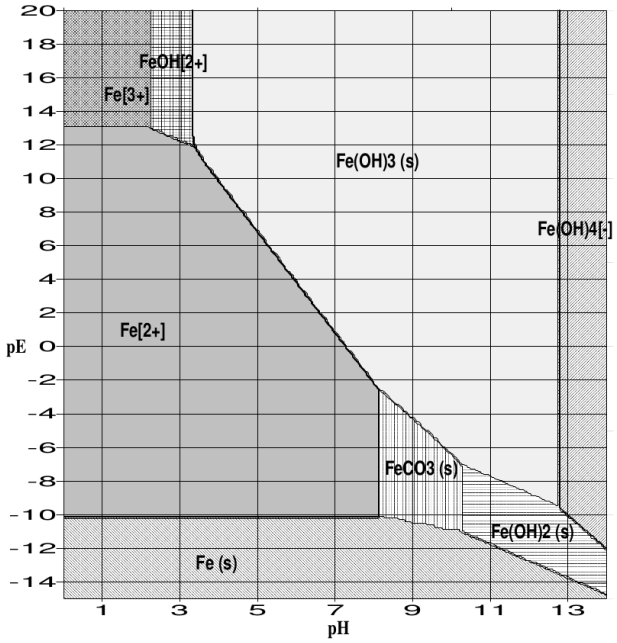

Figure 3.11: pe-pH diagram (Carrayrou [17]).

3.4.3 Summary

In this section we have realized three different test cases of the finding of chemical equilibrium. Performing these tests we verify the capabilities of ChemEqLib code. Summarizing the obtained results we can conclude that:

- ChemEqLib code give the opportunity to define the chemical system of different complexity, chose the type of component activities, the values of total concentration and the root-finding algorithm,
- the used iterative root-finding algorithms converge to the solution of system of equations for chemical equilibrium (3.2).

3.5 One-phase multicomponent transport

3.5.1 Physical model

The transport of a non-reactive component in a porous medium under the influence of advection, diffusion and dispersion is deduced from the mass conservation law and written in the following form:

$$\phi \frac{\partial c}{\partial t} + \nabla.(\overrightarrow{q}c) + \nabla.(-D\nabla c) = f, \tag{3.21}$$

where

- c is the concentration of the component [mol/m^3],
- $\overrightarrow{q}$ is the flow velocity (Darcy' velocity) [m/s],

- ϕ is the porosity [-],
- f is the source term [mol/m^{3}s],
- $D = D_{\text{diff}} + D_{\text{disp}}$ is the diffusion-dispersion tensor.

$$D_{\text{diff}} = d_m I \tag{3.22}$$

where

- d_m is the molecular diffusion coefficient,
- I is the identity tensor.

$$D_{\text{disp}} = |\overrightarrow{q}|(d_l E(\overrightarrow{q}) + d_t(I - E(\overrightarrow{q}))), \tag{3.23}$$

where

- $E_{ij} = \frac{q_i q_j}{|\overrightarrow{q}|^2}$,
- d_l is the longitudinal dispersion coefficient [m],
- d_t is the transversal dispersion coefficient [m].

3.5.2 Numerical simulations

3.5.2.1 Modifications and implementation in Dumux

Numerical model of one-phase multicomponent transport was not implemented in current version of DuMu^X. For this reason we decided to create a new module called **1pNc** which resolves the transport equation with known velocity $\overrightarrow{q}$ for N_c components dissolved in a fluid. As the basis for this new module, we took existing **OnePTwoCModel** (**1p2c**).

The one-phase, two-component model: OnePTwoCModel (1p2c). This model implements a one-phase flow of a compressible fluid, that consists of two components (water and chemical component i dissolved in water). For calculation of the phase velocity, the model uses standard Darcy's law:

$$\overrightarrow{q} = -\frac{K}{\mu}(\nabla p - \rho \overrightarrow{g}). \tag{3.24}$$

The system of balance equations consist of one continuity equation:

$$\phi \frac{\partial \rho}{\partial t} + \nabla.(\rho \overrightarrow{q}) = f, \tag{3.25}$$

and the transport equation for dissolved component i

$$\phi \frac{\partial \rho X^i}{\partial t} + \nabla.(\rho X^i \overrightarrow{q}) + \nabla.(-\rho D \nabla X^i) = f, \tag{3.26}$$

where X^i is the mass fraction of the component i. All equations are discretized using a vertex-centered finite volume as spatial discretization and the implicit Euler method as time discretization. The primary variables are the pressure p and the mass fraction of dissolved component i.

The one-phase, multicomponent transport model: 1pNc. To adapt the model used in **1p2c** module to the model of one-phase multicomponent transport, we have made the following list of changes:

- In contrast to **OnePTwoCModel** the velocity of multicomponent transport is supposed to be known. By this reason we replace realization of Darcy's law by a function that returns the vector of velocity which correspond to known pressure field depending on the position in space.
- The pressure p is eliminated from the list of primary components.
- Under the condition of known velocity, the continuity equation (3.25) is not necessary. Thus we eliminated this equation in numerical scheme.
- We add the possibility to change the number of dissolved components.
- Instead of mass fraction of dissolved components as primary variables, we use their concentration ($c_i = \dfrac{\rho X^i}{M_i}$).

Further we present numerical test cases which demonstrate operability of the created module **1pNc** and verify its ability to simulate one-phase multicomponent transport (H_2O-CO_2).

3.5.2.2 Analytical test case

Description of Test 1. In this test we want to compare the concentration given by the created module **1pNc** implemented in DuMu^X [67] and the two-dimensional analytical solution [40] that corresponds to the following conditions:

- the domain is homogeneous (porosity is constant $\phi = 1$),
- the domain is rectangular of the size 100 m × 40 m,
- imposed flow is one-dimensional and parallel to x-axis ($\overrightarrow{q} = \big(1,\ 0\big)^T$),
- initial concentration is equal to zero ($c(x, y, t = 0) = 0$),
- boundary conditions are of Dirichlet type, concentration is imposed at the left side of the domain: $c(0, y, t) = c_0$ if $|y| < a\ (= 8)$ and $c(0, y, t) = 0$ if $|y| \geq a\ (= 8)$,
- molecular diffusion is neglected ($d_m = 0$),
- $d_l = 2$ m, $d_t = 0.2$ m.

The geometrical configuration of the test is shown in Figure 3.12.
The analytical solution for this configuration is given by [40]:

$$c(x, y, t) = \frac{x c_0}{(16\pi d_l)^{\frac{1}{2}}} \int_0^t \tau^{-\frac{3}{2}} \left(\operatorname{erf}\left(\frac{a+y}{(4d_t\tau)^{\frac{1}{2}}} \right) + \operatorname{erf}\left(\frac{a-y}{(4d_t\tau)^{\frac{1}{2}}} \right) \right) \exp\left(-\left(\frac{x - q\tau}{(4d_l\tau)^{\frac{1}{2}}} \right)^2 \right) d\tau. \tag{3.27}$$

For computation of the integral we use Gauss-Chebyshev's formula based on Chebyshev polynomials of first order:

$$\int_a^b f(x)dx \simeq \frac{b-a}{2} \sum_{k=1}^{n} w(\xi_k) \sqrt{1-\xi_k^2} f\left(\frac{b-a}{2}\xi_k + \frac{b+a}{2} \right), \tag{3.28}$$

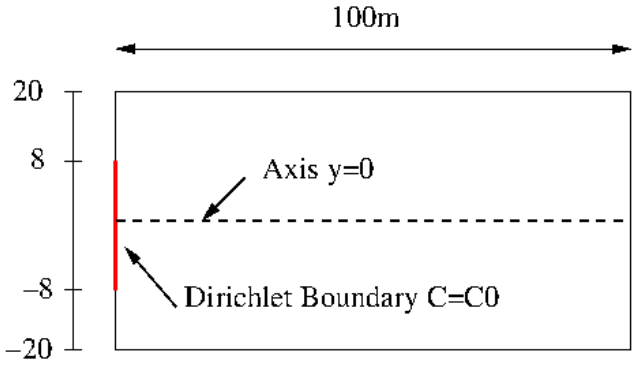

Figure 3.12: Configuration of the test case.

where

$$\xi_k = \cos\frac{(2k-1)\pi}{2n}, \quad w(\xi_k) = \frac{\pi}{n}, \quad k = 1,..,n,$$

and

$$f(\tau) = \tau^{-\frac{3}{2}}\left(\operatorname{erf}\left(\frac{a+y}{(4d_t\tau)^{\frac{1}{2}}}\right) + \operatorname{erf}\left(\frac{a-y}{(4d_t\tau)^{\frac{1}{2}}}\right)\right)\exp\left(-\left(\frac{x-q\tau}{(4d_l\tau)^{\frac{1}{2}}}\right)^2\right).$$

Using this approximation and a change of variable the analytical solution (3.27) can be presented in the following form:

$$c(x,y,t) \simeq \frac{xtc_0}{(64\pi D_l)^{\frac{1}{2}}}\sum_{k=1}^{n}\frac{\pi}{n}\sin\frac{(2k-1)\pi}{2n} f(t\cos^2\frac{(2k-1)\pi}{4n}) \tag{3.29}$$

Results of simulation. The numerical simulation was made by DuMu^X software with the new module **1pNc**. Figure 3.13 represents the distribution of concentration at the time $t = 50$ s.

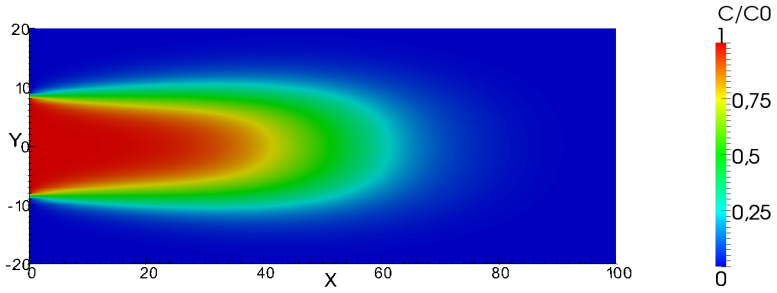

Figure 3.13: Distribution of concentration at $t = 50$ s.

To compare the analytical and numerical solutions, we construct the graphs that represent the dependency of concentration on coordinate x with fixed coordinate $y = 0$ at the time $t = 10,\ 20,\ 30,\ 40,\ 50$ s. These graphs are shown in Figure 3.14.

The slight difference between analytical and numerical solution is due to the presence of an additional numerical diffusion which appears in the numerical scheme.

To demonstrate the convergence of used numerical scheme we evaluate L^2 norm of the difference between analytical and numerical solution at fixed time $t = 5$ s over all

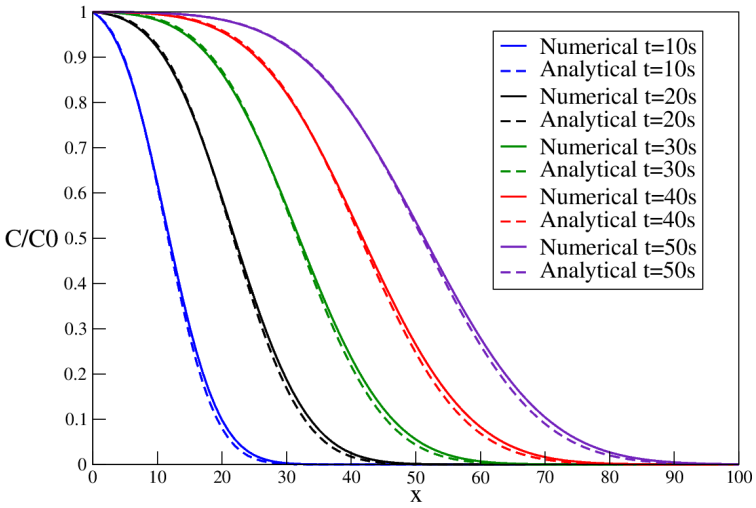

Figure 3.14: Comparison between analytical and numerical solution.

the domain. For this we use uniform meshes with different number of points: 50×20, 100×40, 200×80, 400×160. The obtained dependency between error and number of mesh points is shown in Figure 3.15.

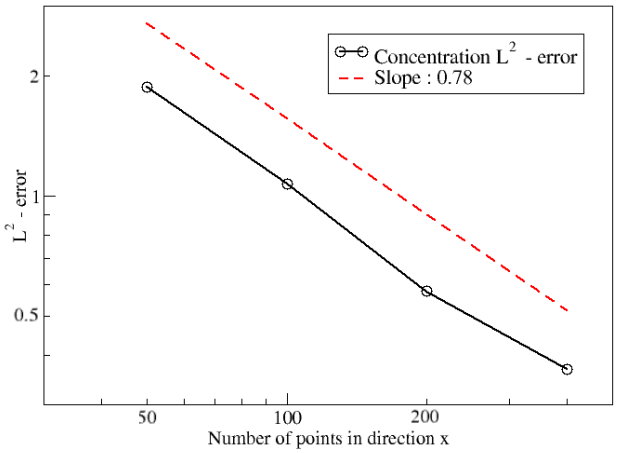

Figure 3.15: Norm of the difference between analytical and numerical solutions for meshes with different number of points at fixed time $t = 5$ s.

The obtained order of numerical scheme for considered test is equal to 0.78. The difference from the theoretically expected order 1 for transport equation can be explained by non-continuous boundary condition at left side of domain.

3.5.3 Summary

In this section we have realized one test case for one-phase multicomponent transport. Performing this test we have verified the capabilities of the created module **1pNc** in DuMu^X simulator. Summarizing the obtained results we can conclude that:

- The **1pNc** module in Dumux satisfies our requirements and gives us tools to define vector field of imposed transport velocity, diffusion-dispersion parameters.
- Our results were compared with known analytical solution. This comparison shows the convergence of used numerical scheme.

3.6 Reactive transport

3.6.1 System of equation

The system of equations for reactive transport is derived from the system of equation for two-phase multicomponent flow (2.67) under the following conditions:

- There are only two phases: mobile liquid phase (l) and immobile solid phase (s). Saturations of the gas phase is supposed to be zero ($S_g = 0$, $S_l = 1$).
- The pressure and velocity of liquid phase are supposed to be known.
- Capillary pressure law and closure relations for saturation are no longer needed.
- In the considered cases of this section we also suppose that all chemical reactions are at equilibrium, so $r_k = \varnothing$.

The obtained system can be written in the following way:

$$\begin{cases} \dfrac{\partial(\phi T_l)}{\partial t} & + & \dfrac{\partial((1-\phi)T_s)}{\partial t} + L_l(T_l) = 0, \\ \log c_{sl} & = & \log K_{c_{sl}} + \mathbb{S}_{ll}\log c_{pl} + \mathbb{S}_{ls}\log c_{ps}, \\ \log c_{ss} & = & \log K_{c_{ss}} + \mathbb{S}_{sl}\log c_{pl} + \mathbb{S}_{ss}\log c_{ps}. \end{cases} \tag{3.30}$$

where

- $T_\alpha = \mathbb{U}\mathbb{M}_\alpha c \quad \alpha = l,s$ is the vector of total liquid and solid concentrations,
- $\mathbb{S}_e = \begin{pmatrix} -\mathbb{I} & 0 & \mathbb{S}_{ll} & \mathbb{S}_{ls} \\ 0 & -\mathbb{I} & \mathbb{S}_{sl} & \mathbb{S}_{ss} \end{pmatrix}$,
- $\mathbb{U} = \begin{pmatrix} \mathbb{S}_{ll}^T & \mathbb{S}_{sl}^T & \mathbb{I} & 0 \\ \mathbb{S}_{ls}^T & \mathbb{S}_{ss}^T & 0 & \mathbb{I} \end{pmatrix}$,
- $\mathbb{M}_l = \begin{pmatrix} \mathbb{I} & & & \\ & 0 & & \\ & & \mathbb{I} & \\ & & & 0 \end{pmatrix}$, $\mathbb{M}_s = \begin{pmatrix} 0 & & & \\ & \mathbb{I} & & \\ & & 0 & \\ & & & \mathbb{I} \end{pmatrix}$.

As primary variables we use the vector of the component concentrations $c = \left(c_{sl},\ c_{ss},\ c_{pl},\ c_{ps}\right)^T$. The number of equations and number of variables in the system is the same and is equal to N_c. T_l and T_s are functions of the vector c, but for further numerical simulations we want to reformulate this system in the terms of the total concentrations T_l, T_s.

Toward this aim, consider the system of equations obtained in section 3.4.1.1:

$$\begin{cases} \log c_{sl} &= \log K_{c_{sl}} + \mathbb{S}_{ll}\log c_{pl} + \mathbb{S}_{ls}\log c_{ps}, \\ \log c_{ss} &= \log K_{c_{ss}} + \mathbb{S}_{sl}\log c_{pl} + \mathbb{S}_{ss}\log c_{ps}. \\ \begin{pmatrix} \phi\mathbb{S}_{ll}^T c_{sl} + (1-\phi)\mathbb{S}_{sl}^T c_{ss} + \phi c_{pl} \\ \phi\mathbb{S}_{ls}^T c_{sl} + (1-\phi)\mathbb{S}_{ss}^T c_{ss} + (1-\phi)c_{ps} \end{pmatrix} &= T(=\mathbb{U}\theta c = \phi T_l + (1-\phi)T_s). \end{cases} \tag{3.31}$$

If the value of the vector T is given then the system (3.31) is closed and we can find the concentrations of all component $c = (c_{sl}, c_{ss}, c_{pl}, c_{ps})^T$. Thus, we can introduce the function γ ("black box") such that $\gamma(T)$ equals to the total solid concentration vector calculated from the concentration vector c, the solution of system (3.31) (vector c).

Then, in the same manner as in [11] , using the new variables (T_l and T_s) and the function γ we can rewrite the system (3.31) in the following form:

$$\begin{cases} \phi\dfrac{\partial}{\partial t}(T_l) + (1-\phi)\dfrac{\partial}{\partial t}(T_s) &+ L(T_l) = 0, \\ T &= \phi T_l + (1-\phi)T_s, \\ T_s &= \gamma(T). \end{cases} \tag{3.32}$$

3.6.2 Solution method. Sequential Iterative Approach (SIA)

As numerical algorithm for the solution of the system (3.32), we choose a sequential iterative approach (SIA) [71]. To describe this approach, we introduce the following notation:

- N_t - the number of time iterations,
- N_g - the number of grid points,
- T^n, T_l^n, T_s^n - the values of vectors at the time step t_n,
- $T^{n,k}$, $T_l^{n,k}$, $T_s^{n,k}$ - intermediate preliminary values of vectors at the iteration k at the time step t_n.

Each unknown concentration depends on both the grid point index, and the chemical species index. We will use a notation inspired from **Matlab**. For a concentration u_{ij}, where $i \in [1, N_g]$ represents the spatial index and $j \in [1, N_c]$ represents the chemical index, we shall denote by

- $u_{:,j}$ the column vector of concentrations of species j at all grid points,
- $u_{i,:}$ the row vector of concentrations of all chemical species in grid cell x_i.

With these notations, the iterative algorithm (SIA) is expressed in Algorithm 1:

Algorithm 1 Sequential Iterative Approach

for $n = 1, N_t$ **do**
  while $\frac{||T_l^{n+1,k+1} - T_l^{n+1,k}||}{||T_l^{n+1,k+1}||} + \frac{||T_s^{n+1,k+1} - T_s^{n+1,k}||}{||T_s^{n+1,k+1}||} < \varepsilon$ **do**
    for $j = 1, N_c$ **do**
      Solve the transport problem: $\phi \frac{T_{l\ :,j}^{n+1,k+1} - T_{l\ :,j}^{n}}{\Delta t} + (1-\phi)\frac{T_{s\ :,j}^{n+1,k} - T_{s\ :,j}^{n}}{\Delta t} + L(T_{l\ :,j}^{n+1,k+1}) = 0$
    end for
    $T^{n+1,k+1} = \phi T_l^{n+1,k+1} + (1-\phi) T_s^{n+1,k}$
    for $i = 1, N_g$ **do**
      Solve the chemical equilibrium: $T_{s\ i,:}^{n+1,k+1} = \gamma(T_{i,:}^{n+1,k+1})$
    end for
    k=k+1
  end while
end for
return

3.6.3 Implementation in DuMu^X

In the implementation of the algorithm, there are three main points:

- solution of the system of transport equations,
- finding the value of the function γ,
- implementation of iteration loop.

Since an important part of the algorithm is the solution of one-phase multicomponent transport we decided to base on the developed module **1pNc** of DuMu^X. As was explained in section 3.5.2.1, we solve the system of transport equation with imposed velocity for N_c component. We added a number of changes in this module for the implementation of the main loop of SIA. Calculation of the function γ is performed by linked module. This module is based on the code ChemEqLib [1] presented in section 3.4.1.3.

3.6.4 Numerical simulations

3.6.4.1 Test 1. Ions exchange: PHREEQC

The description of the first test is taken from [51](Example 11 - Transport and Cation Exchange). The chemical system in this test consists of 8 components:

- 4 liquid primary components - sodium ion Na^+, potassium ion K^+, calcium ion Ca^{2+}, chlorine ion Cl^-,
- 1 fixed primary component - rock X^-,
- 3 secondary fixed components - compounds with rock NaX, KX, CaX_2,

and 3 equilibrium reactions:

$$\begin{aligned} NaX &\rightleftharpoons Na^+ + X^-, \\ KX &\rightleftharpoons K^+ + X^-, \\ CaX_2 &\rightleftharpoons Ca^{2+} + 2X^-. \end{aligned} \tag{3.33}$$

Chemical description can be represented in the following Morel's tableau (Table 3.15). In Table 3.15 we can see that Cl^- doesn't participate in chemical reactions. This com-

	Ca^{2+}	Na^+	K^+	Cl^-	X	log K
CaX_2	1	0	0	0	2	3.4576
NaX	0	1	0	0	1	0
KX	0	0	1	0	1	0.7
Total	T_{Ca}	T_{Na}	T_K	T_{Cl}	T_X	

Table 3.15: Parameters for ion exchange test (PHREEQC).

ponent is added as tracer and allows us to compare the distribution of components participated in chemical reaction with tracer component the distribution of which is defined only by advection with $\overrightarrow{q}$ velocity.

The values of equilibrium constants log K are given under condition that we use mmol/l as units for concentration of components.

In this test we consider column of length l. Initially in the column a mixture of sodium and calcium at chemical equilibrium is present. At the left part of the column we inject mixture of chlorine and calcium. The transfer is performed in the column at a constant velocity $\overrightarrow{q}$. The values of the flow parameters are given in Table 3.16. Boundary and initial concentrations of liquid primary components are given in Table 3.17.

Darcy's velocity $\overrightarrow{q}$	2.78 10^{-6} [m/s]
Diffusion coefficient D	5.56 10^{-9} [m^2/s]
Column length l	0.08 [m]

Table 3.16: Flow parameters for ion exchange test (PHREEQC).

Components	c_{init} [mmol/l]	c_{inflow} [mmol/l]
Ca	0	0.6
Na	1	0.
K	0.2	0.
Cl	0	1.2

Table 3.17: Boundary and initial concentrations for ion exchange test (PHREEQC).

The cation exchange capacity equals 1.1 mmol/l ($T_X = 1.1$).

The period of simulation is equal to 1 day. The time step is fixed to 720 s. The mesh size is equal to 5. 10^{-4} m.

The results of simulation are represented in Figure 3.16 which shows the evolution of concentrations of primary components Ca^{2+}, Na^{+}, K^{+}, Cl^{-} at the right side of column. For comparison, in Figure 3.17 we show the results from [51] obtained by **PHREEQC simulator**.

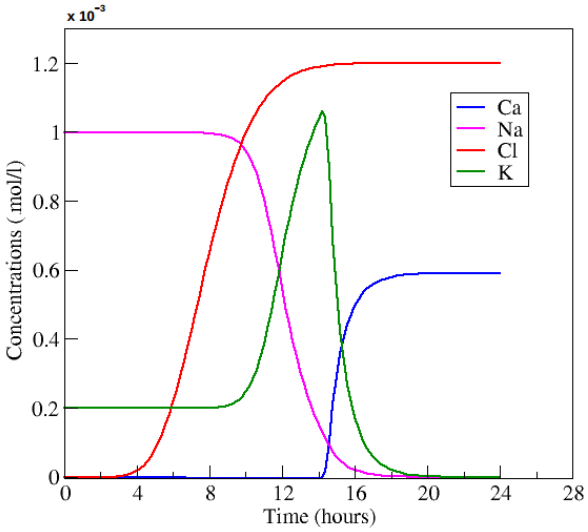

Figure 3.16: Evolution of concentrations (**1pNc**).

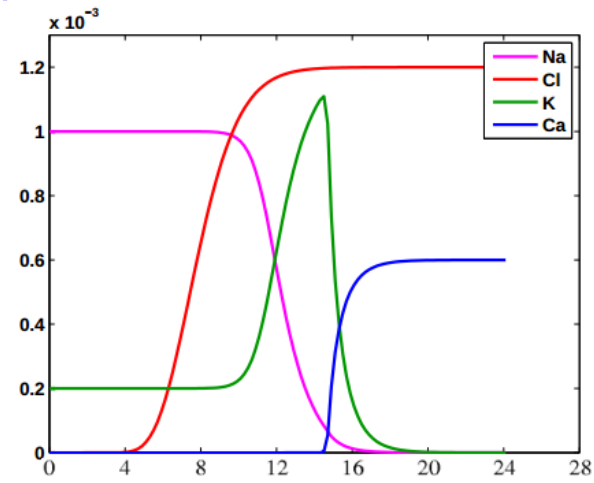

Figure 3.17: Evolution of concentrations ("**PHREEQC**").

Both numerical simulators demonstrate a similar picture of the evolution of primary component concentrations.

3.6.4.2 Test 2. Ions exchange: Valocchi

The description of the second test is taken from [66] (Valocchi et al). The chemical system in this test consists of 8 components:

- 4 liquid primary components - sodium ion Na^+, calcium ion Ca^{2+}, magnesium ion Mg^{2+}, chlorine ion Cl^-,
- 1 fixed primary component - soil S,
- 3 secondary fixed components - compounds with soil S—Na, S_2—Ca, S_2—Mg,

and 3 equilibrium reactions:

$$\begin{aligned} S\text{—}Na &\rightleftharpoons Na^+ + S, \\ S_2\text{—}Ca &\rightleftharpoons K^+ + 2S, \\ S_2\text{—}Mg &\rightleftharpoons Ca^{2+} + 2S. \end{aligned} \tag{3.34}$$

Chemical description can be represented in the following Morel's tableau (Table 3.18).

	Na^+	Ca^{2+}	Mg^{2+}	Cl^-	S	$\log K$
S—Na	1	0	0	0	1	4
S_2—Ca	0	1	0	0	2	8.602
S_2—Mg	0	0	1	0	2	8.355
Total	T_{Na}	T_{Ca}	T_{Mg}	T_{Cl}	T_S	

Table 3.18: Parameters for ion exchange test (Valocchi).

In this test, like in previous one, we consider a column of length l. At the left end of the column four liquid components (Na^+, Ca^{2+}, Mg^{2+} and Cl^-) are injected into an homogeneous landfill. The transfer is performed in the column at a constant velocity $\overrightarrow{q}$. The values of the flow parameters are given in Table 3.19. Boundary and initial concentrations of liquid primary components are given in Table 3.20.

Darcy's velocity $\overrightarrow{q}$	0.2525 [m/h]
Diffusion coefficient D	0.74235 [m^2/h]
Column length l	16 [m]
porosity ϕ	0.35

Table 3.19: Flow parameters for ion exchange test (Valocchi).

Components	c_{init} [mmol/l]	c_{inflow} [mmol/l]
Na^+	248	9.4
Ca^{2+}	165	2.12
Mg^{2+}	158	0.494
Cl^-	161	9.03
S	750	

Table 3.20: Boundary and initial concentrations for ion exchange test (Valocchi).

The period of simulation is equal to 5000 h. The mesh size is equal to 0.08 m.

Figure 3.18 shows the evolution of Mg^{2+} and Ca^{2+} concentrations at the right end of the column. Also we add to this plot the experimental data of Valocchi et al. [66]. From comparison of the concentration graphs, we can see that the developed module **1pNc** give results which are very close to the experimental values.

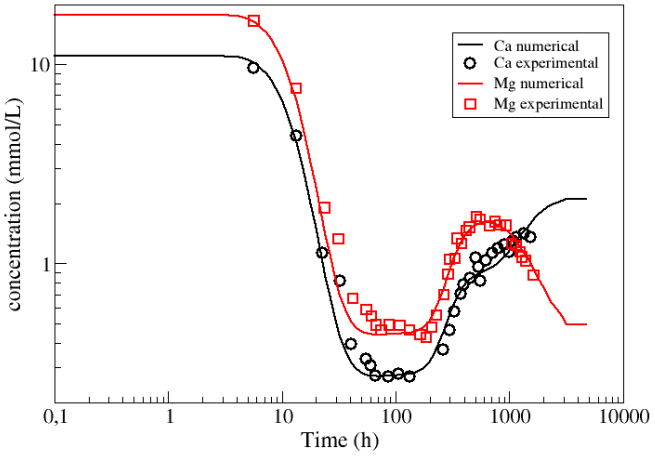

Figure 3.18: Comparison of the concentrations of Ca^{2+} and Mg^{2+} in the outlet of the domain between our results (numerical) and experimental results (taken from Valocchi *et al*).

3.6.4.3 Test 3. Alkaline water injection

The description of the third test is taken from [24]. The chemical system in this test consists of 6 components:

- 3 primary liquid components - Na^+, OH^-, H_4SiO_4,
- 2 secondary liquid components - H^+, H_3SiO_4,
- 1 fixed precipitated component - quartz SiO_2,

2 usual equilibrium reactions:

$$\begin{array}{rcl} H^+ & \rightleftharpoons & H_2O - OH^-, \\ H_3SiO_4 & \rightleftharpoons & OH^- + H_4SiO_4 - H_2O. \end{array} \tag{3.35}$$

and 1 reaction of precipitation:

$$SiO_2 \rightleftharpoons H_4SiO_4 - 2H_2O. \tag{3.36}$$

In addition to indicated components, we also meet the water H_2O. But H_2O is not included in this model because the variation of the amount of water is negligible, thereby chemical description of the test can be represented in the following Morel's tableau (Table 3.21).

	Na^+	OH^-	H_4SiO_4	$\log K$
H^+	0	-1	0	-14
H_3SiO_4	0	1	1	4.2
SiO_2	0	0	1	3.6
Total	T_{Na}	T_{OH^-}	$T_{H_4SiO_4}$	

Table 3.21: Parameters for alkaline water injection test.

The values of equilibrium constants $\log K$ are given under condition that we use mol as units for concentration of components.

In this test, we consider a column of length l. Initially in the column there is only pure quartz. At the left end of the column initial solution is in contact with alkaline water. Transport is performed only by diffusion from the left end with Dirichlet boundary condition inside the column. The values of the flow parameters are given in Table 3.22. Boundary and initial concentrations of liquid primary components are given in Table 3.23.

Darcy's velocity $\overrightarrow{q}$	0.0 [m/s]
Diffusion coefficient D	$3\ 10^{-10}$ [m^2/s]
Column length l	$1.6m$ [m]
Porosity ϕ	1

Table 3.22: Flow parameters for alkaline water injection test.

Components	T_{init} [mol/l]	T_{inflow} [mol/l]
Na	$1\ 10^{-20}$	$2\ 10^{-2}$
OH^-	$1\ 10^{-20}$	$2\ 10^{-2}$
H_4SiO_4	10	$1.62\ 10^{-2}$

Table 3.23: Boundary and initial concentrations for alkaline water injection test.

The period of simulation is equal to 100 days. The time step is fixed to 20 minutes. We used 4 different one dimensional meshes with 100, 200, 400, 800 points.

Results of simulation are represented in Figure 3.19 which shows concentrations of primary components Na, OH^-, H_4SiO_4 in the column at $t = 100$ days.

Since Darcy's velocity in this test is equal to $\overrightarrow{0}$, we can find an analytical solution of the problem. Sodium Na^+ doesn't participate in the chemical reaction and therefore its concentration satisfies the following diffusive transport equation:

$$\phi \frac{\partial c_{Na}}{\partial t} = D \frac{\partial^2 c_{Na}}{\partial x}. \tag{3.37}$$

The analytical solution of this equation in the domain $x \in (0, \infty)$, $t > 0$ is known and can be written in the following form:

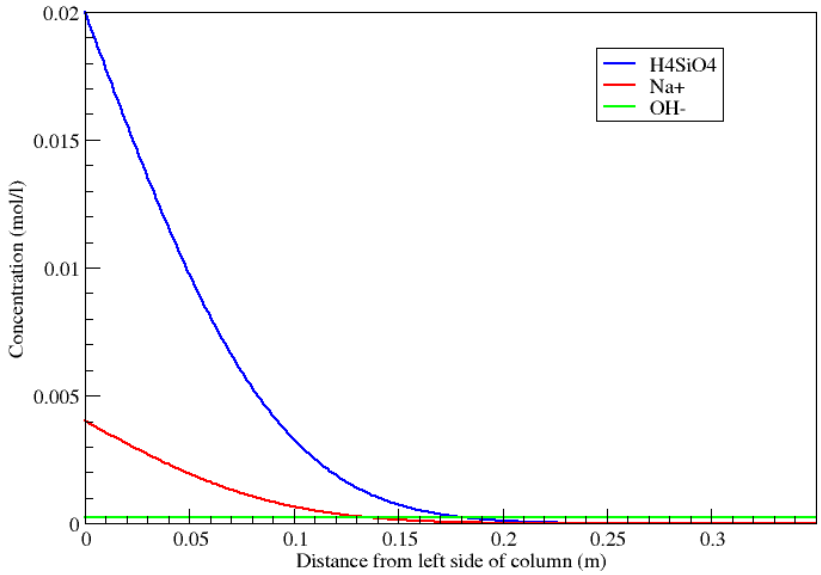

Figure 3.19: Concentrations of primary components ($t = 100$ days).

$$c_{Na^+}(x,t) = c_{Na^+,D}\text{erfc}\left(\frac{x}{2\sqrt{\frac{Dt}{\phi}}}\right) + c_{Na^+,0}\text{erf}\left(\frac{x}{2\sqrt{\frac{Dt}{\phi}}}\right), \tag{3.38}$$

where $c_{Na^+,D}$ is the value of Na^+ concentration at the left border and $c_{Na^+,0}$ is the initial value of Na^+ concentration inside the column.

Using the mass action law, we can express the concentration of other components through Na^+ concentration. For example :

$$c_{H^+} = \sqrt{\frac{c_{Na^+}^2}{2} + \frac{K_{H^+}K_{H_3SiO_4}}{K_{SiO_2}} + K_{H^+}} - c_{Na^+} \tag{3.39}$$

and

$$c_{OH^-} = \frac{K_{H^+}}{c_{H^+}}. \tag{3.40}$$

A detailed derivation of equations (3.39), (3.40) is given in [24].

Under the condition of fixed activity of SiO_2 (mineral component) and H_2O (negligible variation of concentration) the concentration of primary component H_4SiO_4 is immediately deduced from the mass action law of reaction (3.36):

$$c_{H_4SiO_4} = K^{-1}_{H_4SiO_4}. \tag{3.41}$$

Thus we can validate the third test by measuring L^2 norm of the difference ($Error_i$) between the analytical and numerical solutions of the concentration of the component

i at the points of the mesh at each day over the period of 100 days proposed in article [24]:

$$Error_i = \sqrt{\frac{1}{N_m N_n} \sum_{n}^{N_n} \sum_{m}^{N_m} (c_i(x_m, t_n) - \overline{c_i}(x_m, t_n))^2} \tag{3.42}$$

where N_n is the number of measurement times, N_m is the number of points in the mesh, c_i is the numerical solution of component i concentration and $\overline{c_i}$ is the analytical solution of component i concentration.

Table 3.24 contains the values of error of concentrations for primary components. .

Number of points	Δx [m]	$Error_{Na^+}$	$Error_{OH^-}$	$Error_{H_4SiO_4}$
100	0.016	$2.53\ 10^{-5}$	$5.08\ 10^{-6}$	0.0
200	0.008	$7.1\ 10^{-6}$	$1.43\ 10^{-6}$	0.0
400	0.004	$2.0\ 10^{-6}$	$4.02\ 10^{-7}$	0.0
800	0.002	$6.76\ 10^{-7}$	$1.36\ 10^{-7}$	0.0

Table 3.24: Absolute errors in L^2 norm for concentrations of primary components between t = 0 and t = 100 days for different meshes.

As we can see in (3.41), the concentration of the primary component is constant and independent from initial and boundary conditions. For this reason the difference between the analytical and the numerical solution is always zero. To show the convergence of the numerical scheme we use the obtained values of error of concentrations for other two primary components and construct the graph (Figure 3.20) of dependency between the concentration error and the fineness of the grid.

The obtained order of the numerical scheme for the considered test is equal to 1.75. The difference from the theoretically expected order 2 for diffusion (heat) equation can be explained by presence of chemical reactions between components and by the presence of the iterative algorithm required for finding of chemical equilibrium.

3.6.4.4 Test 4. The SHPCO2 Benchmark

The description of the fourth test is taken from [30]. The chemical system in the fourth test consists of 8 components:

- 5 liquid primary components - water H_2O, hydrogen ion H^+, carbon dioxide dissolved in water $CO_{2(l)}$, calcium ion Ca^{2+}, chlorine Cl,
- 2 secondary liquid components - hydroxyde OH^-, hydrogen carbonate HCO_3^-,
- 1 fixed precipitated component - calcite $CaCO_3$,
- 1 gas component - gaseous carbon dioxide $CO_{2(g)}$.

In this test, we make the assumption that the gas phase is immobile $\overrightarrow{q_g} = \overrightarrow{0}$ and therefore gaseous carbon dioxide $CO_{2(g)}$ can be considered like a fixed precipitated component.

Among the components of the system there are 4 chemical reactions :

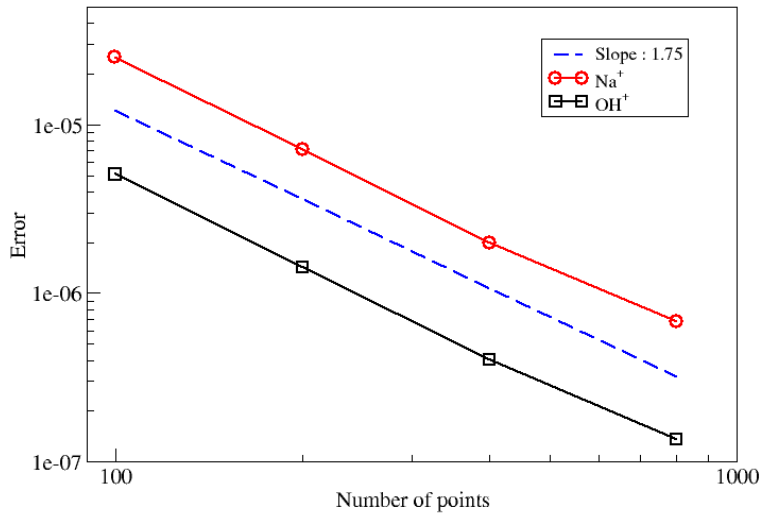

Figure 3.20: Dependence of error on the fineness of the grid.

- 2 aqueous equilibrium reactions

$$\begin{aligned} OH^- &\rightleftharpoons H_2O - H^+, \\ HCO_3^- &\rightleftharpoons H_2O - H^+ + CO_{2(l)}, \end{aligned} \tag{3.43}$$

- 2 reaction of precipitation:

$$\begin{aligned} CO_{2(g)} &\rightleftharpoons CO_{2(l)}, \\ CaCO_3 &\rightleftharpoons H_2O - 2H^+ + CO_{2(l)} + Ca^{2+}. \end{aligned} \tag{3.44}$$

Chlorine Cl does not participate in chemical reactions and is used as tracer.

Chemical description of the test can be represented in the following Morel's tableau (Table 3.25) :

	H_2O	H^+	$CO_{2(l)}$	Ca^{2+}	Cl	$\log K$
OH^-	1	-1	0	0	0	-13.2354
HCO_3^-	1	-1	1	0	0	-6.22
$CO_{2(g)}$	0	0	1	0	0	-0.2226
$CaCO_3$	1	-2	1	1	0	-7.7454
Total	T_{H_2O}	T_{H^+}	$T_{CO_{2(l)}}$	$T_{Ca^{2+}}$	T_{Cl}	

Table 3.25: Parameters for the SHPCO2 Benchmark.

The values of equilibrium constants $\log K$ are given under condition that we use mol/l as units for concentration of components.

In this test we consider a two dimensional rectangular domain. A detailed geometry of this domain is shown in Figure 3.21.

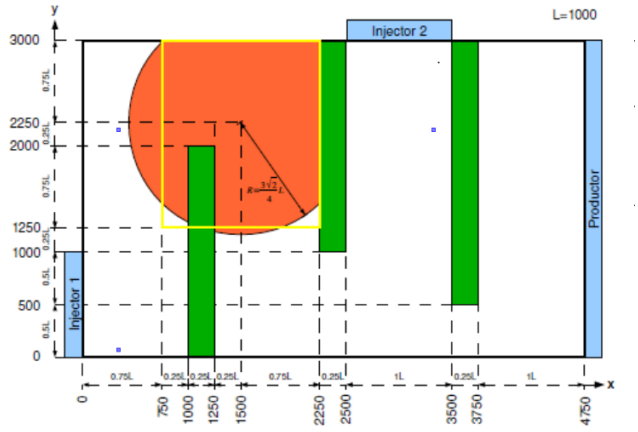

Figure 3.21: Geometry of domain for the SHPCO2 Benchmark.

The domain is divided into two zones :

- "barrier" - zone with low permeability $K_{\text{barrier}} = 1.\ 10^{-15}$ m^2(marked by a green color in the Figure 3.21),
- "drain" - the remaining part of the domain with higher permeability $K_{\text{drain}} = 1.\ 10^{-13}$ m^2.

The transport in the domain is performed with the velocity $\overrightarrow{q} = -\frac{1}{\mu}K\nabla p$ (Figure 3.22) where the pressure p is solution of the steady one-phase flow with the following boundary conditions:

- parts of the boundary marked as "Injector1", "Injector2", "Productor" - Dirichlet boundary conditions such that $p_{injector1} = 1.1\ 10^7$ Pa, $p_{injector2} = 1.05\ 10^7$ Pa, $p_{productor} = 1.0\ 10^7$ Pa,
- rest part - impermeable Neumann boundary conditions.

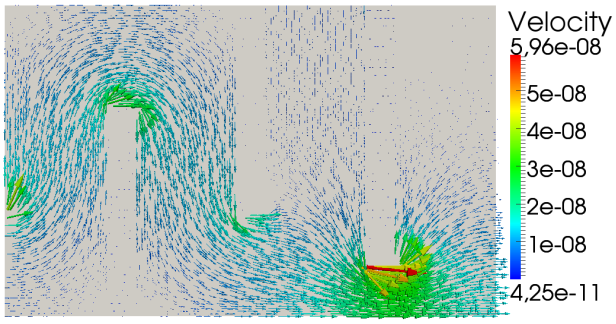

Figure 3.22: Velocity field for the SHPCO2 Benchmark.

For the transport problem, initially in the domain we have two zones with different initial values of total concentrations. The first zone is a sphere with injected gaseous carbon dioxide $CO_{2(g)}$ marked in Figure 3.21 by orange color. In the second zone (rest

of the domain), concentration of $CO_{2(g)}$ is equal to zero. All boundaries of domain have Dirichlet conditions equal to initial concentration. The values of the flow parameters are given in Table 3.26. Boundary and initial concentrations of liquid primary components are given in Table 3.27.

Diffusion coefficient D	10^{-9} [m^2/s]
Porosity ϕ	0.2
Reference length L	1000 m

Table 3.26: Flow parameters for the SHPCO2 Benchmark.

Components	$T_{init,out\ of\ sphere}$ [mol/l]	$T_{init,sphere}$ [mol/l]
H_2O	77.19	77.21
H^+	−43.36	−43.39
$CO_{2(l)}$	21.68	24.38
Ca^{2+}	21.72	21.73
Cl	0	2

Table 3.27: Initial total concentrations for the SHPCO2 Benchmark.

The period of simulation is equal to 2500 years. We have used a two dimensional mesh of size 475 × 300 (142500 points).

In Figures 3.23, 3.24, we compare the values of $CO_{2(g)}$ concentration obtained by our simulator with B. Gueslin and M. Kern's results. As it was mentioned above in the considered test case we suppose that the gas phase is immobile. For this reason, in Figures 3.23, 3.24 we can see that the position of zone of $CO_{2(g)}$ presence does not change with time but the size of this zone is significantly reduced. This is explained by the fact that part of $CO_{2(g)}$ dissolves in liquid phase and is transported by flow outside the injection zone.

Cl component doesn't participate in chemical reactions in this test. This component is introduced as tracer. The evolution of its concentration represented in Figure 3.25 shows how chemical component is transported under the influence only of advection and diffusion. Comparing the evolution of Cl (Figure 3.25) and $CO_{2(l)}$ (Figure 3.26) concentration we can find out that participation in chemical reactions has a strong influence on picture of chemical transport. Thus, in contrast to Cl, $CO_{2(l)}$ has additional source related with the dissolution of $CO_{2(g)}$.

In Figure 3.27 we see that the distribution of H^+ is strongly connected with $CO_{2(l)}$ concentration. High concentration of $CO_{2(l)}$ causes the increasing of the liquid phase acidity.

In the Figure 3.28 we can see that the concentration of fixed component $CaCO_3$ is connected both with distribution of $CO_{2(g)}$ and distribution of $CO_{2(l)}$.

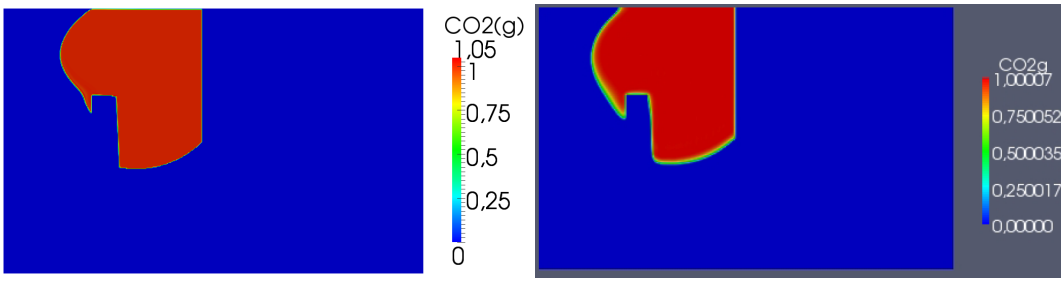

$CO_{2(g)}$ concentration at $t = 400$ years (obtained results)

$CO_{2(g)}$ concentration at $t = 400$ years (M.Kern's results)

Figure 3.23: Comparison between our results and results shown in unpublished Gueslin/ Kern report at $t = 400$ ans.

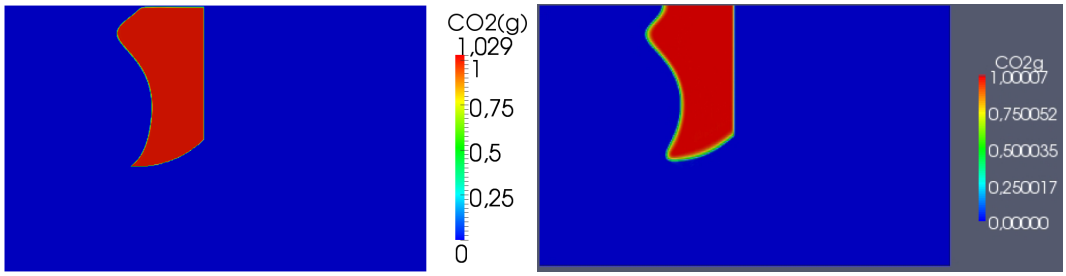

$CO_{2(g)}$ concentration at $t = 1200$ years (obtained results)

$CO_{2(g)}$ concentration at $t = 1200$ years (M.Kern's results)

Figure 3.24: Comparison between our results and results shown in unpublished Gueslin/ Kern report at $t = 1200$ ans.

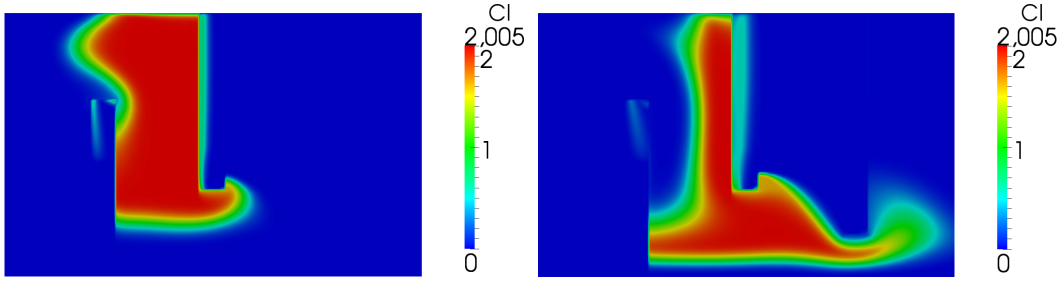

Cl concentration at $t = 400$ years

Cl concentration at $t = 1200$ years

Figure 3.25: Results of numerical simulations for component Cl.

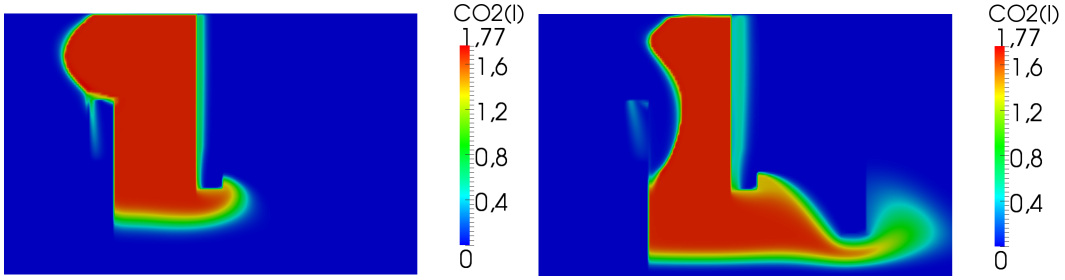

$CO_{2(l)}$ concentration at $t = 400$ years $CO_{2(l)}$ concentration at $t = 1200$ years

Figure 3.26: Results of numerical simulations for component $CO_{2(l)}$.

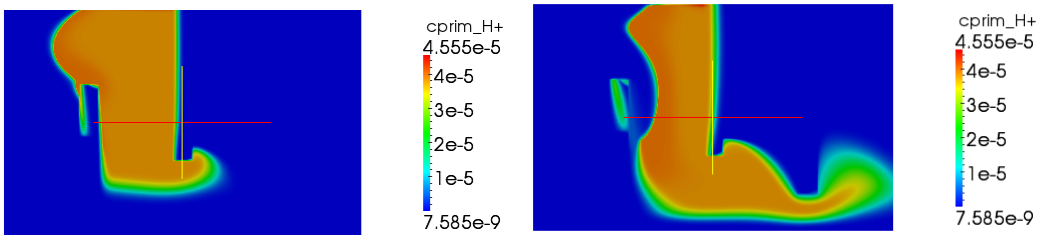

H^+ concentration at $t = 400$ years H^+ concentration at $t = 1200$ years

Figure 3.27: Results of numerical simulations for component H^+.

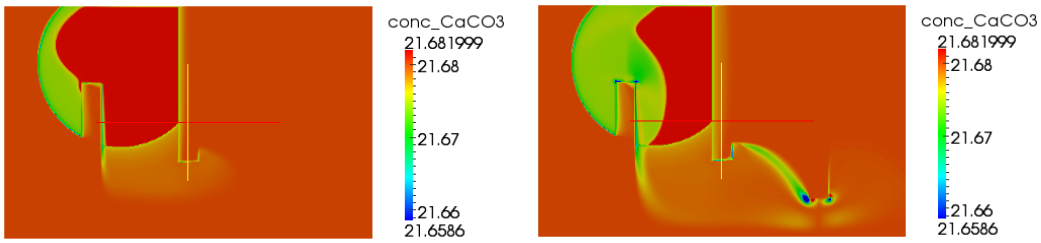

$CaCO_3$ concentration at $t = 400$ years $CaCO_3$ concentration at $t = 1200$ years

Figure 3.28: Results of numerical simulations for component $CaCO_3$.

3.6.5 Summary

In this section, we have realized four different test cases for reactive multicomponent transport. Performing these tests we have verified the capabilities of the module **1pNc** of DuMu^X simulator. Summarizing the obtained results we can conclude that:

- the iterative Algorithm 1 (SIA) was successfully implemented in the **1pNc** module. The obtained numerical simulator satisfies our requirements and gives us tools to define multicomponent chemical system with equilibrium chemical reaction, vector field of imposed transport velocity and other physical parameters.
- Comparison of our results with the results obtained by other authors in the ion exchange test (PHREEQC) (Section 3.6.4.1) shows that the developed reactive multicomponent transport simulator is capable to demonstrate similar evolution of component concentration as other numerical simulator **PHREEQC**.
- In the ion exchange test (Valocchi) (Section 3.6.4.2) we demonstrate that results obtained by the module **1pNc** are good approximation of concentration values observed in real experiments.
- The alkaline water injection test (Section 3.6.4.3) allows to compare the results obtained by the **1pNc** module with known analytical solution. This comparison shows the convergence of used numerical algorithm.
- Performing of the SHPCO2 Benchmark (Section 3.6.4.4) shows that the developed simulator is able to define inhomogeneous initial conditions and not constant velocity field. The results obtained in this test case shows behavior consistent with what is theoretically expected.

Chapter 4

Numerical simulation of two-phase multicomponent flow with reactive transport in porous media. Application to geological storage of CO_2

Contents

4.1 Introduction

The main objective of this chapter is the construction of a numerical simulator for two-phase multicomponent flow with reactive transport. The physics of this problem was detailed in chapter 2. It was mentioned that the elaborated physical model is strongly coupled and a numerical solution of the entire system of equations for such a system faces with various difficulties. To decrease the complexity of the considered problem we present in this chapter a sequential algorithm that enables us to reduce the original problem to the sequential solution of simple sub-problems. The idea underlying the implementation of this algorithm is the separation of primary components into two groups of dominant and minor components. The main attribute of this separation is the influence on the physical parameters. The dominant components almost completely form the liquid phase and have a strong influence on flow parameters such as density, viscosity, pressure etc. The minor components, in contrast, have much lower concentrations in the liquid phase and don't have a significant impact on the physical parameters of the system. Using this separation we can distinguish in the original physical model less coupled sub-problems for dominant and minor components. Multiple consequential solution of these sub-problems at each time step will give the solution of the original problem.

In the second section of this chapter, we introduce the preliminary separation between minor and dominant components and give the reformulation of original physical model of two-phase multicomponent flow, taking into account this new differentiation of components.

In the third section we propose a formulation to decouple the system and formulate a sequential strategy for its resolution. We outline in detail the algorithm and show how the sub-steps are related to the systems studied in chapter 3.

Further, in the fourth section we illustrate the proposed decoupling algorithm for the specific case of geological storage of CO_2.

Using this sequential algorithm, we construct a numerical simulator for two-phase multicomponent flow on the basis of previously developed simulators for two-phase two-component flow and reactive transport. In the fifth section of this chapter, we present this new numerical simulator and demonstrate its capabilities performing three different test cases.

4.2 Reformulation of two-phase multicomponent flow with reactive transport in porous media by separation between dominant and minor components

4.2.1 Reformulation of the chemical system

Consider the chemical system with the following properties:

- in the system we have components in three different phases: liquid, gas and solid,
- all chemical reactions are at equilibrium,
- all primary components are liquid.

In this chemical system we artificially divide the primary liquid components into two groups of dominant and minor components. The main criterion for this separation is the influence on the physical parameters of the system. Dominant components almost completely form liquid phase and have a strong influence on flow parameters. Additionally, we make the assumption that secondary gas components participate only in exchange chemical reactions with dominant components. The minor components, in contrast, have much lower concentrations in the liquid phase and do not have a significant impact on the physical parameters of the system.

According to the separation of primary components into dominant components we introduce additional notations for the corresponding sub-vectors of components:

- $c_{pld} \in \mathbb{R}^{N_{pld}}$ is the vector of concentration of primary dominant components,
- $c_{plm} \in \mathbb{R}^{N_{plm}}$ is the vector of concentration of primary minor components,

where $N_{pld} + N_{plm} = N_p$ since all primary components are liquid.

In this case the entire vector of component concentrations has the following form: $c = (c_{sl}, c_{ss}, c_{sg}, c_{pld}, c_{plm})^T$.

Also here we emphasize that in this chapter we temporarily change the definition of concentration of solid components. Previously we understood by concentration the number of molecules of solid component i in unit volume of the solid phase. In this chapter, for ease of expression of porosity dependence, we change the definition of concentration of solid components to the following: number of molecules of solid component i in entire unit volume. The new formulation is related to the previous one by the following relation:

$$c_{i,new} = (1-\phi)c_{i,old}. \tag{4.1}$$

Further in the chapter, we will use everywhere the new definition of concentration. This explains the slight differences with the second chapter in the form of balance equations. All this changes correspond to the relations between the different concentration definitions as in (4.1).

We suppose that only the liquid components are chosen as primary and all gas and solid components are secondary. Such choice is possible if the chemical reactions satisfy the following two conditions:

Firstly, the gas components participate only in exchange reactions with their own liquid forms. In this case the liquid form is chosen as primary component and the gas form as secondary.

Secondly, the solid components participate only precipitation-dissolution reactions that describe interaction between one secondary solid component and primary liquid components.

The chemical reactions are formulated in following form:

$$\mathbb{S}_e \overline{c} \rightleftharpoons 0 \tag{4.2}$$

where $\mathbb{S}_e \in \mathbb{R}^{N_r \times N_c}$ is the stoichiometric equilibrium matrix of the chemical system.

We can rewrite the reactions (4.2) in a more detailed form by separation on groups for reactions for liquid, solid and gas secondary components:

$$\begin{pmatrix} -I & 0 & 0 & \mathbb{S}_{lld} & \mathbb{S}_{llm} \\ 0 & -I & 0 & \mathbb{S}_{sld} & \mathbb{S}_{slm} \\ 0 & 0 & -I & \mathbb{S}_{gld} & \mathbb{S}_{glm} \end{pmatrix} \begin{pmatrix} \overline{c}_{sl} \\ \overline{c}_{ss} \\ \overline{c}_{sg} \\ \overline{c}_{pld} \\ \overline{c}_{plm} \end{pmatrix} \rightleftharpoons 0 \tag{4.3}$$

or

$$\begin{pmatrix} \overline{c}_{sl} \\ \overline{c}_{ss} \\ \overline{c}_{sg} \end{pmatrix} \rightleftharpoons \begin{pmatrix} \mathbb{S}_{lld} & \mathbb{S}_{llm} \\ \mathbb{S}_{sld} & \mathbb{S}_{slm} \\ \mathbb{S}_{gld} & \mathbb{S}_{glm} \end{pmatrix} \begin{pmatrix} \overline{c}_{pld} \\ \overline{c}_{plm} \end{pmatrix}. \tag{4.4}$$

where sizes of sub-matrices $\mathbb{S}_{\alpha l \beta}$ are the following:

- $\mathbb{S}_{lld} \in \mathbb{R}^{N_{scl} \times N_{pld}}$ (index lld is decrypted in the following way: first l - block of rows for reaction of forming of secondary **liquid** component, second l and d - subset of columns for primary **liquid dominant** components),
- $\mathbb{S}_{llm} \in \mathbb{R}^{N_{scl} \times N_{plm}}$,
- $\mathbb{S}_{sld} \in \mathbb{R}^{N_{scs} \times N_{pld}}$,
- $\mathbb{S}_{slm} \in \mathbb{R}^{N_{scs} \times N_{plm}}$,
- $\mathbb{S}_{gld} \in \mathbb{R}^{N_{scg} \times N_{pld}}$,
- $\mathbb{S}_{glm} \in \mathbb{R}^{N_{scg} \times N_{plm}}$ ($\mathbb{S}_{glm} = 0$ since secondary gas components do not participate in reaction with minor liquid components).

As already mentioned in this section, we suppose that all chemical reactions are at equilibrium. Thereby the vector of rates of kinetic reactions is void $r_k = \varnothing$. In the vector of rates of equilibrium reactions we distinguish the groups that correspond to liquid, solid and gas secondary components: $r_e = \begin{pmatrix} r_l \\ r_s \\ r_g \end{pmatrix}$, where $r_e \in \mathbb{R}^{N_r}$, $r_l \in \mathbb{R}^{N_{scl}}$, $r_s \in \mathbb{R}^{N_{scs}}$, $r_g \in \mathbb{R}^{N_{scg}}$.

4.2.2 Mass action laws

The system of mass actions laws is formulated in the following form:

$$\mathbb{S}_e \log \hat{c} + \log K = 0, \tag{4.5}$$

where K is the vector of equilibrium constants (in our case we divide K in three subvectors for each type of secondary components: liquid K_l, solid K_s and gas K_g).

Rewrite (4.5) in detailed form:

$$\begin{cases} \log \hat{c}_{sl} &= \log K_l + \mathbb{S}_{lld} \log \hat{c}_{pld} + \mathbb{S}_{llm} \log \hat{c}_{plm} \\ \log \hat{c}_{ss} &= \log K_s + \mathbb{S}_{sld} \log \hat{c}_{pld} + \mathbb{S}_{slm} \log \hat{c}_{plm} \\ \log \hat{c}_{sg} &= \log K_g + \mathbb{S}_{gld} \log \hat{c}_{pld} \end{cases} \tag{4.6}$$

Distinguish a separate group of equations for gas equations ($\log \hat{c}_{sg} = \log K_g + \mathbb{S}_{gld} \hat{c}_{pld}$). A distinctive feature of this group of mass action laws is that they do not involve primary minor component. For simplicity, we also suppose that in the considered chemical system the number of secondary gas components is equal to the number of dominant primary liquid components ($N_{scg} = N_{pd}$) and $\mathbb{S}_{gld} = \mathbb{I}$. Thereby the mass action laws for gas secondary components in term of activities can be written in the following form:

$$\log \hat{c}_{sg} = \log K_g + \log \hat{c}_{pld} \tag{4.7}$$

or in term of concentration

$$c_{pld} = g(c_{sg}), \tag{4.8}$$

where the function g returns the solution of equation (4.7) using the dependence of chemical activity from the actual component concentration expressed through the activity model (defined in section 2.3.3). The final form of the function g is defined by specific component activity model (see Section 4.4.4).

4.2.3 Conservation laws

Taking into account the change in the definition of solid component concentration, the volumetric factor of solid phase is equal to one $\theta_s = 1$, the volumetric factors of liquid and gas phase remain unchanged $\theta_l = S_l \phi$, $\theta_g = S_g \phi$.

- θ_α is the volumetric factor, part of unit volume which is occupied by phase α ($\theta_l = S_l \phi$, $\theta_g = S_g \phi$, $\theta_s = 1$),
- θ is the volumetric matrix, diagonal matrix such that $\theta_{ii} = \theta_\alpha$ if the component i is present in the phase α,
- $\mathbb{M}_\alpha$ - matrix of presence in the phase, diagonal matrix such that $m_{ii} = 1$ if the component i is present in the phase α and $m_{ii} = 0$ otherwise.

According to the order in the vector of chemical components $\overline{c} = (\overline{c}_{sl}, \overline{c}_{ss}, \overline{c}_{sg}, \overline{c}_{pld}, \overline{c}_{plm})^T$, the volumetric matrix θ and matrices of presence in phase $\mathbb{M}_l$, $\mathbb{M}_s$, $\mathbb{M}_g$ have the following forms:

$$\theta = \begin{pmatrix} S_l\phi\mathbb{I} & & & & \\ & \mathbb{I} & & & \\ & & S_g\phi\mathbb{I} & & \\ & & & S_l\phi\mathbb{I} & \\ & & & & S_l\phi\mathbb{I} \end{pmatrix}, \tag{4.9}$$

$$M_l = \begin{pmatrix} \mathbb{I} & & & & \\ & 0 & & & \\ & & 0 & & \\ & & & \mathbb{I} & \\ & & & & \mathbb{I} \end{pmatrix}, \quad M_s = \begin{pmatrix} 0 & & & & \\ & \mathbb{I} & & & \\ & & 0 & & \\ & & & 0 & \\ & & & & 0 \end{pmatrix}, \quad M_g = \begin{pmatrix} 0 & & & & \\ & 0 & & & \\ & & \mathbb{I} & & \\ & & & 0 & \\ & & & & 0 \end{pmatrix}. \tag{4.10}$$

Recall also the definition of the advection-diffusion operators for each phase:

- Liquid phase:
$$L_{l(S_l,\overrightarrow{q_l})}(c) = \nabla.(c\overrightarrow{q_l}) + \nabla.(-S_l D_l \nabla c), \tag{4.11}$$
- Solid phase:
$$L_s(c) = 0, \tag{4.12}$$
- Gas phase:
$$L_{g(S_g,\overrightarrow{q_g})}(c) = \nabla.(c\overrightarrow{q_g}) + \nabla.(-S_g D_g \nabla c). \tag{4.13}$$

Using these notations we can write the set of quantity balance equations for each component in a vector form:

$$\frac{\partial(\theta c)}{\partial t} + \mathbb{M}_l L_l(c) + \mathbb{M}_g L_g(c) = \mathbb{S}_e^T r_e. \tag{4.14}$$

To eliminate the right term $\mathbb{S}_e^T r$, we use the kernel matrix $\mathbb{U}$ (2.49):

$$\mathbb{U} = \begin{pmatrix} \mathbb{S}_{lld}^T & \mathbb{S}_{sld}^T & \mathbb{S}_{gld}^T & \mathbb{I} & 0 \\ \mathbb{S}_{llm}^T & \mathbb{S}_{slm}^T & 0 & 0 & \mathbb{I} \end{pmatrix}. \tag{4.15}$$

Multiplying (4.16) by $\mathbb{U}$ we obtain a reduced set of quantity conservation laws:

$$\frac{\partial(\mathbb{U}\theta c)}{\partial t} + L_l(\mathbb{U}\mathbb{M}_l c) + L_g(\mathbb{U}\mathbb{M}_g c) = 0, \tag{4.16}$$

where

$$\mathbb{U}\theta c = \begin{pmatrix} (\phi S_l)(c_{pld}) & + & (\phi S_l)(\mathbb{S}_{lld}^T c_{sl}) & + & \mathbb{S}_{sld}^T c_{ss} & + & \phi S_g c_{sg} \\ (\phi S_l)(c_{plm}) & + & (\phi S_l)(\mathbb{S}_{llm}^T c_{sl}) & + & \mathbb{S}_{slm}^T c_{ss} & + & 0 \end{pmatrix}, \tag{4.17}$$

since $\mathbb{S}_{gld}^T = \mathbb{I}$.

Thus, we note that in conservation equations for minor components there is no term from the gas components, in contrast from equations for dominant components.

4.2.4 System of equations

The final system for two-phase multicomponent flow consists of the following sets of equations:

Conservation laws for dominant components:

$$\frac{\partial(\phi S_l c_{pld})}{\partial t} + \frac{\partial(\phi S_g c_{sg})}{\partial t} + \frac{\partial(\phi S_l(\mathbb{S}_{lld}^T c_{sl}))}{\partial t} + \frac{\partial(\mathbb{S}_{sld}^T c_{ss})}{\partial t} + L_{l,(S_l,\overrightarrow{q_l})}(c_{pld} + \mathbb{S}_{lld}^T c_{sl}) + L_{g,(S_g,\overrightarrow{q_g})}(c_{sg}) = 0. \quad (4.18)$$

Conservation laws for minor components:

$$\frac{\partial(\phi S_l c_{plm})}{\partial t} + \frac{\partial(\phi S_l(\mathbb{S}_{llm}^T c_{sl}))}{\partial t} + \frac{\partial(\mathbb{S}_{slm}^T c_{ss})}{\partial t} + L_{l,(S_l,\overrightarrow{q_l})}(c_{plm} + \mathbb{S}_{llm}^T c_{sl}) = 0. \quad (4.19)$$

Mass action laws for gas secondary components: Henry's law and Raoult's law

$$c_{pld} = g(c_{sg}). \quad (4.20)$$

Mass action laws for liquid and solid secondary components

$$\begin{cases} \log \hat{c}_{sl} &= \log K_l + \mathbb{S}_{lld} \log \hat{c}_{pld} + \mathbb{S}_{llm} \log \hat{c}_{plm}, \\ \log \hat{c_{ss}} &= \log K_s + \mathbb{S}_{sld} \log \hat{c}_{pld} + \mathbb{S}_{slm} \log \hat{c}_{plm}. \end{cases} \quad (4.21)$$

Darcy-Muskat's law

$$\overrightarrow{q}_\alpha = -\frac{k_{r\alpha}}{\mu_\alpha} K(\nabla p_\alpha - \rho_\alpha \overrightarrow{g}). \quad (4.22)$$

Density state equation:

For liquid phase

$$\rho_l = \rho_l(p_l, c_{pld}, c_{plm}, c_{sl}). \quad (4.23)$$

For gas phase

$$\rho_g = \rho_g(p_g, c_{sg}). \quad (4.24)$$

Capillary pressure law:

$$p_g - p_l = p_c(S_l). \quad (4.25)$$

Closure relations

For saturations:

$$S_l + S_g = 1. \quad (4.26)$$

For concentrations:

$$\rho_l = M_{mol,pld}^T c_{pld} + M_{mol,sl}^T c_{sl}, \quad (4.27)$$

$$\rho_g = M_{mol,sg}^T c_{sg}, \quad (4.28)$$

where M_{mol} is a vector such that $M_{mol,i}$ is equal to the molar mass of component i and $M_{mol,pld}$, $M_{mol,sl}$, $M_{mol,sg}$ are its sub-vectors for corresponding subsets of components.

In addition to the relations included in the physical model of two-phase multicomponent flow, in this chapter, we take into account the variation of porosity caused by the dissolution or precipitation of solid components. In chapter 2, we did not specify

this type of relations and by default we supposed that porosity was constant. In this chapter we suppose that the entire solid phase consists of chemical solid components represented in the chemical system. For this case we suppose that the density of each solid component i is a known constant $\rho_{s,i}$. Then the porosity can be found through the values of solid component concentrations by the following formula:

$$\phi(c_{ss}) = 1 - \sum_{i}^{N_{scs}} \frac{M_{mol,i} c_{ss,i}}{\rho_{s,i}}. \tag{4.29}$$

where $c_{ss,i}$ is the concentration of the solid component i.

Thus combining all the above equations we obtain a closed coupled system of equations for the following set of unknowns: phase pressures p_l, p_g, phase saturations S_l, S_g and component concentrations c_{pld}, c_{plm}, c_{sl}, c_{ss}, c_{sg}.

In the case of the gas phase disappearance the proposed system of equations keeps the same structure, except that some terms in the conservation equations for the dominant components ($L_{g,(S_g,\vec{q_g})}(c_{sg})$ and $\phi S_g c_{sg}$) become equal to zero. The set of unknowns remains the same. In the case of the liquid phase disappearance the conservation equations for the minor components completely degenerate and the considered system is no more valid, since the number of unknowns becomes bigger than the number of equations. Therefore the presented system of equations can be used only in the case when the liquid phase is present in all points of the considered domain.

In the next section we exploit the additional structure afforded by the introduction of dominant and minor components to propose a consistent decoupled algorithm.

4.3 Decoupling algorithm

4.3.1 Sequential strategy for the decoupling

In comparison with the previously deduced physical model of two-phase multicomponent flow in section 2.3.3, the final system of equations given in section 4.2.4 did not introduce any changes in the form of equations and only gives the reformulation of these equations taking into account the separation between dominant and minor components. It was already mentioned that the obtained system of equations is strongly coupled and the numerical solution of such a system faces significant computational complexity. To reduce the complexity of the problem we try to decouple the entire system in two subsystems corresponding to, respectively, the dominant and minor components such that each of them is weakly dependent on the other. In our case we want to create two subsystems for the following sets of variables:

- c_{pld}, c_{sg}, p_l, p_g, S_l, S_g on one side (dominant components system),
- c_{plm}, c_{sl}, c_{ss} on other side (minor component system).

In order to do this, first we have to make a number of assumptions that will decrease the connections between equations:

1) the gas phase density depends only on pressures and concentrations of dominant components.

2) the same assumptions are done for the liquid phase density and other physical parameters such as phase viscosities $\mu_\alpha = \mu(p_\alpha, c_{pld}, c_{sg})$.

3) we suppose that $M^T_{mol,pld} c_{pld} \gg M^T_{mol,sl} c_{sl}$ and rewrite the relation for concentrations in the liquid phase (4.27) in the following form: $\rho_l = M^T_{mol,pld} c_{pld}$.

The first assumption is a direct consequence of the previously mentioned requirements on the system that the secondary gas components participate in reactions which include **only** dominant components and only in exchange reactions with their own liquid forms. This requirement is equivalent to the gas phase density dependence on concentrations of dominant components as we have Henry's and Raoult's laws $c_{sg} = g^{-1}(c_{pld})$ and $\rho_g = \rho_g(p_g, c_{sg})$. The second and third assumptions were not mentioned before and are new to our model. In fact, these assumptions just define initially artificial separation between dominant and minor components. For example, the second assumption is equivalent to the requirement that dominant components have a strong influence on the physical parameters of flow and, in contrast, minor components do not have a significant impact on the physical parameters of system. The third assumption is equivalent to the requirement that dominant components almost completely form the liquid phase. The second and third assumptions will be valid for the system of interest in CO_2 storage as will be shown in the next section.

Now if we consider the set of the following equations: mass conservation laws for dominant components (4.18), mass action laws for gas secondary components (4.20), Darcy-Muskat's law (4.22), capillary pressure law (4.25), state equations (4.23), (4.24) and closure relations (4.26), (4.27), (4.28), we notice that the number of these equations equals the number of elements in the subset of variables for dominant components system, mentioned above. This subsystem has a similar structure as that of two-phase two-component flow except that, among this list of equations, the conservation laws for dominant components (4.18) contain terms that depend on the second set of variables $(c_{sl}, c_{ss}, c_{plm})$. These terms are $\frac{\partial(\phi S_l(\mathbb{S}^T_{lld} c_{sl}))}{\partial t} + L_{l,(S_l,q_l)}(\mathbb{S}^T_{pld} c_{sl}) + \frac{\partial(\mathbb{S}^T_{sld} c_{ss})}{\partial t}$ and also the porosity $\phi(c_{ss})$. The remaining equations (4.19), (4.21) form the sub-system of reactive transport equations for minor components and are coupled with the first subsystem through pressures, saturations and concentrations of dominant components.

To break the remaining connections between the subsystems of dominant and minor components we use a sequential solution strategy. For this we divide the entire period of simulation $[0, T]$ in time intervals $[t_n, t_{n+1}]$ such that $t_n < t_{n+1}$, $n = 0, \ldots, N$, $t_0 = 0$ and $t_N = T$. We solve at each time interval at first the sub-system of two-phase two-component flow of dominant components and then the sub-system of reactive transport equations of minor component. For the time interval $[t_n, t_{n+1}]$ we take as initial conditions for subsystems of dominant or minor component the values of corresponding subsystem variables at the time t_n obtained from the solution of the subsystems at previous time interval $[t_{n-1}, t_n]$. In the sub-system of two-phase two-component flow of dominant components, we use explicit expression for the terms $\frac{\partial(\phi S_l(\mathbb{S}^T_{lld} c_{sl}))}{\partial t} + L_{l,(S_l,q_l)}(\mathbb{S}^T_{pld} c_{sl}) + \frac{\partial(\mathbb{S}^T_{sld} c_{ss})}{\partial t}$ and porosity $\phi(c_{ss})$ at time t_n from the result of sub-system of reactive transport equations of minor component obtained for previous time interval $[t_{n-1}, t_n]$. In the sub-system of reactive transport equations of minor components we use explicit expression of the liquid phase velocity $\overrightarrow{q}_l$ and the liquid phase saturation S_l at time t_{n+1} obtained from the result of the sub-system of two-phase two-component flow of dominant components calculated at the same time interval $[t_n, t_{n+1}]$

to construct the linear operator L_l. Thereby the sequential strategy for solution for two-phase multicomponent flow with reactive transport is to solve sequentially at each time interval $[t_n, t_{n+1}]$.

To demonstrate the proposed algorithm we consider in detail the form of each subsystem for the time interval $[t_n, t_{n+1}]$ under the assumption that the values of system variables are already known for time $[0, t_n]$.

4.3.2 Two-phase two-component flow sub-problem.

The system of equations devoted to two-phase two-component flow subproblem consists of the following equations:

Conservation laws for dominant components:

$$\frac{\partial(\phi^n S_l c_{pld})}{\partial t} + \frac{\partial(\phi^n S_g c_{sg})}{\partial t} + L_{l,(S_l,\overrightarrow{q}_l)}(c_{pld}) + L_{g,(S_g,q_g)}(c_{sg}) = R^n, \tag{4.30}$$

where

$$R^n = -\frac{\partial(\phi S_l(\mathbb{S}_{lld}^T c_{sl}))}{\partial t} - L_{l,(S_l^n,\overrightarrow{q}_l)}(\mathbb{S}_{lld}^T c_{sl}) - \frac{\partial(\mathbb{S}_{sld}^T c_{ss})}{\partial t}, \tag{4.31}$$

and porosity $\phi^n = 1 - \sum_i^{N_{scs}} \frac{M_{mol,i} c_{ss,i}}{\rho_{s,i}}$ are evaluated at time t_n, using quantities computed in the second subproblem 4.3.3 on the previous time interval $[t_{n-1}, t_n]$.

Mass action laws for gas secondary components: Henry's law and Raoult's law

$$c_{pld} = g(c_{sg}), \tag{4.32}$$

Capillary pressure law:

$$p_g - p_l = p_c(S_l). \tag{4.33}$$

Closure relations

For saturations:

$$S_l + S_g = 1. \tag{4.34}$$

For concentrations:

$$\rho_l = M_{mol,pd}^T c_{pld}, \tag{4.35}$$

$$\rho_g = M_{mol,scg}^T c_{sg}. \tag{4.36}$$

The final system of equations (4.30), (4.32), (4.33) (4.34), (4.35), (4.36) forms the sub-problem of two-phase two-component flow considered in section 2.4. To compute the solution of this problem on the interval $[t_n, t_{n+1}]$ we fix the initial conditions of the system variables c_{pld}, c_{sg},p_l, p_g, S_l, S_g at time t_n and use the numerical simulator for two-phase two-component flow problem described in section 3.3.1 which can choose his own time discretization of time interval $[t_n, t_{n+1}]$.

4.3.3 Reactive transport sub-problem.

The system of equations devoted to reactive transport subproblem consists of the following equations:

Conservation laws for minor components:

$$\frac{\partial(\phi S_l^{n+1} c_{plm})}{\partial t} + \frac{\partial(\phi S_l^{n+1}(\mathbb{S}_{llm}^T c_{sl}))}{\partial t} + \frac{\partial(\mathbb{S}_{slm}^T c_{ss})}{\partial t} + L_l^{n+1}(c_{plm} + \mathbb{S}_{llm}^t c_{sl}) = 0, \quad (4.37)$$

where S_l^{n+1}, $\overrightarrow{q}_l^{n+1}$ are the values of the liquid saturation and the liquid phase velocity at time t_{n+1} calculated in two-phase two-component flow sub-problem at the time interval $t_n \longrightarrow t_{n+1}$, $L_l^{n+1} = L_{l,(S_l^{n+1}, \overrightarrow{q}_l^{n+1})}$ is the liquid phase transport operator constructed from given value of the liquid saturation S_l^{n+1} and the liquid phase velocity $\overrightarrow{q}_l^{n+1}$ previously computed in the first subproblem 4.3.2 at the same time interval $[t_n, t_{n+1}]$.

Mass action laws for liquid and solid secondary components

$$\begin{cases} \log \hat{c}_{sl} &= \log K_l + \mathbb{S}_{lld} \log \hat{c}_{pld}^{n+1} + \mathbb{S}_{llm} \log \hat{c}_{plm}, \\ \log \hat{c_{ss}} &= \log K_s + \mathbb{S}_{sld} \log \hat{c}_{pld}^{n+1} + \mathbb{S}_{slm} \log \hat{c}_{plm}, \end{cases} \quad (4.38)$$

where $\hat{c}_{pld}^{n+1}$ are the values of dominant liquid component activities at time t_{n+1} calculated in two-phase two-component flow sub-problem at the time interval $[t_n, t_{n+1}]$.

The final system of equations (4.37), (4.38) forms the sub-problem of reactive transport considered in section 2.5. To compute the solution of this problem on the interval $[t_n, t_{n+1}]$ we fix the initial conditions of system variables c_{plm}, c_{sl}, c_{ss} at time t_n and use numerical simulator for reactive transport problem described in section 3.6.3 can choose his own time discretization of time interval $[t_n, t_{n+1}]$. After computation we can calculate the new values of right hand term R^{n+1} and porosity ϕ^{n+1}.

4.3.4 Numerical algorithm.

The general scheme of numerical sequential algorithm proposed in this section is demonstrated at the Figure 4.1.

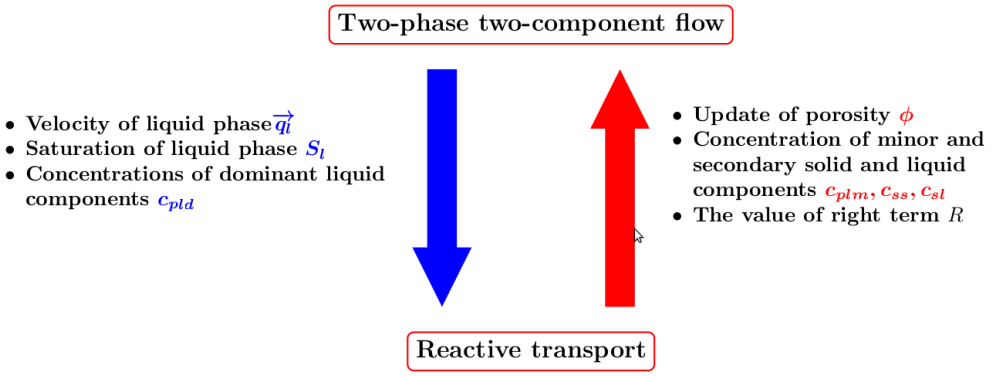

Figure 4.1: Sequential algorithm. Exchange of data (coupling) between flow and reactive transport sub-problems.

There were several coupling terms that we neglected (mass of secondary liquid components in liquid density relation $M^T_{mol,sl}c_{sl}$, physical parameter dependence from concentrations of minor and secondary components), or threated explicitly to arrive at the decoupled system just described. The remaining coupling terms have different influence on the solution. From one side, the reactive transport sub-problems is heavily dependent on the solution of two-phase two-component flow sub-problem. The configuration of liquid flow, the values of dominant component concentrations and liquid phase saturation directly affect on the transport equations. From other side, the inverse connection between subproblems is much weaker. In practice mass changes of dominant components arising from chemical reaction and expressed in form of the right hand side term R are often negligible. At the same time, during dissolution process of secondary solid components, only very small amounts of minerals are transferred to the liquid form and therefore the change in the porosity caused by this process is relatively small. For these reasons, the originally proposed algorithm can be modified to reduce computational complexity without substantial loss in accuracy.

We have tested two variants of such modifications:

- one in which the R^n terms were included, and treated explicitly as in section 4.3.2,
- and one where these terms were simply set to zero.

We compared the two variants on the SHPCO2 example described in section 4.5.1, and found no significant difference between the two results (see remark in Section 4.5.1.3). In the simulations presented later we have used the simplest variant with $R^n = 0$.

Actually, the most important source of coupling from the reactive transport on the flow in performed tests was through the change of porosity, coming from the dissolution/precipitation of minerals.

4.4 Application to geological storage of CO_2

4.4.1 Chemical system. Dominant and minor components

To simulate geological storage of CO_2 we use the chemical system described in SHPCO2 benchmark considered in section 3.6.4.4. But in comparison with the test case in section 3.6.4.4, here we add the process of water vaporization. This difference is explained by the fact that SHPCO2 benchmark considered in section 3.6.4.4 was adapted to one-phase transport in the liquid phase and in this case $H_2O_{(g)}$ was simply neglected. So the chemical system has an additional component $H_2O_{(g)}$ and the full list of components is given in Table 4.1.

Liquid phase (l)	Gas phase (g)	Solid phase (s)
$H_2O_{(l)}$, $CO_{2(l)}$, H^+, OH^-, HCO_3^-, Ca^{2+}	$CO_{2(g)}$, $H_2O_{(g)}$	$CaCO_3$

Table 4.1: Chemical components.

Also we have an additional reaction of water inter-phase exchange. The full list of chemical reactions is the following:

- 2 homogeneous (aqueous) equilibrium reactions

$$\begin{aligned} OH^- &\rightleftharpoons H_2O_{(l)} - H^+, \\ HCO_3^- &\rightleftharpoons H_2O_{(l)} - H^+ + CO_{2(l)}, \end{aligned} \tag{4.39}$$

- 3 heterogeneous equilibrium reactions:

$$\begin{aligned} CaCO_3 &\rightleftharpoons H_2O_{(l)} - 2H^+ + CO_{2(l)} + Ca^{2+}, \\ H_2O_{(g)} &\rightleftharpoons H_2O_{(l)}, \\ CO_{2(g)} &\rightleftharpoons CO_{2(l)}. \end{aligned} \tag{4.40}$$

In the considered chemical system the gas phase is formed by two components: $CO_{2(g)}$ and $H_2O_{(g)}$. By Henry's and Raoult's laws their concentrations are coupled with concentrations of their liquid states $CO_{2(l)}$, $H_2O_{(l)}$. Thereby the density state equation for the gas phase depends on the components $CO_{2(l)}$, $H_2O_{(l)}$.

The liquid phase is formed almost entirely of water $H_2O_{(l)}$ and dissolved carbon dioxide $CO_{2(l)}$. The remaining components are dissolved in water. In practice, $CO_{2(l)}$ has the highest concentration among dissolved components. The components of H^+, OH^-, HCO_3^-, Ca^{2+} have orders of magnitude lower concentration then water. For this reason, in such a system we can assume that the state density equation of liquid phase depends only on concentration of two components $CO_{2(l)}$ and $H_2O_{(l)}$.

Based on the foregoing discussion, we can conclude that for the realization of sequential strategy for the considered chemical system we should choose $CO_{2(l)}$ and $H_2O_{(l)}$ as primary dominant components. With such a choice $c_{pld} = \left(c_{H_2O_{(l)}}, \quad c_{CO_{2(l)}}\right)^T$. H^+ and Ca^{2+} complete the list of primary components and are called primary minor components $c_{plm} = \left(c_{H^+}, \quad c_{Ca^{2+}}\right)^T$. The secondary components are divided into three groups accordingly to their phase: liquid secondary components $c_{sl} = \left(c_{OH^-}, \quad c_{HCO_3^-}\right)^T$, gas secondary components $c_{sg} = \left(c_{H_2O_{(g)}}, \quad c_{CO_{2(g)}}\right)^T$ and solid secondary components $c_{ss} = \left(c_{CaCO_3}\right)^T$.

The stoichiometric matrix for the full vector of concentrations $(c_{OH^-}, c_{HCO_3^-}, |c_{CaCO_3}, |c_{H_2O_{(g)}}, c_{CO_{2(g)}}, |c_{H_2O_{(l)}}, c_{CO_{2(l)}}, |c_{H^+}, c_{Ca^{2+}})^T$ has the following form:

$$\mathbb{S}_e = \left(\begin{array}{cc|c|cc|cc|cc} -1 & 0 & 0 & 0 & 0 & 1 & 0 & -1 & 0 \\ 0 & -1 & 0 & 0 & 0 & 1 & 1 & -1 & 0 \\ \hline 0 & 0 & -1 & 0 & 0 & 1 & 1 & -2 & 1 \\ \hline 0 & 0 & 0 & -1 & 0 & 1 & 0 & 0 & 0 \\ 0 & 0 & 0 & 0 & -1 & 0 & 1 & 0 & 0 \end{array}\right). \tag{4.41}$$

The blocks of columns of the stoichiometric matrix correspond to the arrangement in the concentration vector $c = (c_{sl}, c_{ss}, c_{sg}, c_{pld}, c_{plm})$. The separation of matrix in blocks is the same as in 4.3 (for example $\mathbb{S}_{lld} = \begin{pmatrix} 1 & 0 \\ 1 & 1 \end{pmatrix}$).

The vector of reaction terms $r_e = (r_l, r_s, r_g)^T$ is divided in three sub-vectors which correspond to different types of chemical reactions: $r_l = (r_{OH^-}, r_{HCO_3^-})^T$ are rates of homogeneous liquid reactions that produce secondary liquid components, $r_s = (r_{CaCO_3})$ is rate of heterogeneous reaction that forms solid secondary component and $r_g = (r_{H_2O_{(g)}}, r_{CO_{2(g)}})^T$ are rates of heterogeneous reactions of liquid-gas phase exchange.

We now carry out the elimination procedure explained in section 4.2.3 in the particular case of the considered chemical system. This will help to better understand how this procedure works in practice.

4.4.2 Balance equations

For each component of the chemical system, we can write the following balance equations:

$$\begin{array}{lcccccl}
OH^- & : & \partial_t(\phi S_l c_{OH^-}) & + & L_l(c_{OH^-}) & = & -r_{OH^-}, \\
HCO_3^- & : & \partial_t(\phi S_l c_{HCO_3^-}) & + & L_l(c_{HCO_3^-}) & = & -r_{HCO_3^-}, \\
CaCO_3 & : & & & \partial_t c_{CaCO_3} & = & -r_{CaCO_3}, \\
H_2O_{(g)} & : & \partial_t(\phi S_g c_{H_2O_{(g)}}) & + & L_g(c_{H_2O_{(g)}}) & = & -r_{H_2O_{(g)}}, \\
CO_{2(g)} & : & \partial_t(\phi S_g c_{CO_{2(g)}}) & + & L_g(c_{CO_{2(g)}}) & = & -r_{CO_{2(g)}}, \\
H_2O_{(l)} & : & \partial_t(\phi S_l c_{H_2O_{(l)}}) & + & L_l(c_{H_2O_{(l)}}) & = & r_{OH^-} + r_{CaCO_3} + r_{HCO_3^-} + r_{H_2O_{(g)}}, \\
CO_{2(l)} & : & \partial_t(\phi S_l c_{CO_{2(l)}}) & + & L_l(c_{CO_{2(l)}}) & = & r_{HCO_3^-} + r_{CO_{2(g)}} + r_{CaCO_3}, \\
H^+ & : & \partial_t(\phi S_l c_{H^+}) & + & L_l(c_{H^+}) & = & -r_{OH^-} - 2r_{CaCO_3} - r_{HCO_3^-}, \\
Ca^{2+} & : & \partial_t(\phi S_l c_{Ca^{2+}}) & + & L_l(c_{Ca^{2+}}) & = & r_{CaCO_3}
\end{array} \tag{4.42}$$

where the operators L_l, L_g are defined in (4.11), (4.13).

4.4.3 Elimination procedure. Total concentrations.

The reaction rates of the equilibrium reactions in the right terms of the balance equations (4.42) are unknown. To eliminate reaction terms, we use linear combination of balance equations represented by matrix $\mathbb{U}$. The elimination procedure was described in detail in section 2.3.2. For the considered chemical system, the matrix $\mathbb{U}$ has the following view:

$$\mathbb{U} = \begin{pmatrix} \mathbb{S}_{lld}^T & \mathbb{S}_{sld}^T & \mathbb{S}_{gld}^T & \mathbb{I} & 0 \\ \mathbb{S}_{llm}^T & \mathbb{S}_{slm}^T & 0 & 0 & \mathbb{I} \end{pmatrix} = \left(\begin{array}{cc|c|cc|cc|cc} 1 & 1 & 1 & 1 & 0 & 1 & 0 & 0 & 0 \\ 0 & 1 & 1 & 0 & 1 & 0 & 1 & 0 & 0 \\ \hline -1 & -1 & -2 & 0 & 0 & 0 & 0 & 1 & 0 \\ 0 & 0 & 1 & 0 & 0 & 0 & 0 & 0 & 1 \end{array}\right). \tag{4.43}$$

Applying the linear combination represented by the matrix $\mathbb{U}$, we obtain a new reduced set of balance equations for the total concentrations of the primary components $T = U\theta c = U\theta(M_l + M_s + M_g)c = \phi S_l T_l + T_s + \phi S_g T_g$ (section 2.3.2):

$$
\begin{aligned}
H_2O_{(l)} \quad &: \quad \tfrac{\partial}{\partial t}(\phi S_l T_{l,H_2O_{(l)}} + T_{s,H_2O_{(l)}} + \phi S_g T_{g,H_2O_{(l)}}) + L_l(T_{l,H_2O_{(l)}}) + L_g(T_{g,H_2O_{(l)}}) = 0,\\
\text{where} \quad & T_{H_2O_{(l)}} = \phi S_l (c_{H_2O_{(l)}} + c_{OH^-} + c_{HCO_3^-}) + c_{CaCO_3} + \phi S_g c_{H_2O_{(g)}}\\
& \qquad\qquad = \phi S_l T_{l,H_2O_{(l)}} + T_{s,H_2O_{(l)}} + \phi S_g T_{g,H_2O_{(l)}},\\
CO_{2(l)} \quad &: \quad \tfrac{\partial}{\partial t}(\phi S_l T_{l,CO_{2(l)}} + T_{s,CO_{2(l)}} + \phi S_g T_{g,CO_{2(l)}}) + L_l(T_{l,CO_{2(l)}}) + L_g(T_{g,CO_{2(l)}}) = 0,\\
\text{where} \quad & T_{CO_{2(l)}} = \phi S_l (c_{CO_{2(l)}} + c_{HCO_3^-}) + c_{CaCO_3} + \phi S_g c_{CO_{2(g)}}\\
& \qquad\qquad = \phi S_l T_{l,CO_{2(l)}} + T_{s,CO_{2(l)}} + \phi S_g T_{g,CO_{2(l)}},\\
H^+ \quad &: \quad \tfrac{\partial}{\partial t}(\phi S_l T_{l,H^+} + T_{s,H^+}) + L_l(T_{l,H^+}) = 0,\\
\text{where} \quad & T_{H^+} = \phi S_l (c_{H^+} - c_{OH^-} - c_{HCO_3^-}) - 2c_{CaCO_3}\\
& \qquad\qquad = \phi S_l T_{l,H^+} + T_{s,H^+},\\
Ca^{2+} \quad &: \quad \tfrac{\partial}{\partial t}(\phi S_l T_{l,Ca^{2+}} + T_{s,Ca^{2+}}) + L_l(T_{l,Ca^{2+}}) = 0,\\
\text{where} \quad & T_{Ca^{2+}} = \phi S_l c_{Ca^{2+}} + c_{CaCO_3}\\
& \qquad\qquad = \phi S_l T_{l,Ca^{2+}} + T_{s,Ca^{2+}}.
\end{aligned}
\tag{4.44}
$$

4.4.4 Mass actions law

The set of balance equations for the total concentrations of primary components contains five less equations then unknowns. The missing equations are replaced by mass action laws of equilibrium chemical reactions for secondary components:

$$
\begin{aligned}
OH^- \quad &: \quad \log \hat{c}_{OH^-} = \log K_{OH^-} + \log \hat{c}_{H_2O_{(l)}} - \log \hat{c}_{H^+},\\
HCO_3^- \quad &: \quad \log \hat{c}_{HCO_3^-} = \log K_{HCO_3^-} + \log \hat{c}_{H_2O_{(l)}} - \log \hat{c}_{H^+} + \log \hat{c}_{CO_{2(l)}},\\
H_2O_{(g)} \quad &: \quad \log \hat{c}_{H_2O_{(g)}} = \log K_{H_2O_{(g)}} + \log \hat{c}_{H_2O_{(l)}},\\
CO_{2(g)} \quad &: \quad \log \hat{c}_{CO_{2(g)}} = \log K_{CO_{2(g)}} + \log \hat{c}_{CO_{2(l)}},\\
CaCO_3 \quad &: \quad \log \hat{c}_{CaCO_3} = \log K_{CaCO_3} + \log \hat{c}_{H_2O_{(l)}} - 2\log \hat{c}_{H^+} + \log \hat{c}_{CO_{2(l)}} + \log \hat{c}_{Ca^{2+}}.
\end{aligned}
\tag{4.45}
$$

We assume that the dissolved liquid components (OH^-, HCO_3^-, H^+, $CO_{2(l)}$) in the first and second reactions have ideal activity ($\hat{c}_i = c_i$). The water $H_2O_{(l)}$ activity in these reactions is fixed to one ($\hat{c}_{H_2O_{(l)}} = 1$).

The activity model of components that participate in third and fourth gas-liquid inter-phase reactions was described in section 2.4.5:

$$
\begin{aligned}
\widehat{c}_{H_2O_{(g)}} &= \Phi_{H_2O_{(g)}} p_g x_g^{H_2O},\\
\widehat{c}_{CO_{2(g)}} &= \Phi_{CO_{2(g)}} p_g x_g^{CO_2},\\
\widehat{c}_{H_2O_{(l)}} &= \gamma_{H_2O_{(l)}} x_l^{H_2O},\\
\widehat{c}_{CO_{2(l)}} &= \gamma_{CO_{2(l)}} x_l^{CO_2},
\end{aligned}
\tag{4.46}
$$

where $\Phi_i(p_g, T)$ is the fugacity coefficient of the gas component i for the CO_2-H_2O mixture, γ_i is the activity coefficient of the liquid component i. The function g defined

in (4.8) has the following form:

$$g(c_{H_2O_{(g)}}, c_{CO_{2(g)}}) = g_2(g_1(c_{H_2O_{(g)}}, c_{CO_{2(g)}})) \tag{4.47}$$

where $g_1(c_{H_2O_{(g)}}, c_{CO_{2(g)}}) = \begin{pmatrix} \frac{\Phi_{H_2O_{(g)}}}{\gamma_{H_2O_{(l)}} K_{H_2O_{(g)}}} p_g \frac{c_g^{H_2O_{(g)}}}{c_{CO_{2(g)}} + c_{H_2O_{(g)}}} \\ \frac{\Phi_{CO_{2(g)}}}{\gamma_{CO_{2(l)}} K_{CO_{2(g)}}} p_g \frac{c_g^{CO_2}}{c_{CO_{2(g)}} + c_{H_2O_{(g)}}} \end{pmatrix}$ and g_2 calculates the value of the component concentrations from the values of component molar fractions $g_2(x_{H_2O_{(l)}}, x_{CO_{2(l)}}) = \begin{pmatrix} \frac{\rho_l x_{H_2O_{(l)}}}{M_{H_2O} x_{H_2O_{(l)}} + M_{CO_2} x_{CO_{2(l)}}} \\ \frac{\rho_l x_{CO_{2(l)}}}{M_{H_2O} x_{H_2O_{(l)}} + M_{CO_2} x_{CO_{2(l)}}} \end{pmatrix}$.

The fifth chemical reaction is heterogeneous precipitation-dissolution reaction for the mineral calcite ($CaCO_3$). Modelling of such type of reaction was described in section 3.4.1.2. The liquid dissolved components (H^+, $CO_{2(l)}$, Ca^{2+}) of this reaction have an ideal activity, while the activity of water $H_2O_{(l)}$ and calcite $CaCO_3$ are fixed and equal to one.

4.4.5 Final system of equations. Decoupling procedure

The final coupled system of equations for the considered chemical system consists of the following list of equations:

- Balance equations for total concentrations of primary components (4.44),
- Mass action laws (4.45),
- Capillary pressure law $p_c(S_l) = p_g - p_l$,
- Closure relation for liquid and gas phase densities (4.35), (4.36),
- Closure relation for phases composition $S_l + S_g = 1$.

In the considered chemical system we assume that the solid phase is formed completely by calcite $CaCO_3$. For this reason the porosity of the media depends on calcite concentration under the condition of constant calcite density - $\rho_{CaCO_3} = 2700$ kg/m^3:

$$\phi(c_{CaCO_3}) = 1 - \frac{c_{CaCO_3} M_{CaCO_3}}{\rho_{CaCO_3}}. \tag{4.48}$$

The unknowns of the obtained system are $c_{OH^-}, c_{HCO_3^-}, c_{CaCO_3}, c_{H_2O_{(g)}}, c_{CO_{2(g)}}, c_{H_2O_{(l)}}, c_{H_2O_{(l)}}$, $c_{H^+}, c_{Ca^{2+}}, p_l, p_g, S_l, S_g$.

In the considered physical model the viscosity of the liquid phase depends only on the concentrations of water and dissolved carbon dioxide. Therefore all three assumptions proposed in the previous section are valid, and we can perform the decoupling procedure. To realize the decoupling algorithm proposed in the previous section for the general case, we group the equation into two subsets that correspond to dominant and minor components. Further, we specify these subsets of equations for geological storage of CO_2.

4.4.5.1 Subset of dominant components

The system for the subset of dominant components is formed by the following equations:

1) the balance equation for the total concentration of water H_2O (4.30):

$$\begin{aligned} \frac{\partial(\phi(S_l c_{H_2O_{(l)}} + S_g c_{H_2O_{(g)}}))}{\partial t} &+ L_{l,(S_l,\vec{q_l})}(c_{H_2O_{(l)}}) + L_{g,(S_g,\vec{q_g})}(c_{H_2O_{(g)}}) \\ &= R_{H_2O}(c_{OH^-}, c_{HCO_3^-}, c_{CaCO_3}, p_l, S_l) \end{aligned} \tag{4.49}$$

where $R_{H_2O} = -\dfrac{\partial(\phi S_l(c_{OH^-} + c_{HCO_3^-}))}{\partial t} - \dfrac{\partial c_{CaCO_3}}{\partial t} - L_{l,(S_l,\vec{q}_l)}(c_{OH^-} + c_{HCO_3^-})$,

2) the balance equation for the total concentration of carbon dioxide CO_2 (4.30):

$$\begin{aligned} \frac{\partial(\phi(S_l c_{CO_{2(l)}} + S_g c_{CO_{2(g)}}))}{\partial t} &+ L_{l,(S_l,\vec{q_l})}(c_{CO_{2(l)}}) + L_{g,(S_g,\vec{q_g})}(c_{CO_{2(g)}}) \\ &= R_{CO_2}(c_{HCO_3^-}, c_{CaCO_3}, p_l, S_l) \end{aligned} \tag{4.50}$$

where $R_{CO_2} = -\dfrac{\partial(\phi S_l c_{HCO_3^-})}{\partial t} - \dfrac{\partial c_{CaCO_3}}{\partial t} - L_{l,(S_l,\vec{q}_l)}(c_{HCO_3^-})$,

3) the mass action law for the water exchange reaction (Henry's law (4.32)):

$$\log \hat{c}_{H_2O_{(g)}} = \log K_{H_2O_{(g)}} + \log \hat{c}_{H_2O_{(l)}}, \tag{4.51}$$

4) the mass action law for the carbon dioxide exchange reaction (Raoult's law (4.32)):

$$\log \hat{c}_{CO_{2(g)}} = \log K_{CO_{(g)}} + \log \hat{c}_{CO_{2(l)}}, \tag{4.52}$$

5) the capillary pressure law (4.33):

$$p_c(S_l) = p_g - p_l, \tag{4.53}$$

6) the density state equations for the liquid and the gas phases (4.35), (4.36) :

$$\begin{aligned} \rho_l(p_l) &= M_{H_2O_{(l)}} c_{H_2O_{(l)}} + M_{CO_{2(l)}} c_{CO_{2(l)}}, \\ \rho_g(p_g) &= M_{H_2O_{(g)}} c_{H_2O_{(g)}} + M_{CO_{2(g)}} c_{CO_{2(g)}}. \end{aligned} \tag{4.54}$$

7) closure relation for phase composition

$$S_l + S_g = 1 \tag{4.55}$$

4.4.5.2 Subset of minor components

The system for the subset of minor components is formed by the following equations:

1) the balance equation for the total concentration of ion hydrogen H^+ (4.37):

$$\frac{\partial}{\partial t}\left(\phi S_l(c_{H^+}-c_{OH^-}-c_{HCO_3^-})-2c_{CaCO_3}\right)+L_{l,(S_l,\overrightarrow{q_l})}(c_{H^+}-c_{OH^-}-c_{HCO_3^-})=0, \quad (4.56)$$

2) the balance equation for the total concentration of ion calcium Ca^{2+} (4.37):

$$\frac{\partial}{\partial t}\left((\phi S_l c_{Ca^{2+}})+c_{CaCO_3}\right)+L_{l,(S_l,\overrightarrow{q_l})}(c_{Ca^{2+}})=0, \quad (4.57)$$

3) the mass action law for the water dissociation (4.38):

$$\log \hat{c}_{OH^-}=\log K_{OH^-}-\log \hat{c}_{H^+}+\Psi_{OH^-}(c_{H_2O_{(l)}}), \quad (4.58)$$

where $\Psi_{OH^-}=\log \hat{c}_{H_2O_{(l)}}$,

4) the mass action law for the CO_2 dissolution (4.38):

$$\log \hat{c}_{HCO_3^-}=\log K_{HCO_3^-}-\log \hat{c}_{H^+}+\Psi_{HCO_3^-}(c_{H_2O_{(l)}},c_{CO_{2(l)}}), \quad (4.59)$$

where $\Psi_{HCO_3^-}=\log \hat{c}_{H_2O_{(l)}}+\log \hat{c}_{CO_{2(l)}}$,

5) the mass action law for the precipitation-dissolution of the mineral $CaCO_3$ (4.38):

$$\log \hat{c}_{CaCO_3}=\log K_{CaCO_3}-2\log \hat{c}_{H^+}+\log \hat{c}_{Ca^{2+}}+\Psi_{CaCO_3}(c_{H_2O_{(l)}},c_{CO_{2(l)}}), \quad (4.60)$$

where $\Psi_{CaCO_3}=\log \hat{c}_{H_2O_{(l)}}+\log \hat{c}_{CO_{2(l)}}$.

4.4.6 Decoupling strategy

The subset of equations for the dominant components, under the condition of explicit expression of the functions R_{H_2O}, R_{CO_2} and the calcite concentration c_{CaCO_3} (required for calculation of the porosity value (4.29)) from the result of reactive transport for minor components, forms a closed system of equations for two-phase two-component flow (H_2O-CO_2). The list of system unknowns is the concentrations of dominant component $c_{H_2O_{(g)}}$, $c_{CO_{2(g)}}$, $c_{H_2O_{(l)}}$, $c_{H_2O_{(l)}}$, the phase pressures p_l, p_g and the saturations S_l, S_g. From the values of the phase pressures we also can compute the phase velocities $\overrightarrow{q_l}$, $\overrightarrow{q_g}$ and configuration of the linear operators L_l, L_g.

The subset of equations for the minor components, under the condition of explicit expression of function Ψ_{OH^-}, $\Psi_{HCO_3^-}$, Ψ_{CaCO_3} , the liquid phase velocity $\overrightarrow{q_l}$ and the liquid phase saturation S_l from the result of two-phase two-component flow for the dominant components H_2O and CO_2, forms the closed system of equations for reactive transport of minor components H^+ and Ca^{2+}. The list of system unknowns is the concentrations of the dominant component c_{H^+}, $c_{Ca^{2+}}$, c_{OH^-}, $c_{HCO_3^-}$, c_{CaCO_3}.

4.4.7 Modifications and implementation in DuMu^X

As was already mentioned in section 4.3.1, for simulation of two-phase multicomponent flow with reactive transport in porous media we propose a sequential algorithm. The numerical simulator based on this algorithm contains three main blocks:

Global time management block. This block contains the realization of the main loop of the sequential algorithm. It divides the entire simulation time in necessary number of time intervals. In this block we should consequently pass from one time interval to another and execute numerical simulators for each sub-problems at each time interval with all necessary input data such as initial values of system variables, values of the right term R^n, the liquid phase velocity $\overrightarrow{q}_l^{n+1}$, the liquid phase saturation S_l^{n+1}, the concentration of dominant or minor components. At the end of sub-problems simulation at each time interval, the global time management block extracts the values of the necessary system variables at the final time of considered interval.

Two-phase two-component flow sub-problem block. This block finds the solution of two-phase two-component flow at the necessary time interval with given initial values of system variables, the right hand side term R^n, the minor and the secondary liquid and solid component concentrations c_{plm}, c_{sl}, c_{ss}, the porosity ϕ^n.

Reactive transport sub-problem block. This block finds the solution of reactive transport at the necessary time interval with given initial values of system variables, the liquid phase saturation S^{n+1}, the liquid phase velocity $\overrightarrow{q}_l^{n+1}$, the dominant component concentrations c_{pld}.

The numerical simulators appropriate for two-phase two-component flow problem and reactive transport problem were already developed and demonstrated in the previous chapter (section 3.3.1 and section 3.6.3). Each of these numerical simulators was realised in the forms of DuMu^X modules **2p2c** for two-phase two-component flow and **1pNc** for reactive transport. These simulators have been adapted to the requirements of the sequential algorithm: there was added in the module **1pNc** the possibility to compute external spatial fields such as the right term source R and the porosity ϕ for actual values of saturation, the liquid phase velocity, the concentrations of minor primary and secondary components. Since the simulators for sub-problems were developed in DuMu^X software environment, the global time management block was also realised in the same environment in form of the module **modelcoupling**. This module is responsible for the realisation of the time step in the main loop of the sequential algorithm. This part of the code choose appropriate time step and exchanges data between the two sub-problems. As was already mentioned in section 4.3.4, we have tested two variants of numerical algorithms with the term R computed in the reactive transport module and term $R = 0$. In practice we found out that presence of term do not have significant influence of the flow, and therefore in the application examples presented in the following section we use the variant of numerical simulator in which the global time management block replaces the value of term R by zero.

4.5 Application examples

4.5.1 SHPCO2 Benchmark

4.5.1.1 Test description.

To test case the elaborated numerical simulator, we choose the SHPCO2 Benchmark which was developed to study the process of CO_2 storage. The chemical system used in this benchmark was already described in section 4.4.

As it was explained in section 4.4, the primary components of the chemical system was divided into two groups: the dominant (CO_2 and H_2O) and the minor (H^+ and Ca^{2+}) components. The balance equations for the total concentrations of the dominant components and the mass action laws of phase exchange reactions with the gas secondary components coupled with the dominant components form the first subproblem of two-phase two-component flow. The balance equations for the total concentrations of the minor components and the mass action laws for the secondary liquid and solid components form the second subproblem of reactive transport. Besides the list of components, given in section 4.4, in this test case we incorporate an additional liquid chemical component Cl. The new component doesn't participate in any chemical component and its presence has no influence on any physical parameters of the system. Cl performs the role of the tracer component in the system and should demonstrate the referential concentration evolution of liquid component under the influence of the diffusion and the advection forces. Cl is included in the group of minor primary component. The balance equation for Cl

$$\frac{\partial}{\partial t}(\phi S_l c_{\mathrm{Cl}}) + L_{l,(S_l,\overrightarrow{q_l})}(c_{\mathrm{Cl}}) = 0, \tag{4.61}$$

is added to the system of equations of the second subproblem.

The mathematical model of the mass action laws involved in the first subproblem of two-phase two-component flow is described in section 2.4.5. The activity of chemical component represented in the second subproblem of reactive transport can be ideal (OH^-, HCO_3^-, H^+, $CO_{2(l)}$, Ca^{2+}, Cl) or fixed to constant one (H_2O, $CaCO_3$). The values of equilibrium constants of chemical reactions for reactive transport subproblem are represented in Morel's tableau (Table 4.2).

	H_2O	H^+	$CO_{2(l)}$	Ca^{2+}	Cl	$\log K$
OH^-	1	-1	0	0	0	-13.2354
HCO_3^-	1	-1	1	0	0	-6.22
$CaCO_3$	1	-2	1	1	0	-7.7454
Total	T_{H_2O}	T_{H^+}	$T_{CO_{2(l)}}$	$T_{Ca^{2+}}$	T_{Cl}	

Table 4.2: Morel's tableau for the SHPCO2 Benchmark.

The values of the equilibrium constants $\log K$ are given under the condition that we use mol/l as units for concentration of components.

In this test, we consider a two-dimensional rectangular domain that represents the horizontal section of a three-dimensional volume of the medium. The geometry of this domain is shown in Figure 4.2.

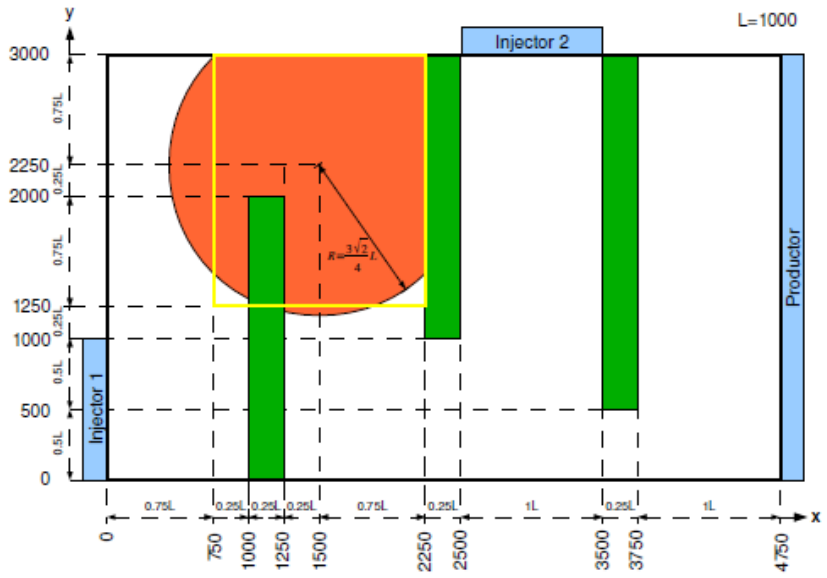

Figure 4.2: Geometry of the domain for the SHPCO2 Benchmark.

The domain is divided into two zones:

- a "barrier" zone with low permeability, marked by green color in Figure 4.2,
- a "drain" zone with high permeability which comprises the rest of the domain.

Since all points of the domain have the same depth, the velocity of the liquid phase doesn't depend on the gravity force:

$$\overrightarrow{q_l} = -\frac{k_{rl}}{\mu_l} K(\nabla p_l). \tag{4.62}$$

Since for numerical simulations we use a sequential algorithm and divide the original problem in two sub-problems, we need to formulate boundary conditions for each subproblem.

The first subproblem of two-phase two-component H_2O-CO_2 flow has the following boundary conditions:

- the parts of the boundary marked as "Injector1", "Injector2", "Productor" have Dirichlet conditions such that the liquid saturation $S_l = 1$, the liquid CO_2 concentration $c_{CO_2(l)} = 0$ mol/l, $p_{injector1} = 1.0\ 10^7$ Pa, $p_{injector2} = 1.05\ 10^7$ Pa, $p_{productor} = 1.1\ 10^7$ Pa,
- the rest of the boundary has Neumann impermeable conditions (no flow).

According to the velocity obtained from two-phase two component H_2O-CO_2 flow we choose the following boundary conditions for reactive transport flow:

- the parts of the boundary marked as "Injector1", "Injector2" have Dirichlet conditions such that the total liquid concentrations of the primary components are equal to initial values,

- the part of the boundary marked as "Productor" has no boundary conditions since $\overrightarrow{q_l} \cdot \overrightarrow{n}_{|"Productor"} > 0$,
- the rest of the boundary has Neumann impermeable conditions (no flow).

As initial conditions for two-phase two-component H_2O-CO_2 flow we use:

- in the zone of CO_2 injection marked by orange color in Figure 4.2, initial liquid saturation $S_l = 0.8$,
- in the rest of the domain, initial liquid saturation $S_l = 1$ and initial CO_2 concentration in the liquid phase $c_{CO_2(l)} = 0$ mol/l.

Initial conditions for the reactive transport are represented in Table 4.3 for zone of CO_2 injection and in Table 4.4 for the rest part of the domain:

	conc. mol/l	total conc. mol/l	total liquid conc. mol/l	total solid conc. mol/l
H^+	$2.596\ 10^{-5}$	-43.36	$-2.597\ 10^{-2}$	-43.36
Ca^{2+}	$3.343\ 10^{-2}$	21.68	$3.343\ 10^{-2}$	21.68
Cl	2.0	2.0	2.0	0.0

Table 4.3: Initial conditions of reactive transport in zone of CO_2 injection for the SHPCO2 Benchmark. **Note**: the total concentration can be negative since its can contain negative terms.

	conc. mol/l	total conc. mol/l	total liquid conc. mol/l	total solid conc. mol/l
H^+	$1.0\ 10^{-7}$	-43.36	$-8.497\ 10^{-5}$	-43.36
Ca^{2+}	$4.007\ 10^{-2}$	21.68	$4.007\ 10^{-2}$	21.68
Cl	0.0	0.0	0.0	0.0

Table 4.4: Initial conditions of reactive transport outside of injection zone.

The concentrations of CO_2 and H_2O are not included in Table 4.3 and in Table 4.4 since their values are imposed from the solution of two-phase two-component H_2O-CO_2 flow.

The physical parameters of the flow parameters are given in Table 4.5.

Constitutive law	Parameters
Capillary pressure law (Brooks-Corey model [16])	
$p_c = \frac{1}{\varepsilon}\left(\frac{S_l - S_{lr}}{1 - S_{lr}}\right)^{-\frac{1}{\lambda}}$,	$\frac{1}{\varepsilon} = 0.01$ MPa $\lambda = 2$ $S_{lr} = 0.2$
Darcy-Muskat's law	
$q_\alpha = -\frac{k_{r\alpha}}{\mu_\alpha} K(\nabla p_\alpha), \quad \alpha = l, g$	$K_{\|\text{barrier}} = 10^{-15}\mathbb{I}$ m^2 $K_{\|\text{drain}} = 10^{-13}\mathbb{I}$ m^2

Relative permeability (Brooks-Corey model [16]) $k_{rl} = \left(\frac{S_l - S_{lr}}{1 - S_{lr}}\right)^{3+\frac{2}{\lambda}}$ $k_{rg} = \left(1 - \frac{S_l - S_{lr}}{1 - S_{lr}}\right)\left(1 - \left(\frac{S_l - S_{lr}}{1 - S_{lr}}\right)^{1+\frac{2}{\lambda}}\right)$	$\lambda = 2$ $S_{lr} = 0.2$
Liquid diffusion/dispersion tensor $D_l = D_m \mathbb{I} + d_L \lvert\overrightarrow{q_l}\rvert + (d_L - d_T)\frac{\overrightarrow{q_l}\,\overrightarrow{q_l}^T}{\lvert\overrightarrow{q_l}\rvert}$	$D_m = 1.\ 10^{-9}$ m^2/s $d_L = 0.$ m $d_T = 0.$ m
Porosity	$\phi = 0.2$
Liquid density $\rho_l(p_l, x_l^{\mathrm{CO_2}}, S, T) = \rho_{brine}(p_l, S, T) + \rho_{\mathrm{H_2O–CO_2}}(p_l, x_l^{\mathrm{CO_2}}, T) - \rho_{\mathrm{H_2O}}$ The model is based on the results of the articles [29] and [9] and implemented in DuMu^X	$S = 0$ (salinity) $T = 50$°C (323 K)
Liquid viscosity	$\mu_l = 4.8\ 10^{-4}$ Pa s
Gas density ρ_g is a tabulated variable. Tabulated values are calculated for the model described in [63]	
Gas viscosity $\mu_g(p_g, T) = \mu_0(T) + \Delta\mu(\rho_g(p_g, T), T)$ The model is based on the results of article [27] and implemented in DuMu^X	

Table 4.5: Physical parameters for the SHPCO2 Benchmark.

Further, we consider two variants of the described test: with immobile and mobile gas phase.

4.5.1.2 Immobile gas phase.

The general purpose of performed simulations is to demonstrate the capabilities of the developed numerical simulator for two-phase multicomponent flow with reactive transport. The particular choice of the SHPCO2 Benchmark as a first test case is explained by the fact that in the previous section we already used one-phase multicomponent analog of this test for validation of one-phase reactive transport solver. The comparison of simulation results should reveal the influence of the gas phase presence.

In section 3.6.4.4 the gas carbon dioxide ($CO_{2(g)}$) is represented in the form of a mineral that doesn't participate in the transport process. In contrast, in the current test, $CO_{2(g)}$ forms a mobile gas phase and participates in the transport process of this phase. In order to bring closer the condition of different physical models for one-phase and two-phase flows, for this test we introduce an additional artificial assumption in physical laws of the SHPCO2 Benchmark. Instead of formula for the relative permeability of gas

phase given by Brooks-Corey model, we use in this first simulation a value of this relative permeability that is ten orders of magnitude less:

$$\widehat{k}_{rg} = 10^{-10} k_{rg(\text{Brooks-Corey})}. \tag{4.63}$$

This assumption in the physical model reduces the velocity of the gas phase almost to zero. In this case the gas carbon dioxide and the entire gas phase are almost **immobile** and do not participate in the transport process, and all changes in the concentration of $CO_{2(g)}$ are caused by the process of $CO_{2(g)}$ dissolution like in the analog test case for one-phase reactive transport.

The period of simulation is equal to 2500 years. The domain is discretized by a mesh of size 190×120.

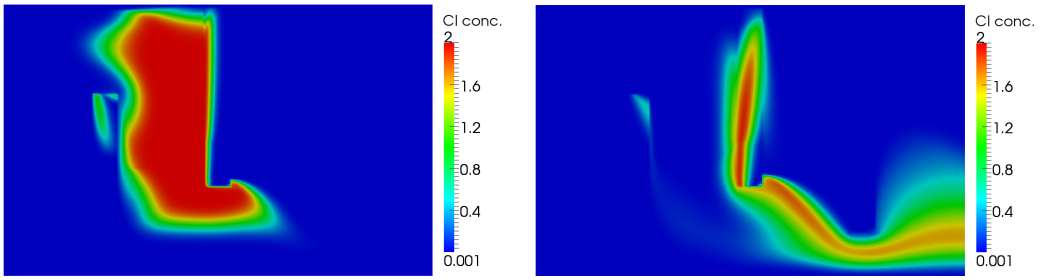

Cl concentration at $t = 400$ years Cl concentration at $t = 1200$ years

Figure 4.3: Results of numerical simulations for component Cl.

The Cl concentration at different period of times is represented in Figure 4.3. Cl is an additional tracer component. Its initial concentration is zero outside of the CO_2 zone injection and non-zero constant inside. The transport of Cl in the system is performed only by advection and diffusion in the liquid phase and does not have any influence from chemical reactions. If we compare this results with the evolution of the Cl concentration obtained for one phase transport, we notice that velocities field of the liquid phase are not identical (Figure 3.25). At the same time we can see that the general configuration of the liquid phase flow is similar to the one-phase case. The main reason of the observed differences is the presence of the strong coupling of the gas and the liquid pressures trough capillary pressure law in the two-phase case. Also the presence of a gas phase changes the value of the relative permeability of the liquid phase through Brook-Corey relations. In the one-phase case the relative permeability of the liquid phase is fixed to one.

The evolution of the gas saturation is represented in Figure 4.4. We can see, as expected, that the CO_2 bubble initially injected is not displaced by advection in the gas phase because of the zero gas phase velocity. The size of the gas phase zone is reduced in a similar way to changes of $CO_{2(g)}$ concentrations in the one-phase case (Figure 3.23 and Figure 3.24). In the same way as in the one-phase case this disappearance of the initially present gas is explained by the fact that a part of $CO_{2(g)}$ dissolves in the liquid phase and is transported by the flow of the liquid phase outside the injection zone. The difference in the evolution of zone with gas carbon dioxide (non-zero concentration of $CO_{2(g)}$ in one-phase case and non-null gas saturation in two-phase case) can be explained by the differences in the forms of $CO_{2(g)}$ activity in mass action law for reaction of $CO_{2(g)}$ dissolution. In the one-phase case, this reaction is considered as a

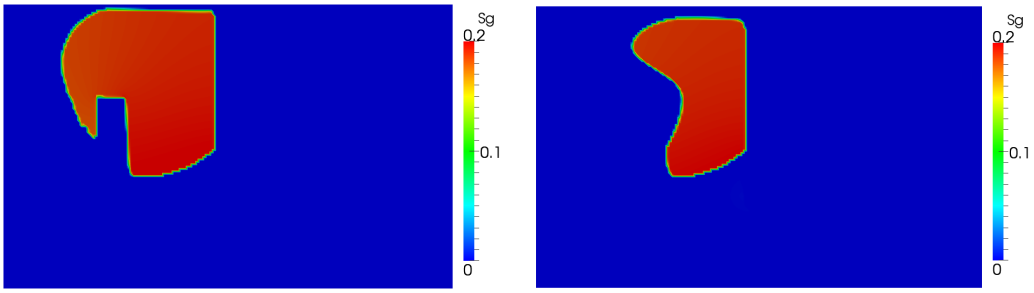

Gas saturation at $t = 400$ years Gas saturation at $t = 1200$ years

Figure 4.4: Results of numerical simulations for the gas saturation S_g.

precipitation-dissolution reaction of mineral component, whereas in the two-phase case the same chemical reaction is considered in the form of Henry's law. Also, previously, we already noticed that the configuration of flow in the liquid phase is slightly different in the two-phase case and thereby, removal of dissolved carbon dioxide in the liquid phase from the zone of gas presence is performed with different velocities causing difference in the rate of $CO_{2(g)}$ dissolution process.

4.5.1.3 Mobile gas phase.

In the second test, we remove the artificial assumption for the gas relative permeability and return to the physical model given in the test description. In this case the gas phase becomes **mobile** and the transport process in the gas phase has a strong influence on the simulation results.

As in the first test, the period of simulation is equal to 2500 years and we use a two dimensional mesh of size 190×120 (22800 points).

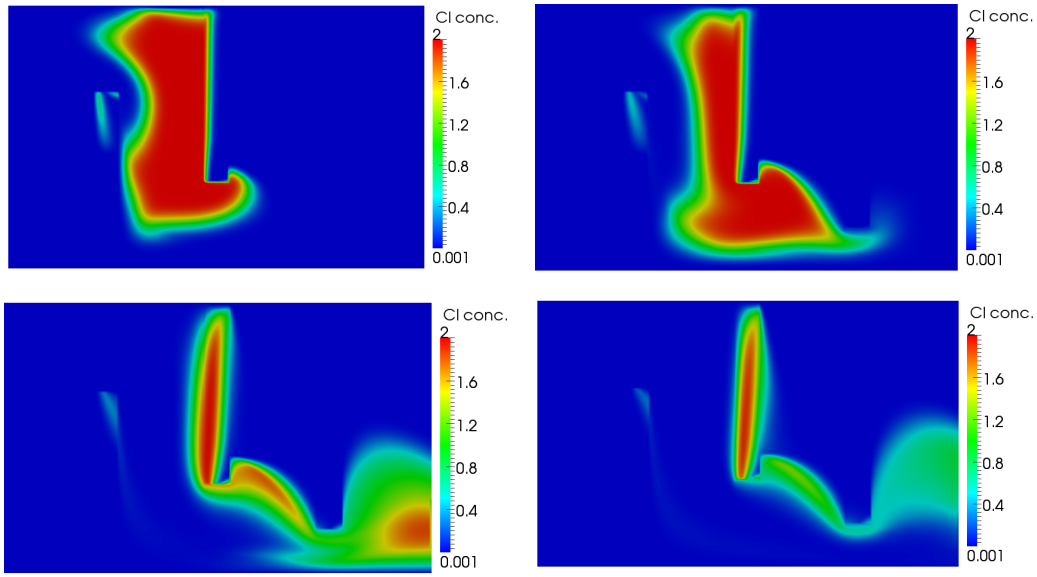

Figure 4.5: Evolution of the Cl concentration. Top left: 400 years. Top right : 800 years. Bottom left: 1200 years. Bottom right : 1600 years.

The Cl concentration at different periods of time is represented in Figure 4.5. As in the previous case, Cl is an additional tracer component. Considering the picture of Cl concentration evolution and comparing with results obtained for immobile gas phase test (Figure 4.3), we notice that the gas phase mobility changes the configuration of the flow in the liquid phase.

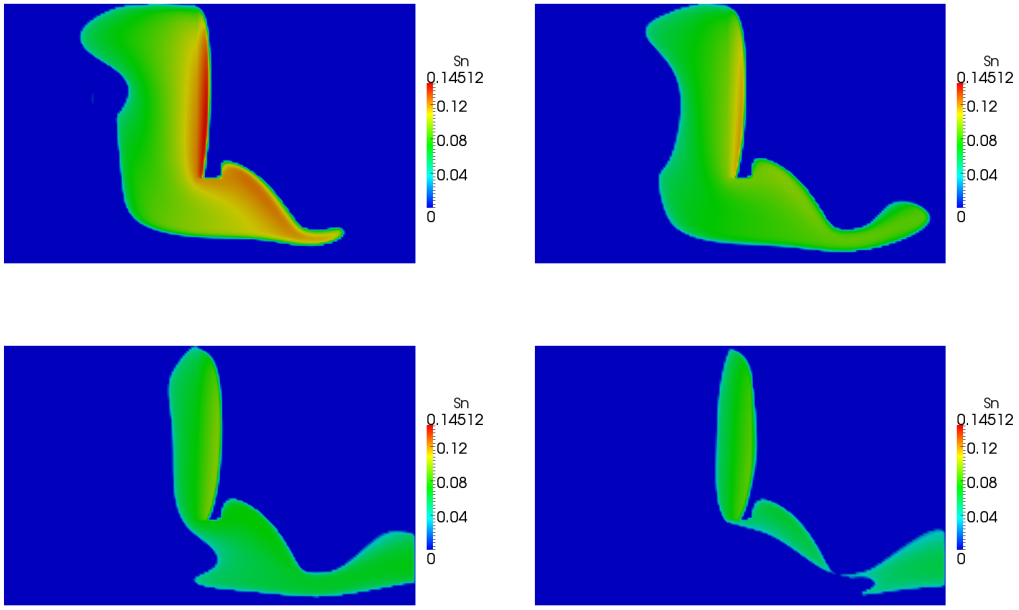

Figure 4.6: Evolution of the gas saturation. Top left: 400 years. Top right : 800 years. Bottom left: 1200 years. Bottom right : 1600 years.

The evolution of the gas saturation is represented in Figure 4.6. We can see that the CO_2 bubble initially injected is now displaced by advection in the gas phase. Comparing the evolution of gas saturation and the Cl concentration (Figure 4.5), we notice that the displacement of the gas is initially faster than displacement in the liquid phase. The velocities of gas and liquid phases are coupled by the capillary pressure law, so that the difference between the phase velocities is proportional to the gradient of the capillary pressure. Since the capillary pressure gradient is initially non-zero only on the boundary of injected CO_2 bubble, the initial difference between the velocities of both phases is large. Comparing the evolution of the gas saturation obtained for mobile gas phase case with results obtained for immobile gas phase case (Figure 4.4), we conclude that the effects caused by the transport processes in the gas phase have a significant influence on the process of carbon dioxide storage and they cannot be neglected like in the previous test with immobile gas phase. At the same time, $CO_{2(g)}$ dissolution observed in the immobile gas phase case (Figure 4.4) also has importance for the evolution of the gas phase, and is responsible for the gradual decrease in the gas saturation in zones with small gas phase velocity.

The liquid CO_2 concentration evolution is represented in Figure 4.7. In the zone where CO_2 was initially injected, some part of $CO_{2(g)}$ dissolves in the liquid phase. Then $CO_{2(l)}$ is transported by advection and diffusion in the liquid phase. Also the process of gaseous CO_2 dissolution continues during the whole period of simulation and some

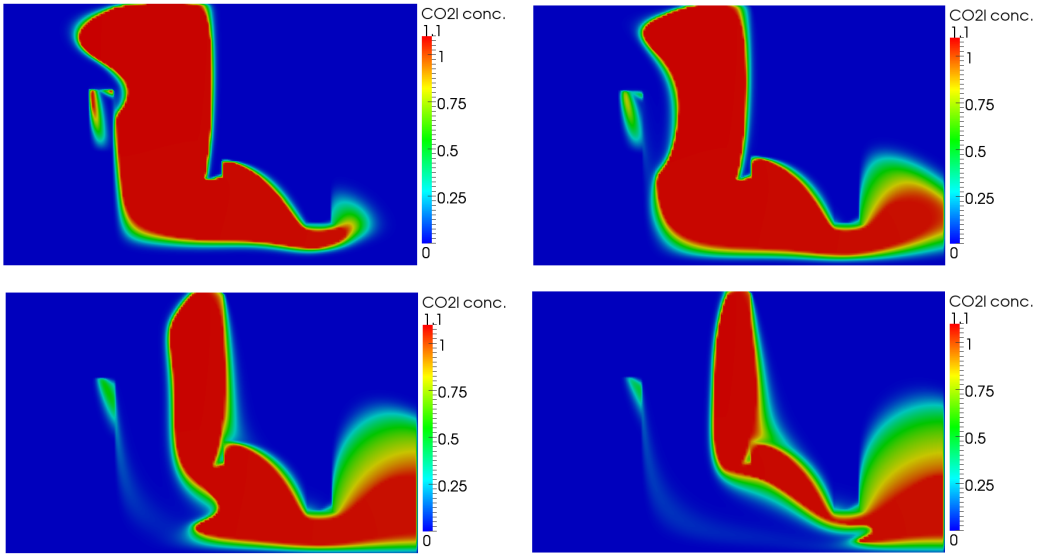

Figure 4.7: Evolution of CO_2 concentration in the liquid phase. Top left: 400 years. Top right : 800 years. Bottom left: 1200 years. Bottom right : 1600 years.

part of the liquid CO_2 comes from the gas phase. In addition to these phenomena the displacement of the liquid CO_2 is influenced by the presence of chemical reactions that involve liquid CO_2. If we compare these results with the results obtained for the tracer component Cl (Figure 4.5), we conclude that the presence of chemical reactions and dissolution of the gas component may have a strong influence on the transport of the liquid CO_2, and this effect has to be taken into account in the physical model.

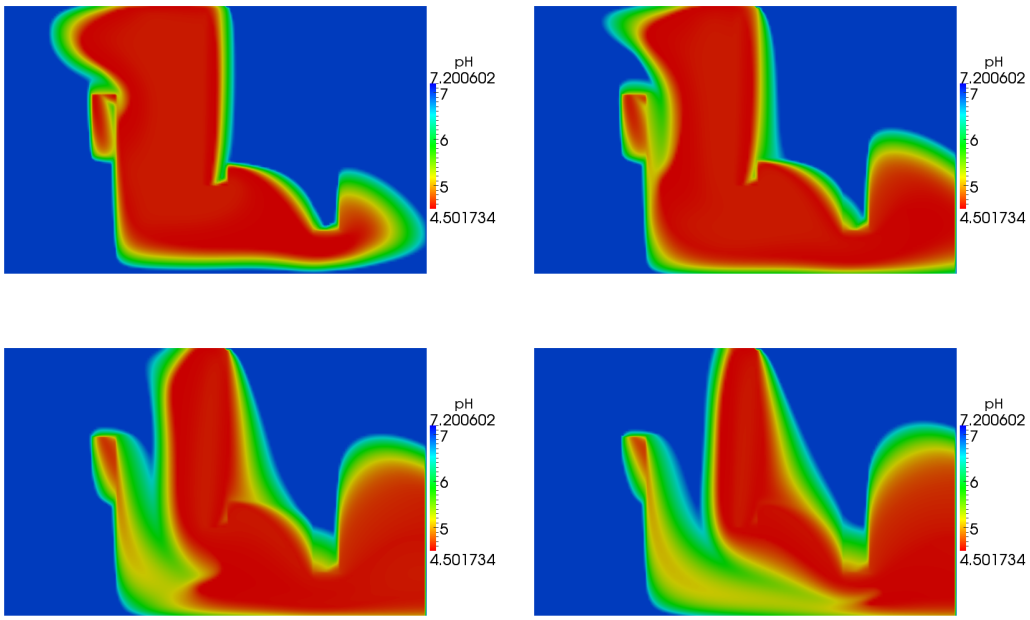

Figure 4.8: Evolution of pH. Top left: 400 years. Top right : 800 years. Bottom left: 1200 years. Bottom right : 1600 years.

Finally, in Figure 4.8 we see that the distribution of H^+ is strongly correlated with the $CO_{2(l)}$ concentration. High concentration of $CO_{2(l)}$ causes an increase of the liquid phase acidity.

Remark

As already mentioned in subsection 4.3.4, the right hand side term R in the balance equations for H_2O and CO_2 was neglected in the numerical simulations presented in sections 4.5.1.2 and 4.5.1.3. To demonstrate that the neglecting of the R terms doesn't cause a significant change, we perform an additional test, identical to the previous SHPCO2 benchmark with mobile gas phase (section 4.5.1.3), but with the R terms included.

At each time step $t_n \to t_{n+1}$, the terms

$$R^n_{\mathrm{H_2O}} = -\frac{\phi^n S_l^n (c^n_{\mathrm{OH^-}} + c^n_{\mathrm{HCO_3^-}}) - \phi^{n-1} S_l^{n-1} (c^{n-1}_{\mathrm{OH^-}} + c^{n-1}_{\mathrm{HCO_3^-}})}{t_n - t_{n-1}} - \frac{c^n_{CaCO_3} - c^{n-1}_{CaCO_3}}{t_n - t_{n-1}} - L_{l(q_l^n, S_l^n)}(c^n_{\mathrm{OH^-}} + c^n_{\mathrm{HCO_3^-}})$$

and

$$R^n_{\mathrm{CO_2}} = -\frac{\phi^n S_l^n c^n_{\mathrm{HCO_3^-}} - \phi^{n-1} S_l^{n-1} c^{n-1}_{\mathrm{HCO_3^-}}}{t_n - t_{n-1}} - \frac{c^n_{CaCO_3} - c^{n-1}_{CaCO_3}}{t_n - t_{n-1}} - L_{l(q_l^n, S_l^n)}(c^n_{\mathrm{HCO_3^-}})$$

of the dominant component balance equations, for the chemical system represented in the SHPCO2 benchmark (see equations (4.49) and (4.50)), should be computed explicitly from the results of the two-phase two-component flow and reactive transport subproblems at the previous time step. However, because of the structure of the DuMu^X code, using the old velocity $\overrightarrow{q}_l^n$ in the advection-diffusion operator L_l is not convenient. For this reason, we decided to replace this by the velocity at the current time $\overrightarrow{q}_l^{n+1}$. In case of a stable flow configuration and a sufficiently small time step, such a replacement should not result in large changes to the solution.

When we compare visually the results of simulations without and with R terms, we observe that both figures are identical, so that we can indeed conclude that the presence of the R terms has very little influence on the flow configuration.

However the presence of R is quite important for the question of mass conservation. In the case without R term, the solution of two-phase two-component flow is conservative with respect to the total concentration of dominant components which contain only concentrations of their liquid and gas forms:

$$\overline{T}_{\mathrm{CO_{2(l)}}} = \phi S_l c_{\mathrm{CO_{2(l)}}} + \phi S_g c_{\mathrm{CO_{2(g)}}},$$

and

$$\overline{T}_{\mathrm{H_2O_{(l)}}} = \phi S_l c_{\mathrm{H_2O_{(l)}}} + \phi S_g c_{\mathrm{H_2O_{(g)}}}.$$

However, the solution of the original equation is conservative with respect to total concentrations that additionally contain concentrations of some secondary components:

$$T_{\mathrm{CO_{2(l)}}} = \overline{T}_{\mathrm{CO_{2(l)}}} + \phi S_l c_{\mathrm{HCO_3^-}} + c_{\mathrm{CaCO_3}},$$

and

$$T_{\mathrm{H_2O_{(l)}}} = \overline{T}_{\mathrm{H_2O_{(l)}}} + \phi S_l c_{\mathrm{HCO_3^-}} + \phi S_l c_{\mathrm{OH^-}} + c_{\mathrm{CaCO_3}}.$$

To demonstrate that the presence of the R term imprives the conservation of the two-phase two-component flow subproblem with respect to the original total concentrations, we compare the overall value of $T_{\mathrm{CO_{2(l)}}}$ ($\int_\Omega T_{\mathrm{CO_{2(l)}}}|_{t_{\mathrm{fix}}}$) in the SHPCO2 Benchmark during the first 200 years of simulations, with and without term R. The results of comparison are shown in Table 4.6:

Time (years)	$\int_\Omega T_{\mathrm{CO_{2(l)}}}$ without R	$\int_\Omega T_{\mathrm{CO_{2(l)}}}$ with R
5 years	335267384	335416542
50 years	334590649	335411173
100 years	334127585	335409334
200 years	333338905	335408767
Absolute change after 200 years	−1928479	−7775
Relative change after 200 years	−0.5752%	−0.0023%

Table 4.6: Evolution of total $T_{\mathrm{CO_{2(l)}}}$ value

Since there are no internal sources of CO_2 inside of the domain, and since during the CO_2 bubble hasn't reached the boundary of domain during the first 200 years, the total value of $T_{\mathrm{CO_{2(l)}}}$ shouldn't change. From Table 4.6 we see that the introduction of the R term makes the numerical algorithm more nearly conservative. At the same time, we can note that the mass transfered from the secondary components (represented by term R) is relatively small in comparison with the initially injected CO_2 mass.

We conclude that, consistent with current practice (reference to TOUGH2, others) it will usually not be necessary to include the R terms. As the mass balance conservation can always be checked a posteriori, those terms can be added if it is found that mass conservation is not sufficient.

4.5.2 Test case of Saaltink et al

To compare the results of the new developed simulators for two-phase multicomponent flow with results of other software we choose the test case described in the article [59]. The authors of this article elaborate a coupled physical model of two-phase multicomponent flow and construct a numerical simulator that solves the entire system using a fully-coupled approach. To reduce the complexity of the considered numerical task, the authors chose a different approach from our method for computing the chemical equilibrium states. Instead of solving a system of mass action laws coupled with expression of the total concentrations (section 3.4.1), the authors use a pre-calculated tabulated function that returns the concentrations of all components at chemical equilibrium according to the value of the gas pressure. This choice simplifies the computation and reduces computing time, but creates a problem for interpreting the test conditions such as values of initial component concentrations and chemical equilibrium constants. These functions for some important chemical components are represented in form of graphs in Figures 1 in the article [59]. For convenience, we duplicate this illustration in Figure 4.9.

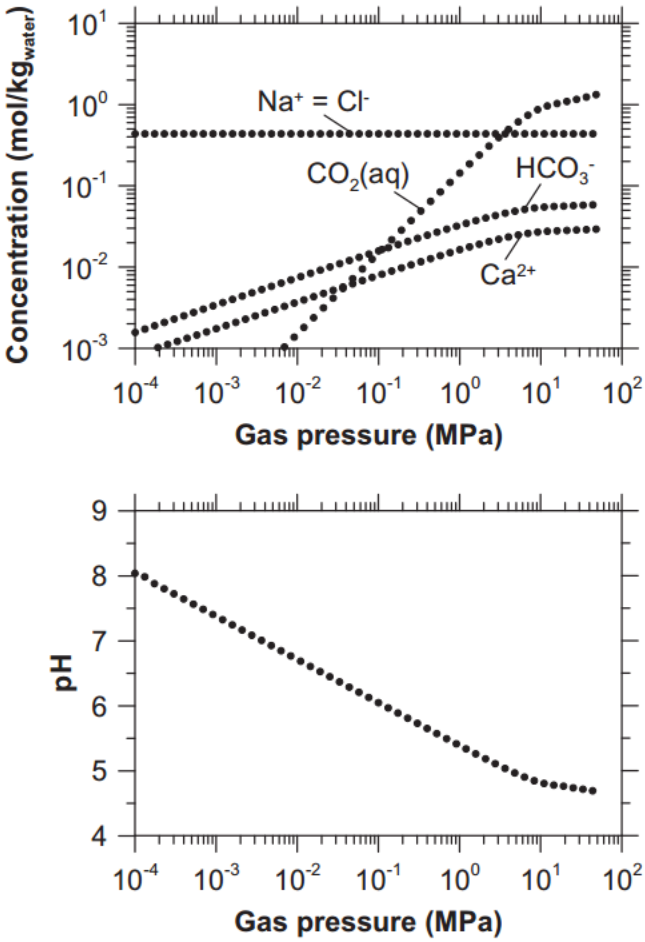

Figure 4.9: Concentrations of the most important chemical components ($CO_{2(l)}$, HCO_3^-, Ca^{2+}, Cl) and pH as a function of the gas pressure. Reproduced from [59]

The necessary values of the equilibrium constants for our physical values were calculated through the presented graphics of the primary component concentration and for this reason can slightly differ from the values used in [59].

4.5.2.1 Test description

The chemical description of the second test coincides with the test in section 4.5.1.1.

Because the considered test is carried out at different temperature from test in section 4.5.1.1, the equilibrium constants of the chemical reactions of reactive transport subsystem reconstructed from the functions of component concentrations (Figure 4.9) are also different. The new values of these constants are represented in the following Morel's tableau (Table 4.7):

	H_2O	H^+	$CO_{2(l)}$	Ca^{2+}	Cl	$\log K$
OH^-	1	-1	0	0	0	-14
HCO_3^-	1	-1	1	0	0	-5.9
$CaCO_3$	1	-2	1	1	0	-8.1
Total	T_{H_2O}	T_{H^+}	$T_{CO_{2(l)}}$	$T_{Ca^{2+}}$	T_{Cl}	

Table 4.7: Parameters for the test case of Saaltink et al.

In this test, we consider a simple axisymmetric 2D geometry of 100 m thick horizontal aquifer at 1500 m depth. The model extends 5 km laterally (radius 2.5 km). An injection well with a radius of 0.15 m is placed at the center of the domain. The geometry of this domain is shown in Figure 4.10.

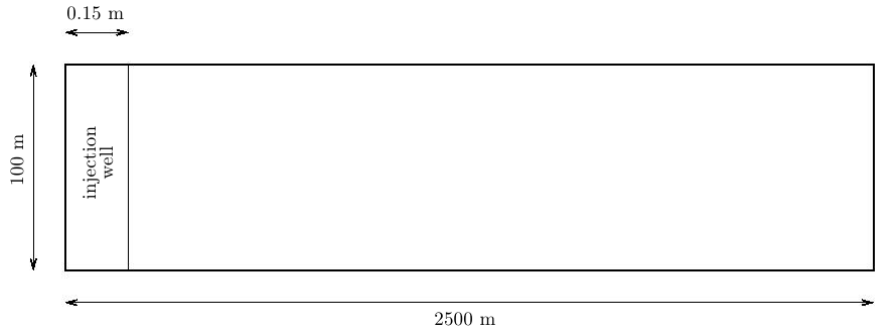

Figure 4.10: Section of the axisymmetric 2D domain for Saaltink et al. test case

The transport in the domain is performed with the velocity of the liquid phase

$$\overrightarrow{q_l} = -\frac{k_{rl}}{\mu_l} K(\nabla p_l - \rho_l \overrightarrow{g}) \tag{4.64}$$

where the pressure p_l is the solution of a two-phase two-component H_2O-CO_2 flow with the following boundary conditions:

- the part of the boundary close to the injection well, $\partial\Omega_1$, has Neumann conditions such that $q_{H_2O|\partial\Omega_1} = 0$ and $\int_{\partial\Omega_1} q_{CO_2} = 2.5\ 10^9$ kg per year,

- the top and the bottom parts of the domain boundary, $\partial\Omega_2$, have Neumann impermeable conditions,
- the outer part of the domain boundary, $\partial\Omega_3$, has Dirichlet conditions (hydrostatic for the pressure and equal to the initial condition for the liquid CO_2 concentration).

According to the velocity obtained from the two-phase two component H_2O-CO_2 flow, we choose the following boundary conditions for reactive transport:

- the part close to the injection well $\partial\Omega_1$ has Dirichlet conditions equal to initial for the total liquid concentrations of primary components,
- the top and the bottom parts of the domain boundary $\partial\Omega_2$ have Neumann impermeable conditions,
- the outer part of the domain boundary $\partial\Omega_3$ has no conditions since $\overrightarrow{q_l} \cdot \overrightarrow{n}_{|\partial\Omega_3} > 0$.

As initial conditions for the two-phase two-component H_2O-CO_2 flow we use:

- hydrostatic condition for the liquid pressure $p_l(x,y,z) = p_{atm} + \rho_l(p_{ref})(1500 - g \cdot y)$ where $p_{ref} = 15$ MPa,
- the initial liquid saturation $S_l = 1$ for the entire domain Ω,
- the initial CO_2 concentration in the liquid phase $c_{CO_2(l)} = 1.223\ 10^{-4}$ mol/l.

Since in the article [59], the concentration of chemical components are computed as explicit functions of the gas pressure, no initial values are needed. In our model, the concentrations of the primary components are system variables, and we need to know their values at the initial time. These values were read off the graph in Figure 4.9 with an initial gas pressure equal to 10^{-3} MPa. The initial concentration of CO_2(l) was already mentioned in the list of the initial conditions for two-phase two-component H_2O-CO_2 flow subproblem. The initial concentrations of other primary components H^+, Ca^{2+}, Cl, represented in Table 4.8, are necessary for the definition of reactive transport subproblem.

	conc. mol/l	total conc. mol/l	total liquid conc. mol/l	total solid conc. mol/l
H^+	$4.1\ 10^{-8}$	-48.6	$-3.5\ 10^{-3}$	-48.6
Ca^{2+}	$1.7\ 10^{-3}$	24.3	$1.7\ 10^{-3}$	24.3
Cl	0.435	0.435	0.435	0

Table 4.8: Initial conditions of reactive transport for the test case of Saaltink et al.

The physical parameters of the flow parameters are given in Table 4.9.

Constitutive law	Parameters

Relation curve (capillary pressure law) $S_l = \left(1 + \left(\frac{p_g - p_l}{P_0}\right)^{\frac{1}{1-m}}\right)^{-m}$	$P_0 = 0.02$ MPa $m = 0.8$
Darcy-Muskat's law $q_\alpha = -\frac{k_{r\alpha}}{\mu_\alpha} K(\nabla p_\alpha - \rho_\alpha \overrightarrow{g}), \quad \alpha = l, g$	$\overrightarrow{g} = \begin{pmatrix} 0 \\ -9.81 \\ 0 \end{pmatrix}$ m/s^2 $K = 10^{-13}\mathbb{I}$ m^2
Relative permeability $k_{r\alpha} = S_\alpha^n, \quad \alpha = l, g$	$n = 1$
Liquid diffusion/dispersion tensor $D_l = D_m\mathbb{I} + d_L\lvert\overrightarrow{q_l}\rvert + (d_L - d_T)\frac{\overrightarrow{q_l}\overrightarrow{q_l}^T}{\lvert\overrightarrow{q_l}\rvert}$	$D_m = 1.6\ 10^{-8}$ m^2/s $d_L = 5$ m $d_T = 0.5$ m
Solid density	$\rho_s = 2700$ kg/m^3
Porosity $\phi = 1 - \frac{c_{\mathrm{CaCO_3}} M_{\mathrm{CaCO_3}}}{\rho_s}$	$M_{\mathrm{CaCO_3}} = 0.1$ kg/mol
Liquid density $\rho_l = \rho_{l0}\exp(\alpha T + \beta(p_l - p_{l0}) + \gamma S)$	$\alpha = -3.4\ 10^{-4}$ °C^{-1} $\beta = 4.5\ 10^{-4}$ MPa^{-1} $T = 60$°C(333 K) $S = 0.025$ $\rho_{l0} = 1037.12$ kg/m^3 $p_{l0} = 0.1$ MPa $\gamma = 0.19$
Liquid viscosity	$\mu_l = 4.8\ 10^{-4}$ Pa s
Gas density ρ_g is a tabulated variable. Tabulated values are calculated for the model described in [63]	
Gas viscosity $\mu_g = \mu_0\left(\sum_{i=1}^{4}\sum_{j=0}^{1}\frac{a_{ij}\rho_R^i}{T_R^j}\right)$ $\rho_R = \rho_g/\rho_{cr}$ $T_R = T/T_{cr}$ $\mu_0 = T_R^{0.5}\left(27.22 - \frac{16.63}{T_R} + \frac{4.67}{T_R^2}\right)$ μPa	$\rho_{cr} = 468$ kg/m^3 $T_{cr} = 304$ K $T = 333$ K $a_{10} = 0.249$ $a_{11} = 0.00489$ $a_{20} = -0.373$ $a_{21} = 1.23$ $a_{30} = 0.364$ $a_{31} = -0.774$ $a_{40} = -0.0639$ $a_{41} = 0.143$

Table 4.9: Physical parameters for the test case of Saaltink et al.

4.5.2.2 Numerical results

The period of simulation is equal to 1 year. We have used a two dimensional mesh of size 500×20 (10000 points).

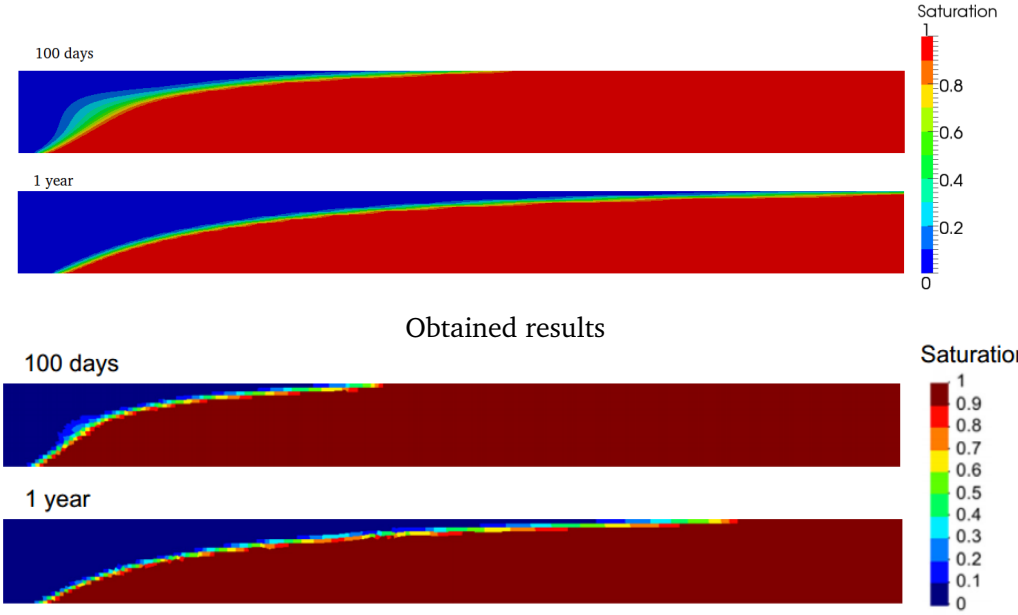

Obtained results

Saatlink's results

Figure 4.11: Comparison of the liquid saturation S_l between ours and Saatlink et al. results after 100 days and 1 year of CO_2 injection. Only the 1.1 km closest to the injection is presented.

The comparison of the liquid phase saturation distribution between the results of our numerical simulator and Saatlink et al. results at different periods of time is represented in Figure 4.11. The gaseous CO_2 injected at the left border migrates upward by buoyancy effect until it reaches the top of the domain with no-flux conditions and then is driven to the right border by advective forces and almost completely displaces the liquid phase in zone of gas phase presence. Comparing the two results, we observe that the form and the propagation velocity of the gas phase front in both simulation have no significant differences.

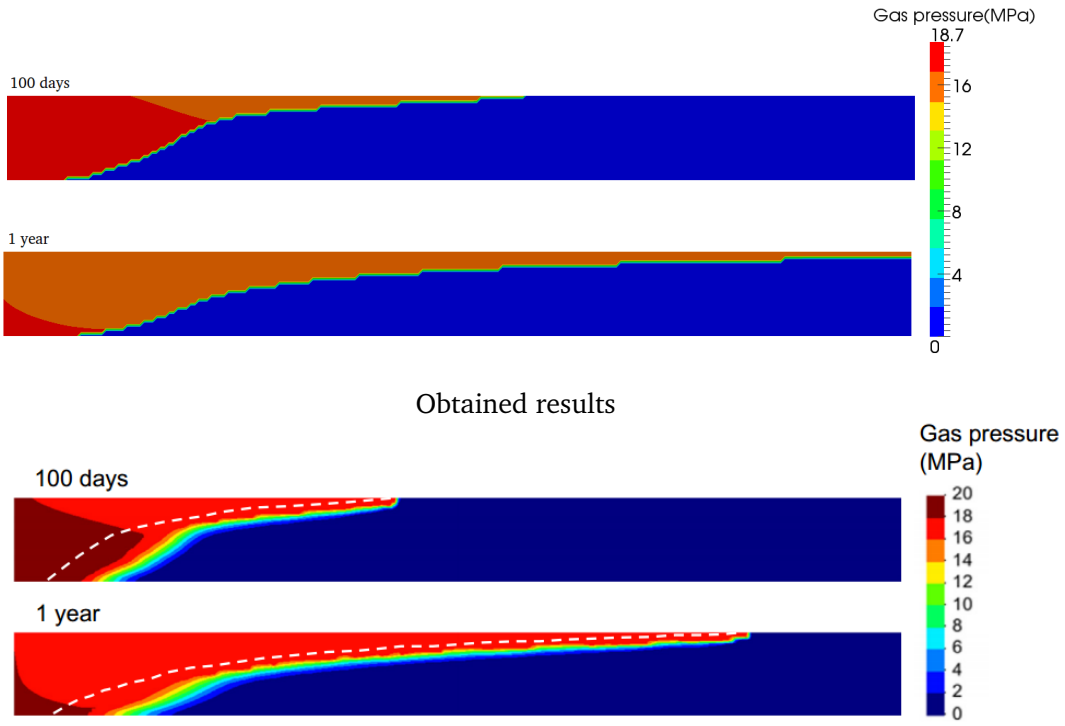

Figure 4.12: Comparison of the gas pressure p_g between our and Saatlink et al. results after 100 days and 1 year of CO_2 injection. Only the 1.1 km closest to the injection is presented. The white discontinuous line in Saatlink et al. results indicates the extension of the CO_2 plume (saturation equal to 0.5)

The comparison of the gas pressure evolution between the results of our numerical simulator and Saatlink et al. results at different periods of time is represented in Figure 4.13. The evolution of the gas pressure is strongly coupled with the evolution of the gas phase. The gas pressure reaches its highest values on the left boundary because of the continuous process of CO_2 injection. As it approaches the boundary of the gas phase spread,the gas pressure is slowly decreasing. In the zone without the gas phase presence, we assume that the gas pressure is zero. Comparing the results of our numerical simulator and Saatlink et al. results we observe that the general picture of the gas pressure evolution coincide, but at the same time gas pressure in our simulation does not reach the maximal values observed in Saatlink et al. simulations. The possible explanation of such difference will be given later. The distribution of the liquid density represented in Figure 4.13 is strongly coupled with the distribution of the gas pressure because that increase of the gas pressure causes an increase of amount of the dissolved CO_2 that in its turn causes an increase of the liquid phase density. At the same time we observe that the region containing the dissolved CO_2 is larger than the gas CO_2 plume, especially in the lower part of the aquifer below the gas CO_2 plume close to the injection left border. This is caused by vertical dispersion of the liquid CO_2 and by vertical downward flux appearing due to the fact that the denser CO_2 saturated liquid phase is placed on top of lighter non-saturated zone.

Figure 4.14 compares calcite dissolution after 100 days of CO_2 injection, obtained in our and Saatlink et al. results. Both simulations show dissolution of calcite in the

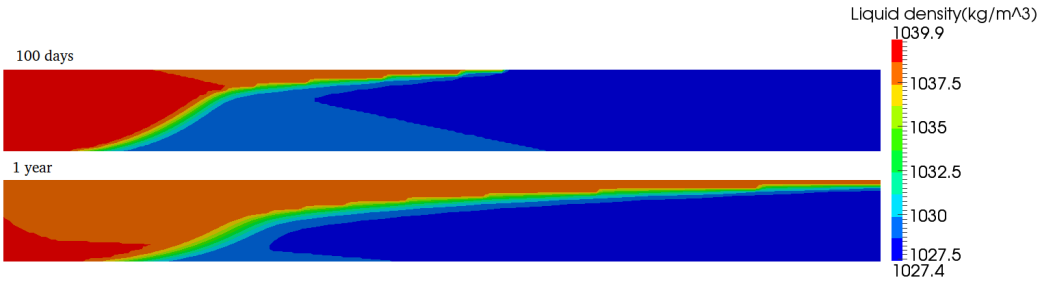

Obtained results

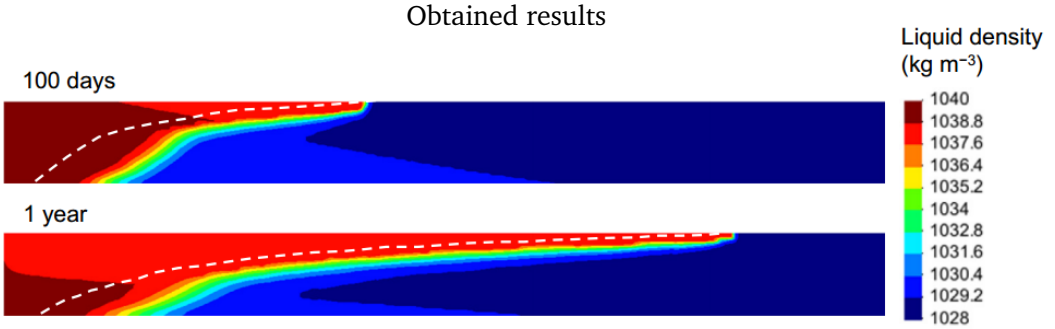

Saatlink et al. results

Figure 4.13: Comparison of the liquid density ρ_l between our and Saatlink et al. results after 100 days and 1 year of CO_2 injection. Only the 1.1 km closest to the injection is presented. The white discontinuous line in Saatlink et al. results indicates the extension of the CO_2 plume (saturation equal to 0.5)

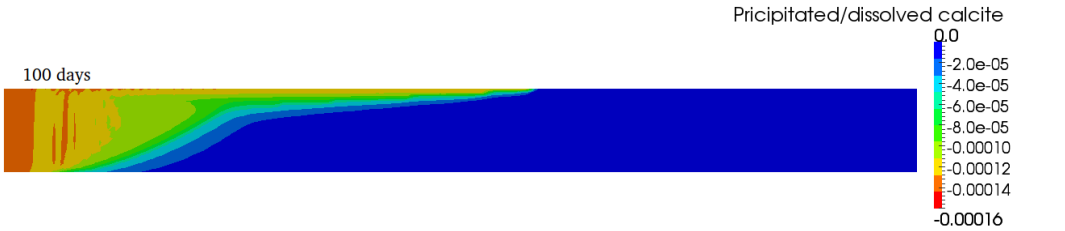

Obtained results

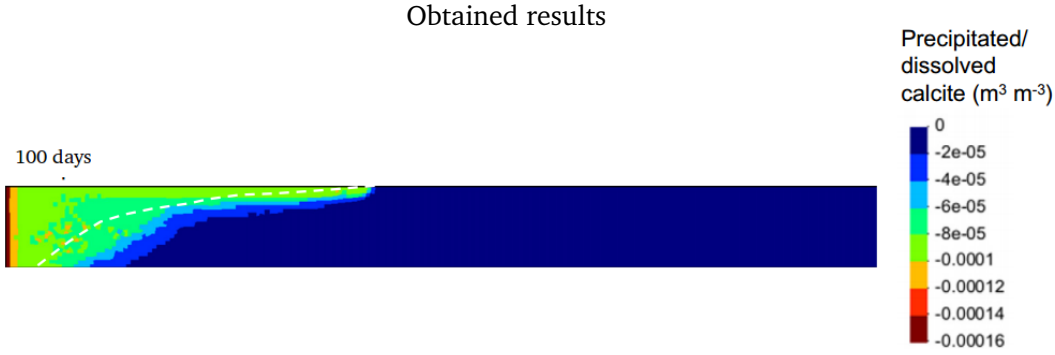

Saatlink et al. results

Figure 4.14: Comparison of value of precipitated/dissolved calcite volume fraction between our and Saatlink et al. results after 100 days of CO_2 injection. Dissolution is indicated by negative values. Only the 1.1 km closest to the injection is presented. The white discontinuous line in Saatlink et al. results indicates the extension of the CO_2 plume (saturation equal to 0.5)

vicinity of the CO_2 plume and give similar pictures of the dissolution process: the calcite dissolves in the zones where the liquid phase contains the dissolved carbon dioxide reacting with mineral calcite. The amount of dissolved calcite is maximal close to the injection border and gradually decreases as it approaches the boundary of the liquid CO_2 spread. Although the described trend is observed in both simulations, the actual amounts of dissolved calcite inside of CO_2 plume differ. To demonstrate these differences we give a more precise comparison of the simulations in Figure 4.15, giving the graph of precipitated/dissolved calcite volume fraction after 100 days of CO_2 injection at two depths as a function of distance from the left side of the domain. We observe that the quantity of the dissolved calcite decreases with the distance from the border with CO_2 injection. The forms of the graphs obtained in our and in Saatlink et al. simulations are similar, but actual values are different. This difference can be explained by difficulties for finding the necessary values of equilibrium constants. The values reconstructed from the graphs of component concentrations may differ from those actually used in Saatlink et al. simulations.

Figures 4.16 and 4.17 display the temporal evolution of the gas pressure and the liquid density obtained in our and Saatlink et al. simulations. At the initial period, the gas phase is not present and the gas pressure is equal to zero at investigated point. At the same time the liquid density slightly increases under the influence of the rising pressure in the liquid phase. At some moment the CO_2 plume comes to the considered point and the gas phase appears and the gas pressure reaches its maximum values. The part of arrived gas dissolves in the liquid phase and causes a large jump in the liquid density. During the remaining time of simulation, the gas pressure slowly decreases. A similar change in the liquid pressure leads to the slight decreasing of liquid pressure. The described evolution of physical parameters is observed in both results, but in our simulations the time of the gas phase appearance comes earlier. The reason for this may lie in the differences of the used numerical simulators. For example, DuMu^X simulator switch the case of only liquid phase to the case with both phase presence when mole fraction of dissolved CO_2 higher then known maximum mole fraction value. The actual value of the maximum mole fraction is defined by form of Henry's and Raoult's laws. Since we do not have precise information about form of these laws used in Saatlink et al. numerical simulator, the value of the maximum mole fraction could be more, and in this case it takes more time to reach necessary fraction of dissolved CO_2 at which the gas phase appears. The same reason possibly can explain 3 percent difference in maximum values of the gas pressure.

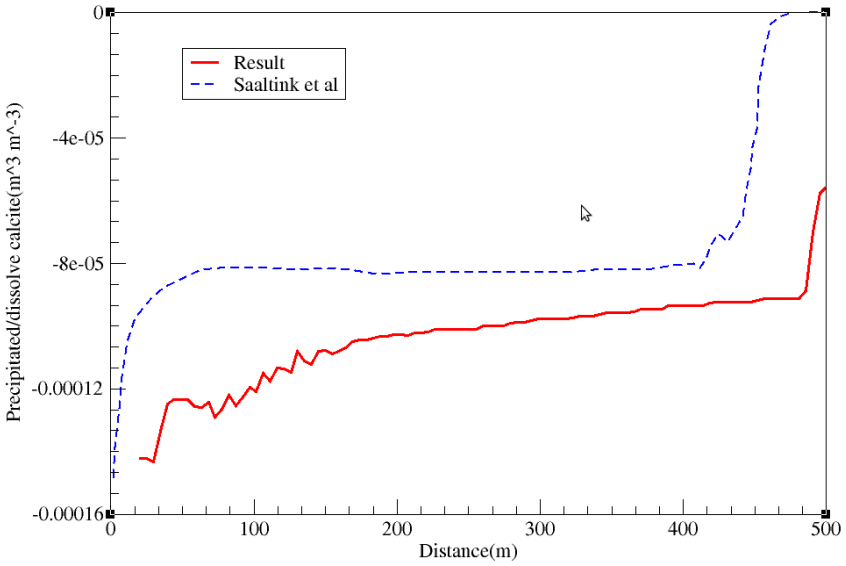

Depth 10 m

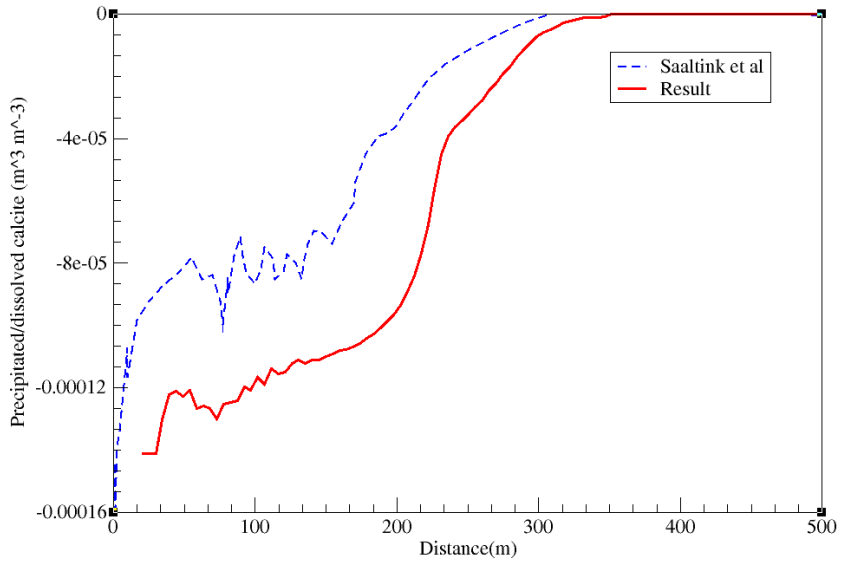

Depth 50 m

Figure 4.15: Precipitated/dissolved calcite volume fraction after 100 days of CO_2 injection at two depths. Red lines represent obtained results. Blue lines represent Saatlink et al. results. Dissolution is indicated by negative value.

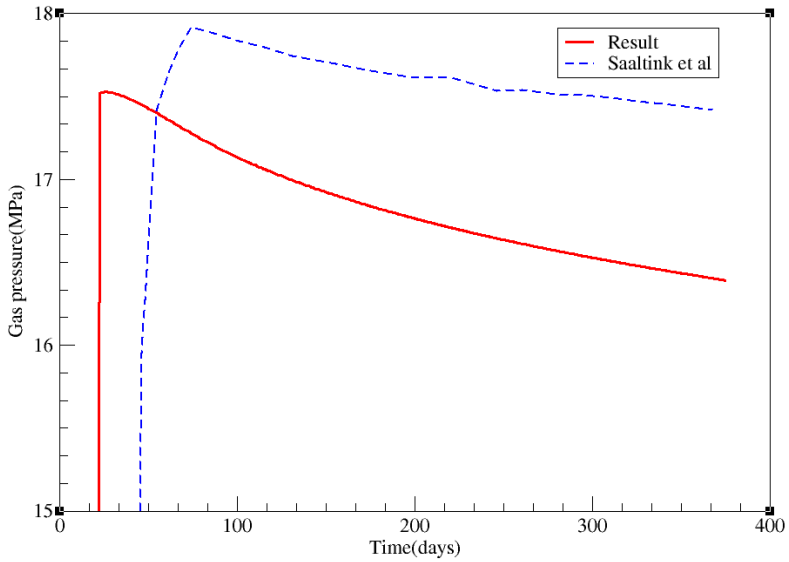

Figure 4.16: Gas pressure evolution at the point placed 200 m away from the injection well and 25 m below the top of the aquifer. Red line represents obtained results. Blue line represents Saatlink et al. results.

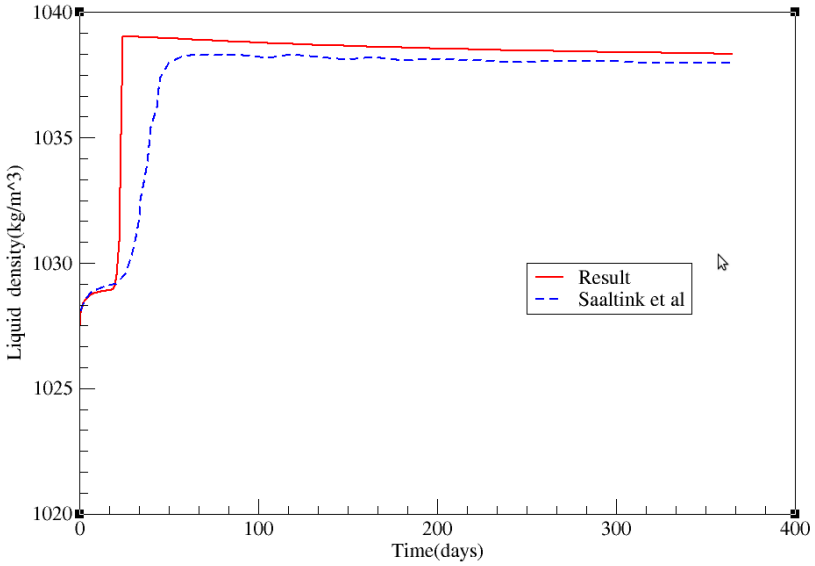

Figure 4.17: Liquid density evolution at a point placed 200 m away from the injection well and 25 mbelow the top of the aquifer. Red line represents obtained results. Blue line represents Saatlink et al. results.

4.5.3 Test case of Fan *et al*

In the previous two tests the investigated domains were two-dimensional. The main aim of our third test is to demonstrate that the code we developed is capable of performing three-dimensional calculations. Such capability naturally arises from the fact that our code was developed on the basis of the well established framework DuMu^X, which already includes the realization of three-dimensional simulations.

We consider the 3D test problem of CO_2 injection described in the work of Fan *et al* [26]. In this work the authors propose to use two variants of complex geochemical systems that include both equilibrium and kinetic reactions. The first system involves four equilibrium reactions and eight kinetic reactions of mineral dissolution/precipitation. The second simplified system takes into account the same equilibrium reactions and only three kinetic reactions from the first system. Because the current version of our simulator is only able to treat equilibrium reactions, we have had to adapt and simplify the second variant of the geochemical system.

The simplified version of the model proposed by Fan et al. included three minerals: anorthite, calcite and kaolinite, and all three reactions were considered kinetic. These three reactions were taken together because they involve the same ions (Ca^{2+}, H^+ and Al^{3+}). In the case of kinetic reactions, the competition between the three reactions is indirect, and does not cause numerical difficulties. This would not be the case if we tried to model the three reactions as equilibrium, as the three minerals would directly compete for the ions, and form a tightly coupled subsystem. With the current version of the chemical code ChemEqLib, it is unfortunately not possible to guarantee that a chemical system including these three reactions can always be solved, irrespective of the initial concentrations. For this reason, we have decided to eliminate two of the minerals (anorthite and kaolinite) and keep only calcite in the system. Furthermore, we have also removed the (aqueous phase) reaction involving aluminum, as it had become decoupled from the rest of the system.

This choice has the consequence that is no longer possible to compare our results with those from the paper [26], so that this test case will not be used as a validation case. But the results can still be interpreted from general physical considerations.

4.5.3.1 Test description

The simplified chemical system used in this test case and derived from the original chemical system [26] is close to the chemical system used in the previous two test cases. It has one new component CO_3^{2-} and one new equilibrium reaction:

$$CO_3^{2-} \rightleftharpoons H_2O - 2H^+ + CO_{2(l)}. \tag{4.65}$$

Also in contrast to the previous tests, we do not introduce the tracer component Cl.

The equilibrium constants of the chemical reactions were not presented in the article [26]. The necessary values were computed from the values of initial molality (simply converted to concentrations) of all chemical components given in Table 3 of this article under the assumption that the concentrations of components of equilibrium reactions at initial time are already at equilibrium and the components have ideal activity, except calcite and water with constant activity equal one. The calculated values of these constants are represented in the following Morel's tableau (Table 4.10):

	H_2O	H^+	$CO_{2(l)}$	Ca^{2+}	$\log K$
OH^-	1	-1	0	0	-13.59
HCO_3^-	1	-1	1	0	-6.46
CO_3^{2-}	1	-2	1	0	-16.408
$CaCO_3$	1	-2	1	1	-8.44
Total	T_{H_2O}	T_{H^+}	$T_{CO_{2(l)}}$	$T_{Ca^{2+}}$	

Table 4.10: Parameters for the test case of Fan et al.

In this test, we consider a 3D domain that is 15 km in both the x and y-directions and 100 m in the z-direction. The model contains $25 \times 25 \times 16 = 10000$ grid blocks. The model contains one injection well perforated in a single grid block located 25 m from the top of the aquifer. A pure CO_2 stream was injected by this well at constant rate during the first 20 years. After the 20 years injection period, a total of 18.6 10^9 kg of CO_2 was injected.

The transport in the domain is performed with the velocity of the liquid phase

$$\overrightarrow{q_l} = -\frac{k_{rl}}{\mu_l} K(\nabla p_l - \rho_l \overrightarrow{g}) \tag{4.66}$$

where the pressure p_l is the solution of a two-phase two-component H_2O-CO_2 flow with Neumann impermeable conditions at all boundaries.

According to the velocity obtained from the two-phase two component H_2O-CO_2 flow, we choose the same Neumann impermeable conditions at all boundaries for reactive transport.

As initial conditions for the two-phase two-component H_2O-CO_2 flow we use:

- hydrostatic condition for the liquid pressure $p_l(x,y,z) = p_{top} - \rho_l(p_{top})(g \cdot z)$ where $p_{top} = 11.8$ MPa is the initial pressure value at the top of the domain,
- the initial liquid saturation $S_l = 1$ for the entire domain Ω,
- the initial CO_2 concentration in the liquid phase $c_{CO_2(l)} = 3.55\ 10^{-3}$ mol/l.

Initial conditions for the reactive transport are similar for the entire domain and represented in Table 4.11.

	conc. mol/l	total conc. mol/l	total liquid conc. mol/l	total solid conc. mol/l
H^+	$5.71\ 10^{-7}$	-44.28	$-2.159\ 10^{-3}$	-44.28
Ca^{2+}	$2.52\ 10^{-2}$	22.14	$2.52\ 10^{-2}$	22.17

Table 4.11: Initial conditions of reactive transport for the test case of Fan *et al.*

The concentrations of CO_2 and H_2O are not included in Table 4.11 since their values are imposed from the solution of the two-phase two-component H_2O-CO_2 flow.

The physical parameters of the flow parameters are given in Table 4.12.

Constitutive law	Parameters
Capillary pressure law $p_c = 0 \ \ (p_l = p_g)$	
Darcy-Muskat's law $\overrightarrow{q}_\alpha = -\frac{k_{r\alpha}}{\mu_\alpha} K(\nabla p_\alpha - \rho_\alpha \overrightarrow{g}), \ \ \alpha = l, g$	$\overrightarrow{g} = \begin{pmatrix} 0 \\ 0 \\ -9.81 \end{pmatrix}$ m/s^2 $K = 10^{-13}\mathbb{I}$ m^2
Relative permeability $k_{rl} = (S_l^*)^4$ $k_{rg} = 0.4(1-S_l^*)^2(1-(S_l^*)^2)$	$S_l^* = \frac{S_l - S_{lr}}{1 - S_{lr}}$ $S_{lr} = 0.2$
Liquid diffusion/dispersion tensor $D_l = D_m\mathbb{I} + d_L\lvert\overrightarrow{q_l}\rvert + (d_L - d_T)\frac{\overrightarrow{q_l}\overrightarrow{q_l}^T}{\lvert\overrightarrow{q_l}\rvert}$	$D_m = 1.6\ 10^{-8}$ m^2/s $d_L = 5$ m $d_T = 0.5$ m
Solid density	$\rho_s = 2700$ kg/m^3
Porosity $\phi = 1 - \frac{c_{\mathrm{CaCO_3}} M_{\mathrm{CaCO_3}}}{\rho_s}$	$M_{\mathrm{CaCO_3}} = 0.1$ kg/mol $\phi_{init} = 0.18$
Liquid density $\rho_l(p_l, x_l^{\mathrm{CO_2}}, S, T) = \rho_{brine}(p_l, S, T) + \rho_{\mathrm{H_2O-CO_2}}(p_l, x_l^{\mathrm{CO_2}}, T) - \rho_{\mathrm{H_2O}}$ The model is based on the results of articles [29] and [9] and implemented in DuMu^X	$S = 0$ $T = 50$°C (323 K)
Liquid viscosity	$\mu_l = 4.8\ 10^{-4}$ Pa. s
Gas density ρ_g is a tabulated variable. Tabulated values are calculated for the model described in [63]	
Gas viscosity $\mu_g(p_g, T) = \mu_0(T) + \Delta\mu(\rho_n(p_g, T), T)$ The model is based on the results of the article [27] and implemented in DuMu^X	

Table 4.12: Physical parameters for the test case of Fan et al.

4.5.3.2 Numerical results

The period of simulation is equal to 2000 years. The calculation was performed on a PC Intel Core i5-2520M CPU @ 2.50GHz×4 with 8 GB of memory. The CPU time was equal to 15 hours 30 minutes.

The evolution of the gas saturation is represented in Figure 4.18. After 20 years,

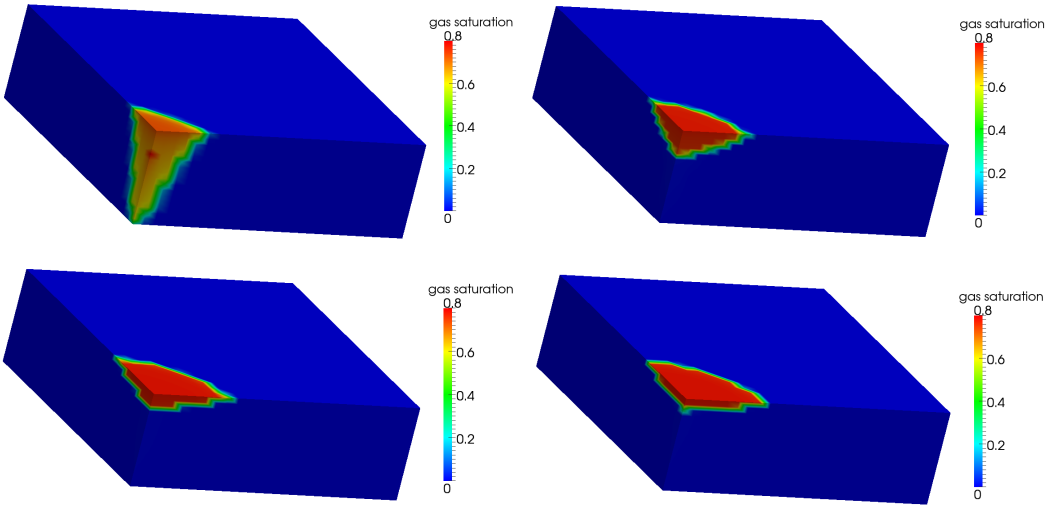

Figure 4.18: Evolution of the gas saturation. Top left: 20 years. Top right : 500 years. Bottom left: 1200 years. Bottom right : 2000 years.

the injected CO_2 forms the gas phase plume near to the injection well. After stop of injection, this plume slowly migrates upward by buoyancy effect until it reaches the top of the aquifer with no-flux conditions and forms a thin gas phase layer, where gaseous CO_2 gradually dissolved into the liquid phase.

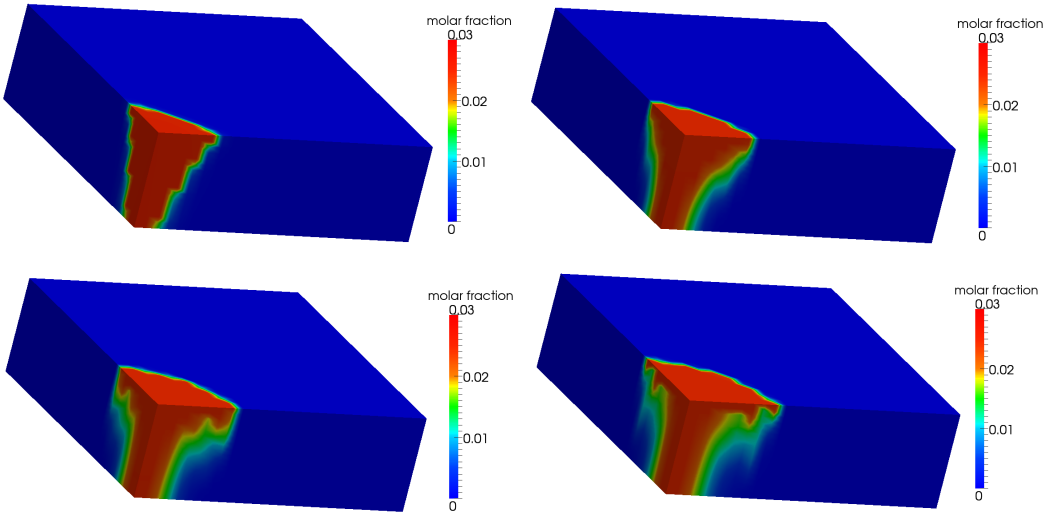

Figure 4.19: Evolution of the dissolved CO_2 mole fractions in liquid phase. Top left: 20 years. Top right : 500 years. Bottom left: 1200 years. Bottom right : 2000 years.

The dissolved CO_2 molar fraction evolution is represented in Figure 4.19. In the zone where the injected CO_2 formed the gas phase, some part of $CO_{2(g)}$ dissolves in the liquid phase. The process of gaseous CO_2 dissolution continues during the whole period of simulation and for this reason the distribution area of the liquid CO_2, after 2000 years of simulation, contains all areas where gas was present. The water with dissolved CO_2, which is heavier than pure water, eventually moves downwards under the gravity. After the long period of simulation, we observe a fingering effect, characteristic of this kind

of simulations (see also section 3.3.2.3).

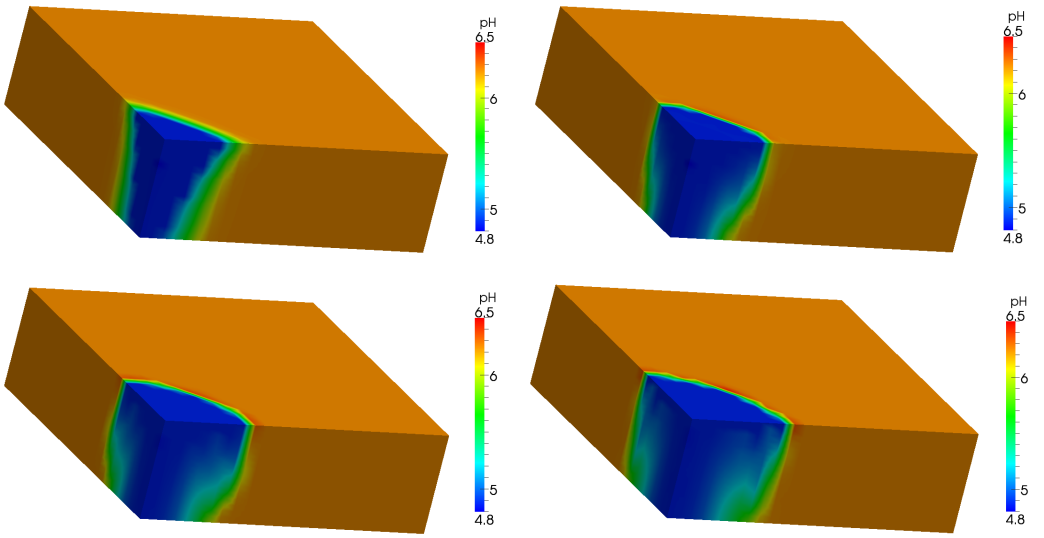

Figure 4.20: Evolution of pH. Top left: 20 years. Top right : 500 years. Bottom left: 1200 years. Bottom right : 2000 years.

The evolution of H^+ concentration (in form of pH$= -\log c_{H^+}$) is represented in Figure 4.20. We see that the distribution of H^+ is strongly correlated with the $CO_{2(l)}$ concentration. High concentration of $CO_{2(l)}$ causes the increasing of the liquid phase acidity.

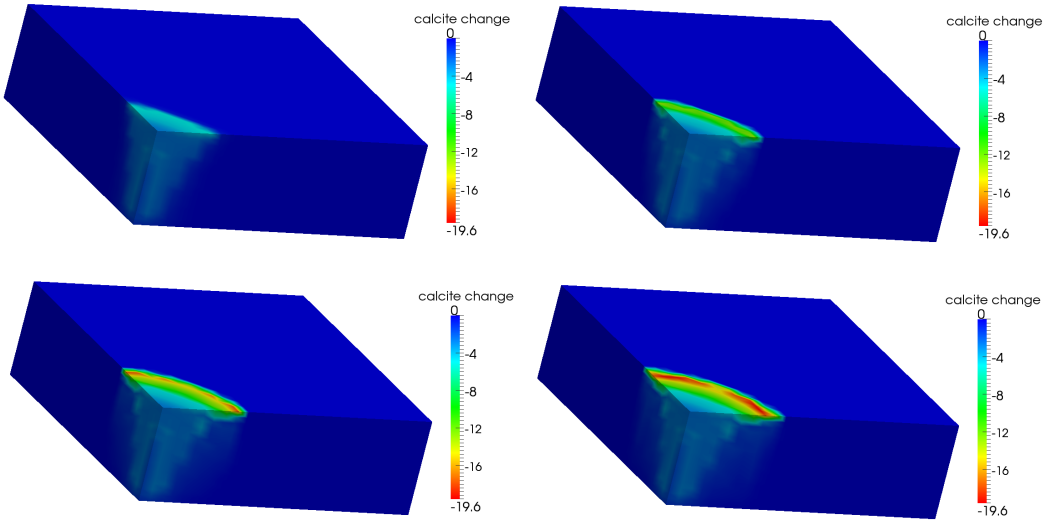

Figure 4.21: Calcite concentration changes (mol/m^3). Negative values indicate dissolution. Top left: 20 years. Top right : 500 years. Bottom left: 1200 years. Bottom right : 2000 years.

The changes of calcite concentration are represented in Figure 4.21. An increase in the concentration of the dissolved CO_2 shifts the equilibrium between calcite and ions presented in the liquid phase, and some part of mineral dissolves. For this reason we

can see that the picture of the calcite concentration changes reflects the evolution of $CO_{2(l)}$ distribution.

As was mentioned before the chemical system used in our simulations is significantly different from the chemical systems investigated in Fan et al. [26]. So we couldn't compare qualitatively our and Fan's results. For example, in the article [26] the process of calcite precipitation is observed for both six- and nine-element chemical system. In our simulations we observe in opposite the calcite dissolution. The main reason for such difference is that in Fan et al. work the reaction between calcium and liquid ions is performed in close connection with other reactions of mineral precipitation/dissolution. In particular, calcium ions are involved not only in chemical reaction with calcite but also with anorthite and dolomite. And in Fan et al. results we observe that the dissolution of anorthite produces the required number of calcium ions for calcite precipitation. In our simulations for the reasons stated previously we had to eliminate all reactions with minerals, except calcite precipitation/dissolution reaction. The obtained chemical system no-longer contains the reaction that produces additional calcium ions and therefore we observe the calcite dissolution and not precipitation.

4.5.4 Concluding remarks on the numerical examples.

After having carried out the three test cases, we are able to draw the following conclusions:

- the numerical simulator developed on the basis of the proposed decoupling algorithm is capable to reproduce test examples taken from the literature,
- comparing two variants of the SHPCO2 Benchmark with immobile and mobile gas phase, we figure out that the transport process in the gas phase has a strong influence on the simulation results,
- the picture of system parameters evolution obtained in numerical simulations for Saatlink et al. test case coincides in many aspects with results of Saatlink *et al*,
- the revealed differences in results of Saatlink et al. test case are possibly explained by not accurate choice of the chemical equilibrium constants and by differences in the implementations of the phase switch,
- the preliminary 3D simulations demonstrated the abilities of developed numerical simulator for performing three-dimensional calculations.

Bibliography

[1] ChemEqLib webpage. https://gforge.inria.fr/projects/chemeqlib.

[2] DuMuX documentation. http://www.dumux.org/doxygen-stable/html-2.2/.

[3] DuMuX handbook. http://www.dumux.org/documents/dumux-handbook-2.5.pdf.

[4] Dune, the distributed and unified numerics environment. http://www.dune-project.org/.

[5] GSL documentation: Multidimensional root-finding. http://www.gnu.org/software/gsl/manual/html_node/Multidimensional-Root_002dFinding.html.

[6] GSL library. http://www.gnu.org/software/gsl/.

[7] A. Abadpour and M. Panfilov. Method of negative saturations for modeling two-phase compositional flow with oversaturated zones. *Transport in Porous Media*, 79(2):197–214, 2009.

[8] A.Bielinski. *Numerical Simulation of CO2 Sequestration in Geological Formations*. Thesis, Universitat Stuttgart, 2007.

[9] J. J. Adams and S. Bachu. Equations of state for basin geofluids: algorithm review and intercomparison for brines. *Geofluids*, 2(4):257–271, 2002.

[10] B. Amaziane, Mladen Jurak, and A. Zgaljić Keko. Modeling compositional compressible two-phase flow in porous media by the concept of the global pressure. *Computational Geosciences*, 18(3-4):297–309, 2014.

[11] L. Amir and M. Kern. A global method for coupling transport with chemistry in heterogeneous porous media. *Computational Geosciences*, 14(3):465–481, 2010.

[12] J. Bear and A. Cheng. *Modeling Groundwater Flow and Contaminant Transport*. Springer, 2010.

[13] C.M. Bethke. *Geochemical Reaction Modeling, Concepts and Applications*. Oxford University Press, 1996.

[14] A. Bourgeat, M. Jurak, and F. Smai. Two-phase, partially miscible flow and transport modeling in porous media; application to gas migration in a nuclear waste repository. *Computational Geosciences*, 13:29–42, 2009. 10.1007/s10596-008-9102-1.

[15] A. Bourgeat, M. Jurak, and F. Smai. On persistent primary variables for numerical modeling of gas migration in a nuclear waste repository. *Computational Geosciences*, 17(2):287–305, 2013.

[16] R.H. Brooks and A.T. Corey. *Hydraulic Properties of Porous Media*. Colorado State University Hydrology Papers. Colorado State University, 1964.

[17] J. Carrayrou. *Modélisation du transport de solutés réactifs en milieu poreux saturé*. Thèse, Université de Strasbourg, 2001.

[18] J. Carrayrou, J. Hoffmann, P. Knabner, S. Kräutle, C. de Dieuleveult, J. Erhel, J. van der Lee, V. Lagneau, K. U. Mayer, and K. T. B. MacQuarrie. Comparison of numerical methods for simulating strongly nonlinear and heterogeneous reactive transport problems-the MoMaS benchmark case. *Computational Geosciences*, 14(3):483–502, 2010.

[19] J. Carrayrou, M. Kern, and P. Knabner. Reactive transport benchmark of MoMaS. *Computational Geosciences*, 14(3):385–392, 2010.

[20] J. Carrayrou, R. Mosé, and P. Behra. Operator-splitting procedures for reactive transport and comparison of mass balance errors. *Journal of Contaminant Hydrology*, 68(3â4):239 – 268, 2004.

[21] Z. Chen, G. Huan, and Y. Ma. *Computational Methods for Multiphase Flows in Porous Media*. Computational Science and Engineering. SIAM, 2006.

[22] H. Class, A. Ebigbo, R. Helmig, H. Dahle, J. Nordbotten, M. Celia, P. Audigane, M. Darcis, J. Ennis-King, Y. Fan, B. Flemisch, S. Gasda, M. Jin, S. Krug, D. Labregere, A. Naderi Beni, R. Pawar, A. Sbai, S. Thomas, L. Trenty, and L. Wei. A benchmark study on problems related to CO2 storage in geologic formations Summary and discussion of the results. *Computational Geosciences*, 13:409–434, 2009. 10.1007/s10596-009-9146-x.

[23] H. Class, R. Helmig, and P. Bastian. Numerical simulation of non-isothermal multiphase multicomponent processes in porous media. 1. An efficient solution technique. *Advances in Water Resources*, 25:533–550, 2002.

[24] C. de Dieuleveult. *Un modèle numérique global et performant pour le couplage géochimie-transport*. Thèse, Université de Rennes 1, 2008.

[25] C. de Dieuleveult, J. Erhel, and M. Kern. A global strategy for solving reactive transport equations. *Journal of Computational Physics*, 228(17):6395 – 6410, 2009.

[26] Y. Fan, L. J. Durlofsky, and H. A. Tchelepi. A fully-coupled flow-reactive-transport formulation based on element conservation, with application to CO2 storage simulations. *Advances in Water Resources*, 42:47–61, 2012.

[27] A. Fenghour, W. A. Wakeham, and V. Vesovic. The Viscosity of Carbon Dioxide. *Journal of Physical and Chemical Reference Data*, 27:31–44, 1998.

[28] P. Gamazo, M. Saaltink, J. Carrera, L. Slooten, and S. Bea. A consistent compositional formulation for multiphase reactive transport where chemistry affects hydrodynamics. *Advances in Water Resources*, 35(0):83 – 93, 2012.

[29] J. E. Garcia. *Fluid Dynamics of Carbon Dioxide Disposal into Saline Aquifers*. PhD thesis, University of California, 2003.

[30] B. Gueslin and M. Kern. Reactive transport for CO2 geological storage. Unpublished, 2011.

[31] G.E. Hammond, P.C. Lichtner, C. Lu, and R.T. Mills. PFLOTRAN: Reactive flow transport code for use on laptops to leadership-class supercomputers. *Groundwater Reactive Transport Models*, pages 141–159, 2012.

[32] G.E. Hammond, A.J. Valocchi, and P.C. Lichtner. Application of jacobian-free newton-krylov with physics-based preconditioning to biogeochemical transport. *Advances in Water Resources*, 28(4):359 – 376, 2005.

[33] Y. Hao, Y. Sun, and J.J. Nitao. Overview of NUFT: A versatile numerical model for simulating flow and reactive transport in porous media. *Groundwater Reactive Transport Models*, pages 212–239, 2012.

[34] J. Jaffré and A. Sboui. Henry's law and gas phase disappearance. *Transport in Porous Media*, 82(3):521–526, 2010.

[35] Xi Jiang. A review of physical modelling and numerical simulation of long-term geological storage of CO2. *Applied energy*, 88:3557–3566, 2011.

[36] S. Kräutle. *General Multi-Species Reactive Transport Problems in Porous Media: Efficient Numerical Approaches and Existence of Global Solutions*. PhD thesis, University of Erlangen–Nuremberg Department of Mathematics, 2008. Habilitation thesis.

[37] S. Kräutle. The semismooth newton method for multicomponent reactive transport with minerals. *Advances in Water Resources*, 34(1):137 – 151, 2011.

[38] S. Kräutle and P. Knabner. A new numerical reduction scheme for fully coupled multicomponent transport-reaction problems in porous media. *Water Resources Research*, 41(9), 2005.

[39] A. Lauser, C. Hager, R. Helmig, and B. Wohlmuth. A new approach for phase transitions in miscible multi-phase flow in porous media. *Advances in Water Resources*, 34(8):957 – 966, 2011.

[40] F. J. Leij and J. H. Dane. Analytical solutions of the one-dimensional advection equation and two- or three-dimensional dispersion equation. *Water Resources Research*, 26(7):1475–1482, 1990.

[41] T. Maldal and I.M. Tappel. CO2 underground storage for Snohvit gas field development. *Energy*, 29(9-10):1403 – 1411, 2004. 6th International Conference on Greenhouse Gas Control Technologies.

[42] E. Marchand and P. Knabner. Results of the MoMaS benchmark for gas phase appearance and disappearance using generalized MHFE. *Advances in Water Resources*, 73(0):74 – 96, 2014.

[43] E. Marchand, T. Muller, and P. Knabner. Fully coupled generalised hybrid-mixed finite element approximation of two-phase two-component flow in porous media. part ii: numerical scheme and numerical results. *Computational Geosciences*, 16(3):691–708, 2012.

[44] E. Marchand, T. Muller, and P. Knabner. Fully coupled generalized hybrid-mixed finite element approximation of two-phase two-component flow in porous media. part i: formulation and properties of the mathematical model. *Computational Geosciences*, 17(2):431–442, 2013.

[45] K.U. Mayer, R.T. Amos, S. Molins, and F. Gérard. Reactive transport modeling in variably saturated media with min3p: Basic model formulation and model enhancements. *Groundwater Reactive Transport Models*, pages 186–211, 2012.

[46] C. Miller, G. Christakos, P. Imhoff, J. McBride, J. Pedit, and J. Trangenstein. Multiphase flow and transport modeling in heterogeneous porous media: challenges and approaches. *Advances in Water Resources*, 21(2):77 – 120, 1998.

[47] F. Morel. *Principles of aquatic chemistry*. J. Wiley, 1983.

[48] R. Neumann, P. Bastian, and O. Ippisch. Modeling and simulation of two-phase two-component flow with disappearing nonwetting phase. *Computational Geosciences*, 17:139–149, 2013.

[49] J. M. Nordbotten and M.A. Celia. *Geological storage of CO2. Modelling approaches for large-scale simulation*. Wiley, 2012.

[50] M. Panfilov and M. Rasoulzadeh. Interfaces of phase transition and disappearance and method of negative saturation for compositional flow with diffusion and capillarity in porous media. *Transport in Porous Media*, 83(1):73–98, 2010.

[51] D. L. Parkhurst and C. A. J. Appelo. Description of input and examples for PHREEQC version 3–a computer program for speciation, batch-reaction, one-dimensional transport, and inverse geochemical calculations. Technical report, US Geological Survey, 2013.

[52] D. Peng and D. Robinson. A New Two-Constant Equation of State. *Industrial Engineering Chemistry Fundamentals*, 15:59–64, 1976.

[53] G. Pinder and W. Gray. *Essentials of Multiphase Flow and Transport in Porous Media*. Wiley, 2009.

[54] M. J. D Powell. A hybrid method for nonlinear algebraic equations. In P. Rabinowitz, editor, *Numerical Methods for Nonlinear Algebraic Equations*, chapter 6, pages 87–114. Gordon Breach, 1970.

[55] C. Prinet, S. Thibeau, M. Lescanne, and J. Monne. Lacq-rousse CO2 capture and storage demonstration pilot: Lessons learnt from two and a half years monitoring. 37:3610–3620, 2013.

[56] J. Rubin. Transport of reacting solutes in porous media: Relation between mathematical nature of problem formulation and chemical nature of reactions. *Water Resources Research*, 19:1231–1252, 1983.

[57] M. W. Saaltink, C. Ayora, and J. Carrera. A mathematical formulation for reactive transport that eliminates mineral concentrations. *Water Resources Research*, 34(7):1649–1656, 1998.

[58] M. W. Saaltink, J. Carrera, and C. Ayora. On the behavior of approaches to simulate reactive transport. *Journal of Contaminant Hydrology*, 48(3â4):213 – 235, 2001.

[59] M. W. Saaltink, V. Vilarrasa, F. De Gaspari, O. Silva, J. Carrera, and T. S. Rötting. A method for incorporating equilibrium chemical reactions into multiphase flow models for CO2 storage. *Advances in Water Resources*, 62, Part C(0):431 – 441, 2013. Computational Methods in Geologic CO2 Sequestration.

[60] J. Samper, C. Yang, L. Zheng, L. Montenegro, T. Xu, Z. Dai, G. Zhang, C. Lu, and S. Moreira. CORE2D V4: A code for water flow, heat and solute transport, geochemical reactions, and microbial processes. *Groundwater Reactive Transport Models*, pages 160–185, 2012.

[61] Javier Samper, Tianfu Xu, and Changbing Yang. A sequential partly iterative approach for multicomponent reactive transport with core2d. *Computational Geosciences*, 13(3):301–316, 2009.

[62] F. Smai. *Développement d'outils mathématiques et numériques pour l'evaluation du concept de stockage géologique*. Thèse, Université de Lyon, 2009.

[63] R. Span and W. Wagner. A new equation of state for carbon dioxide covering the fluid region from the triple-point temperature to 1100 K at pressures up to 800 MPa. *Journal of Physical and Chemical Reference Data*, 25(6), 1996.

[64] N. Spycher and K. Pruess. CO2-H2O mixtures in the geological sequestration of CO2. II. partitioning in chloride brines at 12-100 C and up to 600 bar. *Geochimica et Cosmochimica Acta*, 69(13):3309 – 3320, 2005.

[65] T. Torp and J. Gale. Demonstrating storage of CO2 in geological reservoirs: The sleipner and sacs projects. *Energy*, 29:1361–1369, 2004.

[66] A. J. Valocchi, R. L. Street, and P. V. Roberts. Transport of ion-exchanging solutes in groundwater: Chromatographic theory and field simulation. *Water Resources Research*, 17:1517–1527, 1981.

[67] M. A. C. Van Genuchten. A closed-form equation for predicting the hydraulic conductivity of unsaturated soils. *Soil Sci. Soc. Am. J.*, 1980.

[68] M.F. Wheeler, S. Sun, and S.G. Thomas. Modeling of flow and reactive transport in IPARS. *Groundwater Reactive Transport Models*, pages 42–73, 2012.

[69] M.D. White and Y. Fang. STOMP-ECKEChem: An engineering perspective on reactive transport in geologic media. *Groundwater Reactive Transport Models*, pages 112–140, 2012.

[70] T. Xu, E. Sonnenthal, N. Spycher, G. Zhang, L. Zheng, and K. Pruess. Toughreact TOUGHREACT: A simulation program for subsurface reactive chemical transport

under non-isothermal multiphase flow conditions. *Groundwater Reactive Transport Models*, pages 74–95, 2012.

[71] G. Yeh and V. Tripathi. A critical evaluation of recent developments in hydrogeochemical transport models of reactive multichemical components. *Water Res. Res.*, 25:93–108, 1989.

[72] G.T. Yeh, V.S. Tripathi, J.P. Gwo, H.P. Cheng, J.R.C. Cheng, K.M. Salvage, M.H. Li, Y. Fang, Y. Li, J.T. Sun, F. Zhang, and M.D. Siegel. Hydrogeochem: A coupled model of variably saturated flow, thermal transport, and reactive biogeochemical transport. *Groundwater Reactive Transport Models*, pages 3–41, 2012.

[73] L. Young. A study of spatial approximations for simulating fluid displacements in petroleum reservoirs. *Computer Methods in Applied Mechanics and Engineering*, 47:3 – 46, 1984. Special Issue on Oil Reservoir Simulation.

[74] F. Zhang, G.-T. Yeh, and J.C. Parker. *Groundwater reactive transport models*. Bentham Science Publishers Ltd., 2012.